Porphyrin–Ryleneimide Hybrids: Tuning of Visible and Near-Infrared Absorption by Chromophore Desymmetrization

Supplementary Information

by Sunit Kumar,[†] Yogesh Kumar Maurya,[†] Seongsoo Kang,[‡] Piotr Chmielewski,[†] Tadeusz Lis,[†] Joanna Cybińska,[†,#] Dongho Kim,*[,‡] and Marcin Stępień*[,†]

Table of Contents

Experimental

General. Tetrahydrofuran and diethyl ether were dried using a commercial solvent purification system. Dichloromethane and chlorobenzene were distilled from calcium hydride when used as reaction solvents. All other solvents and reagents were used as received. ^{1}H NMR spectra were recorded on high-field spectrometers (^{1}H frequency 500.13 or 600.13 MHz), equipped with broadband inverse or conventional gradient probeheads. Spectra were referenced to the residual solvent signals (chloroform-d, 7.24 ppm). Two-dimensional NMR spectra were recorded with 2048 data points in the t_2 domain and up to 2048 points in the t_1 domain, with a 1 s recovery delay. All 2D spectra were recorded with gradient selection. ^{13}C NMR spectra were recorded with ^{1}H broadband decoupling and referenced to solvent signals ($^{13}CDCl_3$, 77.0 ppm). High resolution mass spectra were recorded using electrospray or MALDI ionization in the positive mode. Electrochemical measurements (THF and DCM, 0.1 M [$TBAPF_6$], 293 K) were performed on an EA9C Multifunctional Electrochemical Analyzer using a glassy-carbon working electrode, platinum wire as the auxiliary electrode, and silver wire as a reference electrode. The voltammograms were referenced against the half-wave potential of Fc^+ /Fc.

Photoluminescence excitation (PLE) and emission (PL) spectra were taken with the FSL980-sm Fluorescence Spectrometer from Edinburgh Instruments Ltd. A 450 W Xenon arc lamp (PL and PLE) and a Super Continuum Fianium laser were used as excitation sources. Emission spectra were corrected for the recording system efficiency and excitation spectra were corrected for the incident light intensity. PLE and PL spectra and QY were measured using cooled extended red Hamamatsu photomultiplier operating in a range of 200 – 1050 nm. Quantum yield measurements were performed by using an Edinburgh Instruments integrating sphere equipped with a small elliptical mirror and a baffle plate for beam steering and shielding against directly detected light. For the measurement, the integrating sphere replaces the standard sample holder inside the sample chamber. Calculations of quantum yields were made using the software provided by Edinburgh Instruments.

Femtosecond Transient Absorption Spectroscopy. The femtosecond time-resolved transient absorption (TA) spectrometer used for this study consists of a femtosecond optical parametric amplifier (Quantronix, Palitra-FS) pumped by a Ti:sapphire regenerative amplifier system (Quantronix, Integra-C) operating at 1 kHz repetition rate and an accompanying optical detection system. The generated OPA pulses had a pulse width of ~100 fs and an average power of 1 mW in the range of 560 to 680 nm, which were used as pump pulses. For 800 nm excitation, fundamental pulses were used without passing through the OPA system. White light continuum (WLC) probe pulses were generated using a sapphire window (2 mm thick) by focusing of a small portion of the fundamental 800 nm pulses, which were picked off by a quartz plate before entering into the OPA. The time delay between pump and probe beams was carefully controlled by making the pump beam travel along a variable optical delay (Newport, ILS250). Intensities of the spectrally dispersed WLC probe pulses were monitored by a miniature spectrograph (OceanOptics, USB2000+). To obtain the time-resolved transient absorption difference signal (ΔA) at a specific time, the pump pulses were chopped at 500 Hz and absorption spectra intensities were saved alternately with or without pump pulse. Typically, 6000 pulses were used excite samples and to obtain the TA spectra at a particular delay time. The polarization angle between pump and probe beam was set at the magic angle (54.7°) using a Glan- S5 laser polarizer with a half-wave retarder to prevent polarization-dependent signals. The crosscorrelation FWHM in the pump-probe experiments was less than 200 fs, and chirp of WLC probe

pulses was measured to be 800 fs in the 400–800 nm regions. To minimize chirp, all reflection optics were used in the probe beam path, and a quartz cell of 2 mm path length was employed. After completing each set of fluorescence and TA experiments, the absorption spectra of all compounds were carefully checked to rule out the presence of artifacts or spurious signals arising from, for example, degradation or photo-oxidation of the samples in question.

X-ray crystallography. X-ray quality crystals were grown by slow diffusion of n-hexane into a chloroform solution of **2b**-H_2 and **3b**-H_2. Diffraction measurements were performed on a κ-geometry Ruby PX diffractometer (ω scans) with graphite-monochromatized Mo Kα radiation. The data were collected at 100 K, corrected for Lorenz and polarization effects. Data collection, cell refinement, data reduction and analysis were carried out with the Xcalibur PX software, CRYSALIS CCD and CRYSALIS RED, respectively (Oxford Diffraction Ltd., Abignon, England, 2009). An analytical absorption correction was applied with the use of CRYSALIS RED. All structures were solved by direct methods with the SHELXS-97 program and refined using SHELXL-97[1] with anisotropic thermal parameters for non-H atoms. In the final refinement cycles, all H atoms were treated as riding atoms in geometrically optimized positions. CCDC Mercury and CrystalExplorer[2,3] were used for visualization of solvent-accessible surfaces. In the final refinement cycles, all H atoms were treated as riding atoms in geometrically optimized positions. CCDC 2015790 and 2015791 contains the supplementary crystallographic data for this paper. These data can be obtained free of charge from the Cambridge Crystallographic Data Centre via http://www.ccdc.cam.ac.uk/data_request/cif.

Computational methods. Density functional theory (DFT) calculations were performed using Gaussian 16.[4] DFT geometry optimizations were carried out in unconstrained C1 symmetry, using extended tight binding (xTB)[5,6] or semi-empirical models as starting geometries. DFT geometries were refined to meet standard convergence criteria, and the existence of a stationary point was verified by a normal mode frequency calculation. Geometry optimizations, frequency calculations, and thermochemistry calculations were performed using the hybrid functional B3LYP combined with the 6-31G(d,p) basis set.[7-9] In the calculations of absorption spectra, up to 50 electronic transitions were calculated by means of time-dependent DFT (TD-DFT), using the above level of theory, PCM solvation (using dichloromethane parameters).[10]

Synthesis

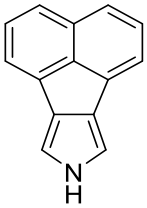

8H-acenaphtho[1,2-c]pyrrole (4). Compound **4** was prepared by following literature procedure.[11] Yield 80 %. **^{1}H NMR** (500 MHz, chloroform-*d* , 300 K): δ 8.16 (1H, b), 7.61 (2H, d, ^3J = 8.4 Hz), 7.56 (2H, d, ^3J = 6.5 Hz), 7.47 (2H, m), 7.02 (2H, s). **^{13}C NMR** (125 MHz, chloroform-*d* , 300 K): δ 137.7, 133.7, 130.9, 128.7, 127.5, 123.9, 118.5, 110.6.

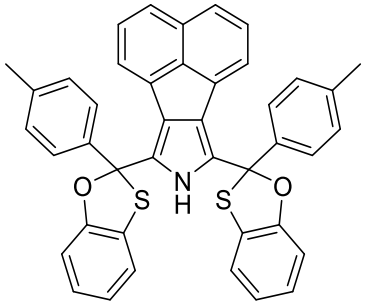

7,9-bis(2-(p-tolyl)benzo[d][1,3]oxathiol-2-yl)-8H-acenaphtho[1,2-c]pyrrole (5). 2-Hydroxythiophenol (0.8 mL, 0.075 mol) and p-toluic acid (1.05 g, 0.075 mol, 1 equiv.) were dissolved in $POCl_3$ (12 mL) in a 25 mL round-bottom flask and heated to 110 °C in an oil bath with continuous stirring for 10 min; the mixture turned deep red. The reaction mixture was cooled to room temperature, and $HBF_4 \cdot Et_2O$ (2.70 mL) was added, followed by the addition of dry ether (20 mL), which precipitated out the benzoxathiolium salt as a yellow powder. The powder was collected by vacuum filtration and used without further purification or characterization (yield: 1.4 g).[12] All of the benzoxathiolium salt was placed into a 250 mL round-bottom flask containing pyrrole (360 mg, 0.018 mol), pyridine (0.413 mL, 0.051 mol), and mixture of acetonitrile and chloroform (5:5 mL) with continuous stirring. The salt got dissolved immediately upon addition and the solution became hot and turned dark yellow. The reaction mixture was stirred for 1 h, and then CH_2Cl_2 (10 mL) and H_2O (10 mL) were added. The aqueous and organic layers were separated, and the aqueous layer was extracted with CH_2Cl_2. The combined organic layers were washed with 5% NaOH (aq) (20 mL) and water and then dried over sodium sulfate, and the solvent was evaporated. The crude product was purified by silica gel column chromatography using petroleum ether/ethyl acetate (90:10, v/v) which afforded pure compound **5** as a yellow solid (900 mg, 75%). **^{1}H NMR** (500 MHz, chloroform-*d* , 300 K): δ 8.84 (1H, b), 7.62 (4H, m), 7.53 (2H, d, ^3J = 8.1 Hz), 7.25 (2H, m), 7.18 (4H, q, ^3J = 8.1 Hz), 7.14 (2H, m), 7.05 (2H, m), 6.94 (4H, m), 6.68 (2H, t, ^3J = 7.6 Hz), 2.37 (6H, s). **^{13}C NMR** (125 MHz, chloroform-*d* , 300 K): δ 154.5, 154.5, 139.2, 139.1, 138.1, 138.0, 137.1, 132.3, 130.3, 129.6, 129.3, 128.8, 128.7, 127.3, 126.8, 126.7, 126.4, 125.7, 124.6, 124.4, 124.3, 123.0, 122.9, 122.1, 122.0, 121.3, 111.0, 110.9, 98.6, 98.5, 21.2. **HRMS** (ESI–TOF): *m/z*: $[M + Na]^+$ Calcd for $C_{42}H_{29}NO_2S_2Na$: 666.1532; Found 666.1543.

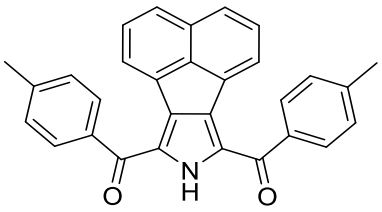

(8H-acenaphtho[1,2-c]pyrrole-7,9-diyl)bis(p-tolylmethanone) (6). 7,9-bis(2-(p-tolyl)benzo[d][1,3]oxathiol-2-yl)-8H-acenaphtho[1,2-c]pyrrole (**5**; 1.0 g, 0.015 mol) was added to the hydrolysis reagent constituted of mercury (II) oxide (0.74 g, 0.033 mol) in THF (25 mL) and 48% aqueous tetrafluoroboric acid (1 mL). The reaction was exothermic, and mercury(II) oxide was dissolved at once. The mixture was allowed to stir at room temperature for 3 h until the disappearance of the starting material (TLC test: petroleum ether/ethyl ether, 80:20). The reaction mixture was then extracted with dichloromethane and the extracts were washed successively with 10% potassium iodide solution, 5% sodium hydroxide solution, and water. After evaporation of the solvent, The crude 2,5-dipivaloylacenapthopyrrole (**6**) was purified The crude product was purified by silica gel column chromatography using petroleum ether/ethyl acetate (80:20, v/v) and afforded pure compound **6** as a yellow solid (530 mg, 80%). **^{1}H NMR** (500 MHz, chloroform-*d* , 300 K): δ 9.67 (1H, b), 7.92 (4H, d, ^3J = 8.1 Hz), 7.74 (2H, d, ^3J = 7.9 Hz), 7.38 (6H, m), 7.09 (2H, q^3J = 7.1 Hz), 2.25 (6H, s). **^{13}C NMR** (125 MHz, chloroform-*d* , 300 K): δ 186.4, 143.8, 137.1, 135.5,133.9, 131.2, 130.2, 129.7,129.2, 127.5, 126.7, 123.8, 21.8. **HRMS** (ESI–TOF): *m*/*z*: [M + H]$^+$ Calcd for $C_{30}H_{22}NO_2$: 428.1645; Found 428.1629.

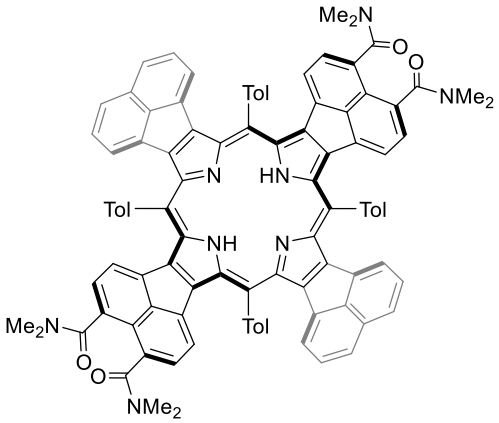

tD$_2$A$_2$ porphyrin (2a-H$_2$**).** To the solution of the diacylated acenapthopyrrole **6** (200 mg, 0.46 mmol) in 48 mL of THF/MeOH (3:2 v/v), was added $NaBH_4$ (880 mg, 23.20 mmol) under N_2 atmosphere. The reaction was stirred at room temperature for an additional 2 h at room temperature. After completion of the reaction, as indicated by TLC analysis, the reaction was quenched with a saturated aqueous solution of NH_4Cl (10 mL) and extracted with dichloromethane (2 × 25 mL). The combined organic layers were dried over anhydrous sodium sulfate, and the solvent was removed on a rotary evaporator under high vacuum to afford dicarbinols as yellow sticky solids. The appropriate crude dicarbinol without further purification was treated with 1 equiv. of NDA pyrrole[13] (149 mg, 0.48 mmol) in the presence of a catalytic amount of *p*-Toluenesulfonic acid monohydrate(PTSA) (53.36 mg, 0.29 mmol) in chloroform/methanol (80.8 mL, 100:1 v/v) under nitrogen atmosphere for 1 h. Then 2,3- dichloro-5,6-dicyano-1,4-benzoquinone (DDQ, 153.99 mg, 0.67 mmol) was added and the mixture was stirred for additional 2 h. The solvent was evaporated and the residue was purified by

column chromatography on alumina (grade V) with dichloromethane/methanol (100:0.3 v/v) to give the product as violet solid (80 mg, 12%). **^{1}H NMR** (500 MHz, chloroform-*d* , 300 K): δ 8.64 (8H, b), 7.72 (8H, m), 7.64 (4H, b), 7.18 (4H, b), 7.01 (4H, b), 5.79 (4H, b), 5.64 (4H, b), 3.07 (6H, s), 3.02 (12H, s), 2.82 (6H, s), 2.81 (6H, s), 2.67 (6H, b), -0.51 (2H, b). **^{13}C NMR** (151 MHz, chloroform-*d* , 300 K): δ 170.8, 170.7, 140.1, 140.0, 139.7, 139.6, 137.0, 134.5, 134.0, 133.3, 131.0, 130.7, 129.5, 127.3, 126.8, 124.4, 123.3, 39.4, 39.3, 34.8, 34.7, 21.7. **HRMS** (ESI–TOF): *m*/*z*: $[2M+H]^{2+}$ Calcd for $C_{200}H_{150}N_{16}O_8$: 1452.5938; Found 1452.5948.

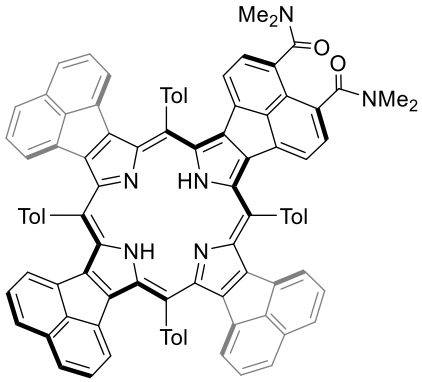

D_3A porphyrin (3a-H_2). Porphyrin **3a**-H_2 was synthesized by following the same procedure as given for **tD_2A_2** porphyrin **2a**-H_2 by using dicarbinal-acenapthopyrrole **5** (195 mg, 0.44 mmol), acenapthopyrrole[11] **4** (42.81 mg, 0.22 mmol), NDA pyrrole[13] (74.63 mg, 0.22 mmol), *p*-toluenesulfonic acid monohydrate (55.36 mg, 0.29 mmol) and DDQ (153.99 mg, 0.67 mmol). The crude compound was purified by column chromatography on alumina (grade V) with dichloromethane to give the product as violet solid (60 mg, 10%). **^{1}H NMR** (500 MHz, chloroform-*d* , 300 K): δ 8.66 (8H, b), 7.73 (8H, m), 7.63 (6H, b), 7.17 (6H, b), 7.00 (2H, b), 5.78 (6H, b), 5.65 (2H, b), 3.05 (3H, s), 3.07 (6H, s), 3.02 (6H, s), 2.82 (3H, s), 2.81 (3H, s), 2.66 (3H, b), -0.53 (2H, b). **^{13}C NMR** (151 MHz, chloroform-*d* , 300 K): δ 170.6, 170.0, 158.3, 158.1, 157.8, 157.6, 142.5, 142.2, 141.2, 141.1, 141.0, 140.6, 140.1, 140.0, 139.8, 139.7, 138.1, 138.0, 137.4, 137.3, 136.0, 135.6, 135.1, 134.7, 132.7, 131,4, 130.6, 129.7, 129.2, 127.7, 127.4, 127.3, 126.2, 125.8, 125.7, 123.2, 120.9, 120.8, 120.6, 117.3, 115.4, 113.5, 39.5, 39.4, 34.9, 21.8, 21.7. **HRMS** (ESI–TOF): *m*/*z*: $[M + H]^+$ Calcd for $C_{94}H_{65}N_6O_2$: 1310.5196; Found 1310.5235.

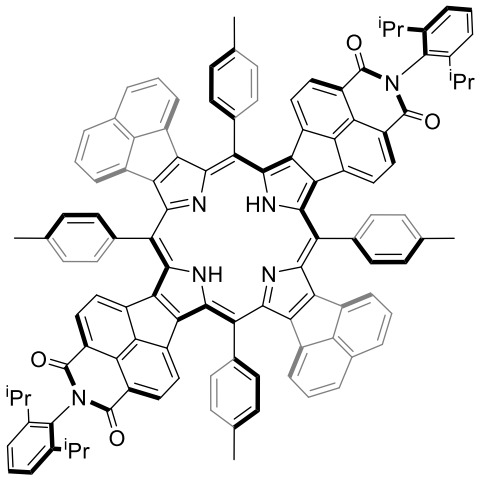

tD$_2$A$_2$ porphyrin (2b-H_2**).** A solution of compound **2a**-H_2 (50 mg, 0.034 mmol) in concentrated hydrochloric acid (5 mL) was refluxed for overnight. The resulting dark-blue precipitate was filtered, washed with water and diethyl ether, and dried in vacuum to give product **2c**-H_2 in quantitative yield as a dark blue powder (45 mg). The solid was suspended in glacial acetic acid (0.2 mL), and 2,6-diisopropylaniline (128 µL, 0.64 mmol) was added. The mixture was purged with nitrogen for 5 min and refluxed in a pressure tube at 160 °C in an oil bath for 24 h. The reaction mixture was cooled down, diluted with water, and extracted with dichloromethane. The organic phase was washed with aqueous sodium bicarbonate and brine, dried over anhydrous sodium sulfate, and concentrated in vacuum. The crude compound was purified by alumina (grade V) column chromatography on with dichloromethane to give the product as dark blue solid (40 mg, 72%-over two steps). **^{1}H NMR** (500 MHz, chloroform-*d*, 300 K): δ 8.62 (8H, m), 8.03 (4H, d, ^3J = 7.6 Hz), 7.81 (4H, d, ^3J = 6.7 Hz), 7.75 (4H, d, ^3J = 6.9 Hz), 7.71 (4H, d, ^3J = 7.9 Hz), 7.44 (2H, t, ^3J = 7.8 Hz), 7.32 (2H, dd, ^3J = 8.0 Hz), 7.23 (6H, m), 5.82 (4H, d, ^3J = 7.2 Hz), 5.68 (4H, d, ^3J = 7.6 Hz), 2.88 (14H, m), 2.62 (2H, sept, ^3J = 6.9 Hz), 1.23 (12H, d, ^3J = 6.7 Hz), 1.00 (12H, d, ^3J = 6.9 Hz), -0.34 (2H, b). **^{13}C NMR** (151 MHz, chloroform-*d* , 300 K): δ 164.0, 148.64, 145.8, 142.0, 140.9, 139.3, 137.5, 136.7, 135.0, 134.2, 132.8, 132.1, 131.0, 130.9,129.5, 129.3, 128.5, 128.0, 127.4, 125.8, 125.4, 125.0, 123.9, 123.8, 123.5, 121.9, 121.3, 29.1, 28.9, 24.1, 23.8, 22.3, 21.9 . **HRMS** (ESI–TOF): *m*/*z*: $[M + H]^+$ Calcd for $C_{116}H_{85}N_6O_4$: 1626.6660; Found 1626.6772.

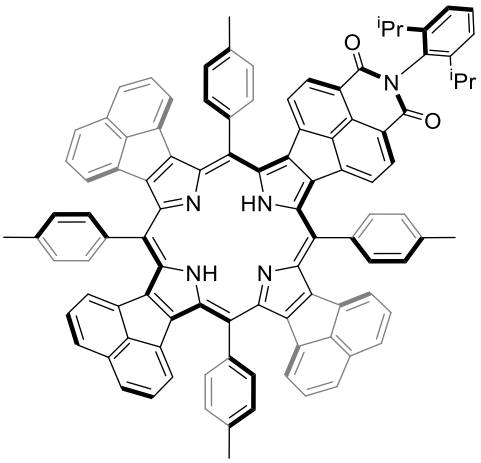

D_3A porphyrin (3b-H_2**).** Porphyrin **3b**-H_2 was synthesized by following the same procedure as given for **tD_2A_2** porphyrin **2b**-H_2 by using porphyrin **3a**-H_2 (50 mg, 0.038 mmol), hydrochloric acid (5 mL), 2,6- diisopropylaniline (144 µL, 0.75 mmol) and glacial acetic acid (0.2 mL). The crude compound was purified by column chromatography on alumina (grade V) with dichloromethane to give the product as violet solid (35 mg, 66% over two steps). **^{1}H NMR** (500 MHz, chloroform-*d* , 300 K): δ 8.64 (8H, m), 8.02 (2H, m), 7.80 (2H, d, ^3J = 7.9 Hz), 7.75 (6H, m), 7.67 (6H, b), 7.44 (1H, t, ^3J = 7.9 Hz), 7.32 (1H, d, ^3J = 8.0 Hz), 7.25(1H, b, overlap with $CDCl_3$), 7.20 (6H, m), 5.77 (6H, b), 5.66 (2H, b), 2.86 (13H, m), 2.63 (1H, sept, ^3J = 6.7 Hz), 1.24 (6H, d, ^3J = 6.7 Hz), 1.00 (6H, d, ^3J = 6.9 Hz) -0.34 (2H, b). **^{13}C NMR** (151 MHz, chloroform-*d* , 300 K): δ 164.0, 151.8, 148.3, 145.9, 141.4, 140.6, 140.1, 139.5, 139.4, 137.1, 135.0, 133.1, 132.1, 131.1, 130.8, 129.5,129.3, 127.3, 125.4, 123.9, 123.7, 121.7, 121.1, 120.7, 29.7, 29.1, 28.8, 24.1, 23.8, 21.8, 21.7. **HRMS** (ESI–TOF): *m*/*z*: $[M + H]^+$ Calcd for $C_{102}H_{70}N_5O_2$: 1397.5557; Found 1397.5596.

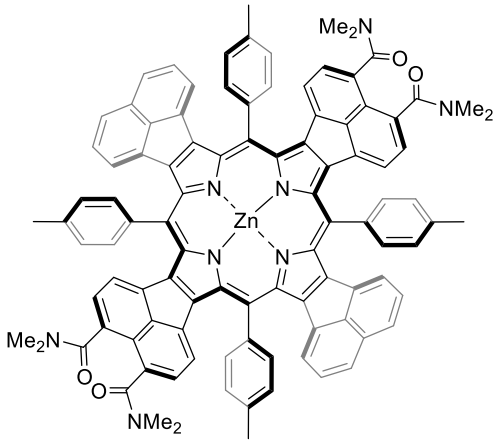

tD_2A_2 porphyrin (2a-Zn**).** An excess of $Zn(OAc)_2.2H_20$ (20 mg, 0.068 mmol) was added to a solution of porphyrin **2a**-H_2 (20 mg, 0.013 mmol) in $CHCl_3$/MeOH (18 ml, 5:1) and the mixture was allowed to stir for 2 h at room temperature. Upon completion of the reaction, the solution was washed with water and dried over anhydrous sodium sulfate. The solvent was evaporated and the crude compound was purified on a column of alumina (grade V) (DCM/MeOH, 100:0.1) to give the product as a violet amorphous solid (18 mg, 87%). **^{1}H NMR** (500 MHz, chloroform/pyridine-*d* , 300 K): δ 8.56 (8 H, m), 7.66 (8H, m), 7.55 (4H, d, ^3J = 8.0 Hz), 7.11 (4H, t, ^3J = 7.5 Hz), 6.95 (4H, m), 5.61 (4H, t, ^3J = 7.7 Hz), 5.50 (4H, m), 3.04 (6H, s), 3.01 (6H, s), 2.99 (6H, s), 2.79 (6H, s), 2.77 (6H, s), 2.67 (6H, s). **^{13}C NMR**

(151 MHz, chloroform/pyridine-*d* , 300 K): δ 171.0, 146.5, 146.1, 145.9, 145.7, 141.1, 141.0, 139.4, 139.3, 137.5, 137.4, 137.3, 135.7, 134.9, 134.0, 133.7, 133.4, 130.8, 130.6, 130.1, 129.6, 129.4, 128.8, 127.0, 126.7, 126.6, 126.4, 124.9, 124.4, 123.4, 121.7, 39.5, 39.3, 34.8, 34.6, 29.6, 21.6. **HRMS** (ESI–TOF): *m*/*z*: $[2M+2H]^+$ Calcd for $C_{200}H_{146}N_{16}O_8Zn_2$: 1516.0058; Found 1516.0491.

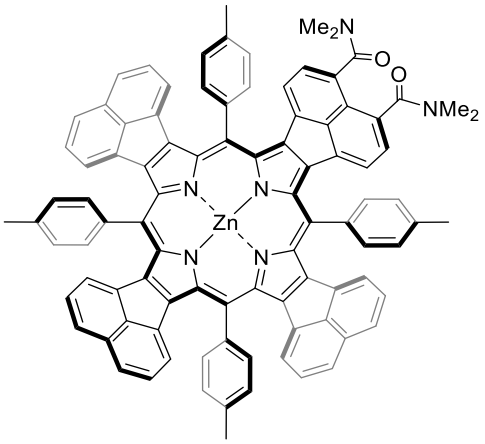

D_3A porphyrin (3a-Zn**).** Porphyrin **3a**-Zn was synthesized by following the same procedure as given for **tD_2A_2** porphyrin **2a**-Zn by using porphyrin **3a**-H_2 (20 mg, 0.015 mmol), zinc acetate (16.6 mg, 0.075 mmol), and $CHCl_3$/MeOH (18 ml, 5:1). The crude compound was purified by column chromatography on alumina (grade V) with dichloromethane to give the product as violet solid (17 mg, 82%). **^{1}H NMR** (500 MHz, chloroform-*d* , 300 K): δ 8.59 (8 H, m), 7.75 (6H, m), 7.61 (8H, m), 7.13 (8H, m), 5.68 (8H, m), 2.85 (24H, m). **^{13}C NMR** (151 MHz, chloroform-*d* , 300 K): δ 145.8, 145.2, 144.9, 140.9, 140.6, 139.5, 137.2, 136.8, 134.9, 134.8, 134.7, 134.0, 133.8, 130.8, 130.7, 129.5, 129.4, 129.1, 127.1, 127.0, 126.8, 125.1, 121.99, 121.6, 39.1, 34.6, 31.93, 29.7, 29.3, 22.6, 21.6, 21.5. **HRMS** (MALDI-TOF): *m*/*z*: $[M+MeOH+H]^+$ Calcd for $C_{95}H_{67}N_6O_3Zn$: 1405.4538; Found 1405.4335.

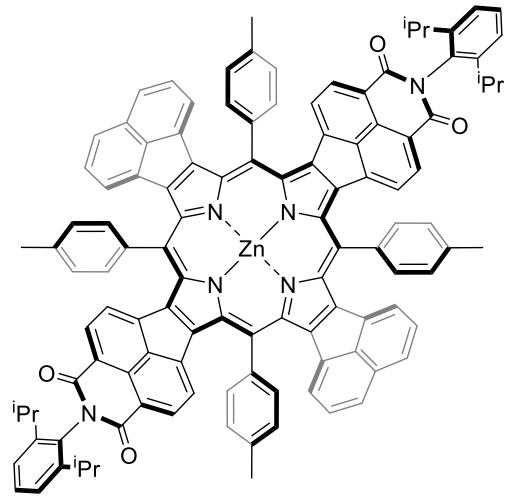

tD_2A_2 porphyrin (2b-Zn**).** Porphyrin **2b**-Zn was synthesized by following the same procedure as given for **tD_2A_2** porphyrin **2a**-Zn by using porphyrin **2b**-H_2 (20 mg, 0.012 mmol), zinc acetate (13.3 mg, 0.061 mmol), and $CHCl_3$/MeOH (18 ml, 5:1). The crude compound was purified by column chromatography on alumina (grade V) with CH_2Cl_2/n-hexane (80:20) to give the product as dark blue solid (19 mg, 92%). **^{1}H NMR** (500 MHz, chloroform-*d* , 300 K): δ 8.57 (8H, m), 8.05 (4H, d, ^3J = 7.6 Hz),

7.82 (4H, d, ^3J = 7.4 Hz), 7.75 (4H, d, ^3J = 7.5 Hz), 7.66 (4H, d, ^3J = 7.9 Hz), 7.45 (2H, t, ^3J = 8.0 Hz), 7.33 (2H, dd, ^3J = 8.2 Hz), 7.26 (2H, m), 7.17 (4H, t, ^3J = 7.7 Hz), 5.67 (4H, d, ^3J = 7.3 Hz), 5.61 (4H, d, ^3J = 7.7 Hz), 2.89 (14H, m), 2.62 (2H, sept, ^3J = 6.9 Hz), 1.25 (12H, d, ^3J = 6.7 Hz), 1.00 (12H, d, ^3J = 6.8 Hz). **^{13}C NMR** (151 MHz, chloroform-*d* , 300 K): δ 164.0, 147.6, 147.0, 146.4, 145.8, 145.4, 140.5, 140.2, 139.7, 137.0, 136.8, 134.7, 134.4, 134.3, 132.1, 131.0, 130.9, 129.4, 129.3, 129.1, 129.0, 128.3, 128.2, 127.5, 127.1, 125.4, 125.4, 125.3, 125.3, 123.9, 123.8, 123.7, 123.1, 122.4, 121.7, 29.1, 28.9, 24.1, 23.8, 21.8. **HRMS** (ESI–TOF): *m*/*z*: $[M]^+$ Calcd for $C_{116}H_{82}N_6O_4Zn$: 1688.5743; Found 1688.5785.

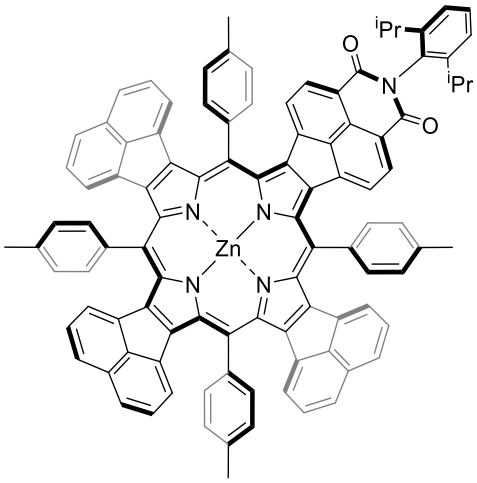

D_3A porphyrin (3b-Zn**).** Porphyrin **3b**-Zn was synthesized by following the same procedure as given for **tD_2A_2** porphyrin **2a**-Zn by using porphyrin **3b**-H_2 (20 mg, 0.014 mmol), zinc acetate (15.5 mg, 0.070 mmol), and $CHCl_3$/MeOH (18 ml, 5:1). The crude compound was purified by column chromatography on alumina (grade V) with CH_2Cl_2/n-hexane (70:30) to give the product as dark blue solid (19 mg, 91%). **^{1}H NMR** (500 MHz, chloroform-*d* , 300 K): δ 8.59 (8H, m), 8.03 (2H, d, ^3J = 7.6 Hz), 7.81 (2H, d, ^3J = 6.9 Hz), 7.75 (6H, m), 7.64 (6H, d, ^3J = 7.9 Hz), 7.44 (1H, t, ^3J = 7.9 Hz), 7.33 (1H, d, ^3J = 6.9 Hz), 7.26 (1H, overlap with $CDCl_3$), 7.17 (6H, m), 5.68 (6H, m), 5.60 (2H, ^3J = 7.6 Hz), 2.88 (6H, s), 2.87 (1H, m, merged with singlets), 2.88 (6H, s), 2.63 (^{1}H, sept, ^3J = 6.8 Hz), 1.25 (6H, d, ^3J = 6.7 Hz), 1.00 (6H, d, ^3J = 6.9 Hz). **^{13}C NMR** (151 MHz, chloroform-*d* , 300 K): δ 170.9, 164.1, 147.5, 147.3, 147.0, 146.5, 146.3, 146.2, 145.9, 145.2, 144.4, 140.5, 140.4, 140.3, 140.0, 139.8, 138.3, 137.1, 136.8, 134.7, 134.5, 133.6, 133.5, 132..1, 131.1, 131.0, 130.9, 129.4, 129.31, 127.4, 127.3, 127.2, 127.1, 125.50, 125.3, 125.1, 123.9, 123.7, 122.2, 121.8, 121.5, 118.0, 29.7, 29.1, 28.9, 24.1, 23.8, 21.8, 21.6. **HRMS** (MALDI–TOF): *m*/*z*: $[M]^+$ Calcd for $C_{102}H_{67}N_5O_2Zn$: 1459.4640; Found 1659.4700.

Additional Figures

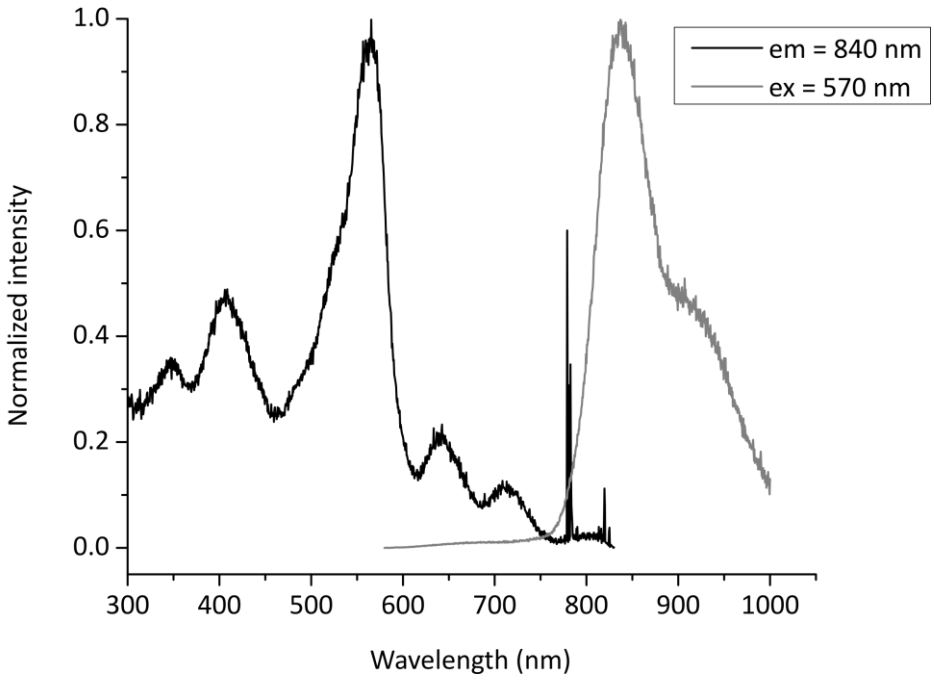

Figure S1. Normalized emission (excited at 570 nm) and excitation spectra (monitored at 840 nm) of compound **2a**-H_2 recorded in DCM .

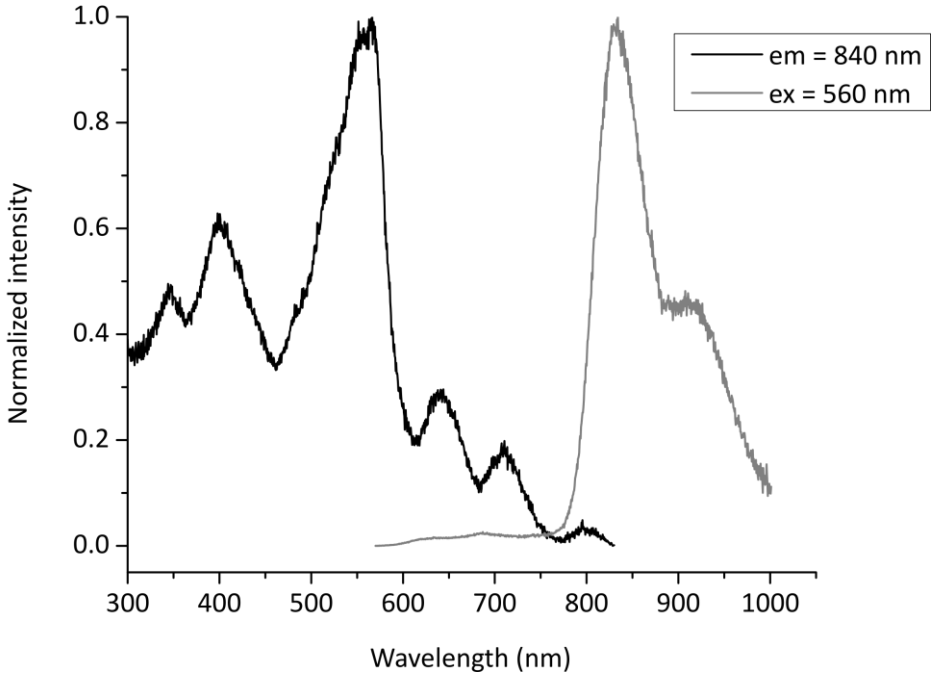

Figure S2. Normalized emission (excited at 560 nm) and excitation spectra (monitored at 840 nm) of compound **3a**-H_2 recorded in DCM .

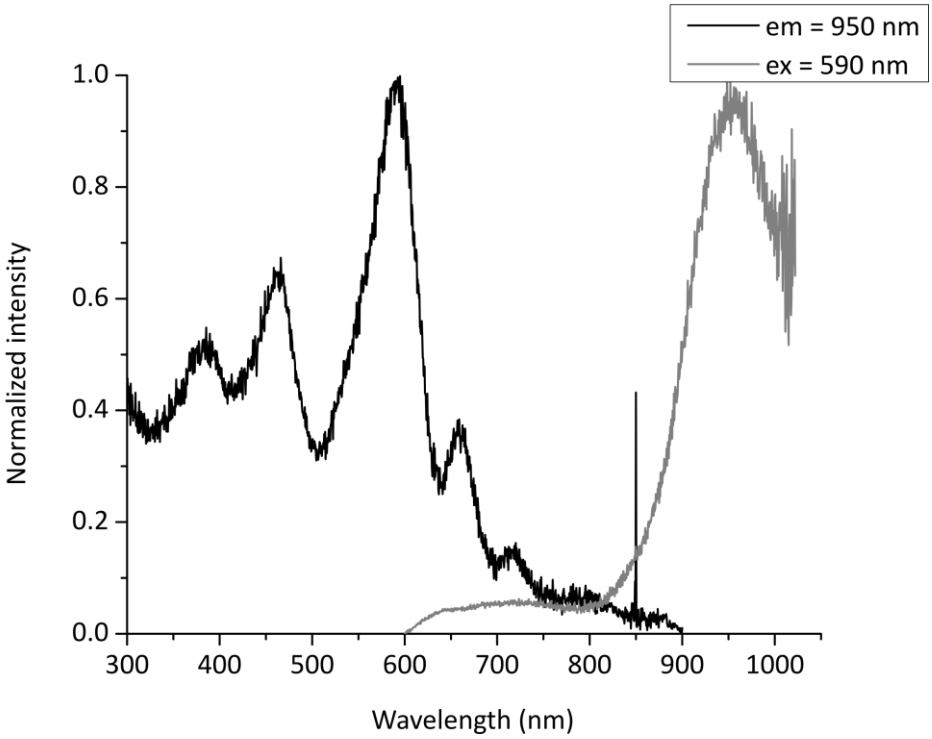

Figure S3. Normalized emission (excited at 590 nm) and excitation spectra (monitored at 950 nm) of compound **2b**-H_2 recorded in DCM .

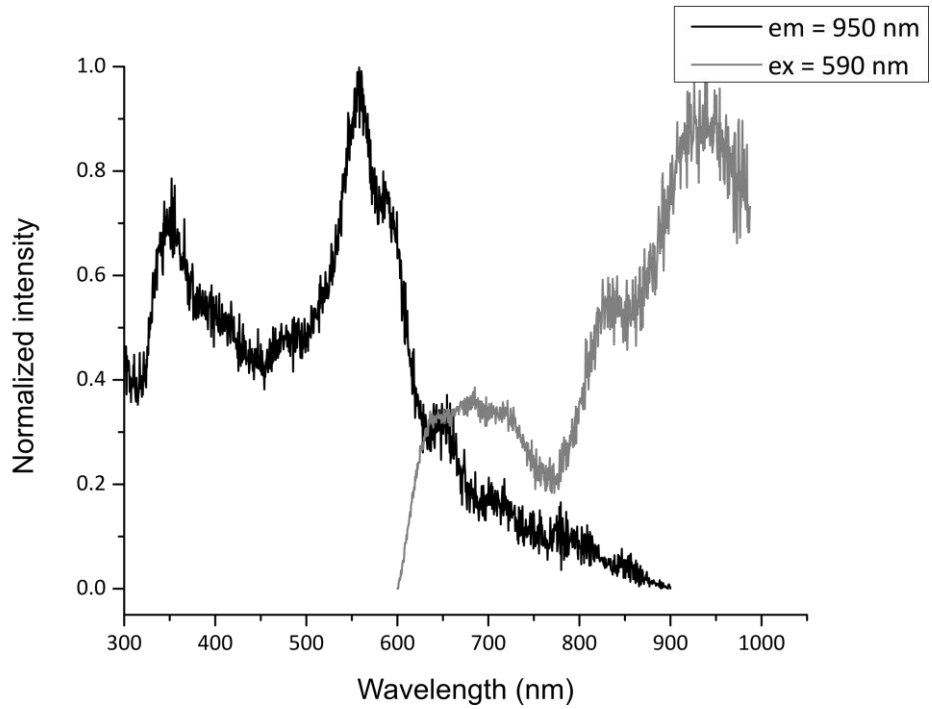

Figure S4. Normalized emission (excited at 590 nm) and excitation spectra (monitored at 950 nm) of compound **3b**-H_2 recorded in DCM .

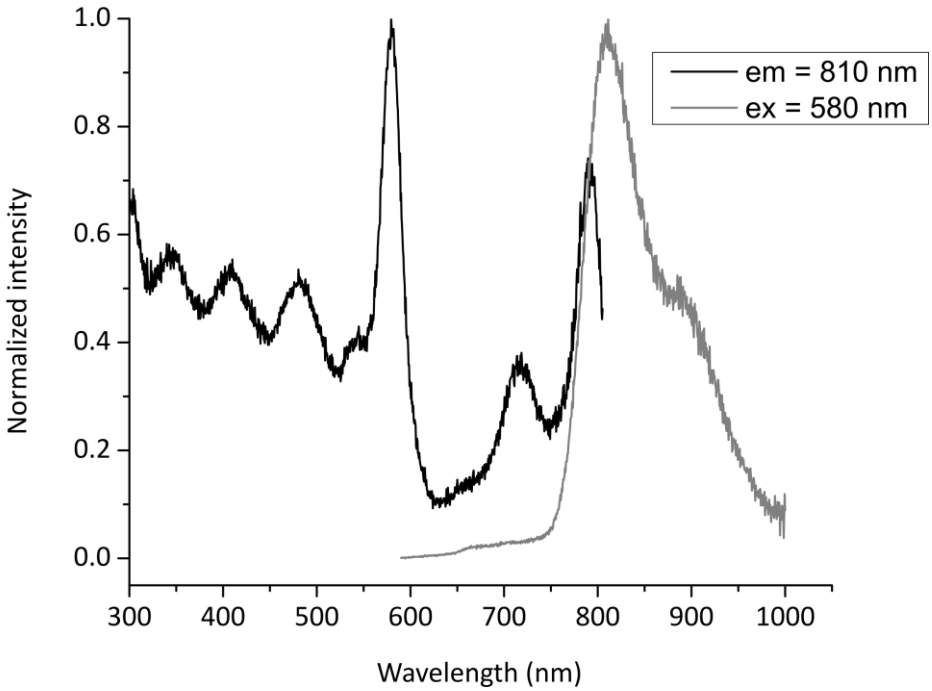

Figure S5. Normalized emission (excited at 580 nm) and excitation spectra (monitored at 810 nm) of compound **2a**-Zn recorded in toluene + 1% pyridine.

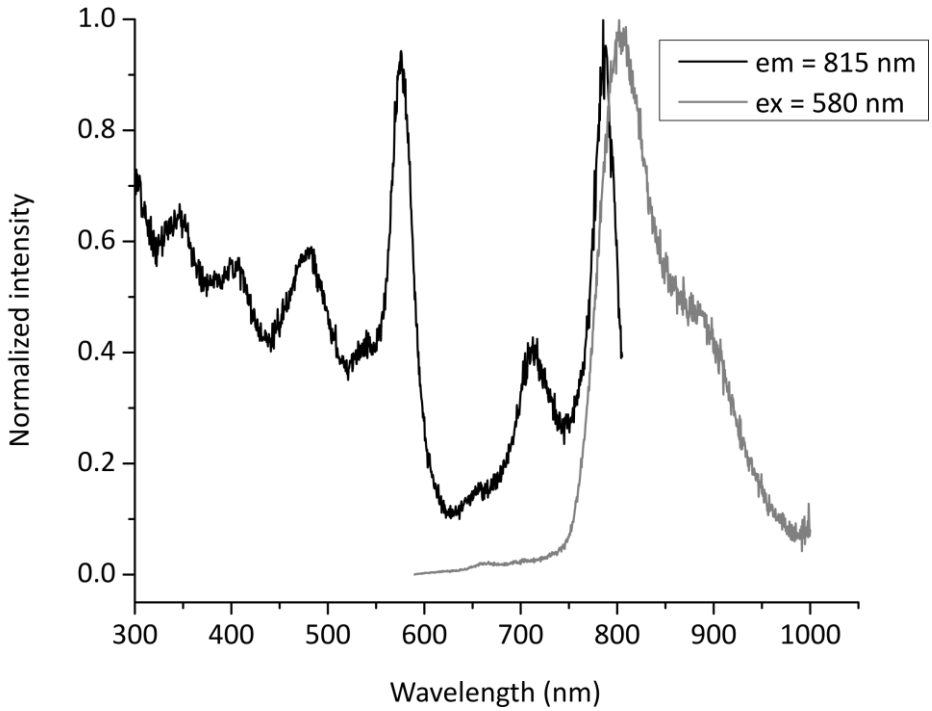

Figure S6. Normalized emission (excited at 580 nm) and excitation spectra (monitored at 815 nm) of compound **3a**-Zn recorded in toluene + 1% pyridine..

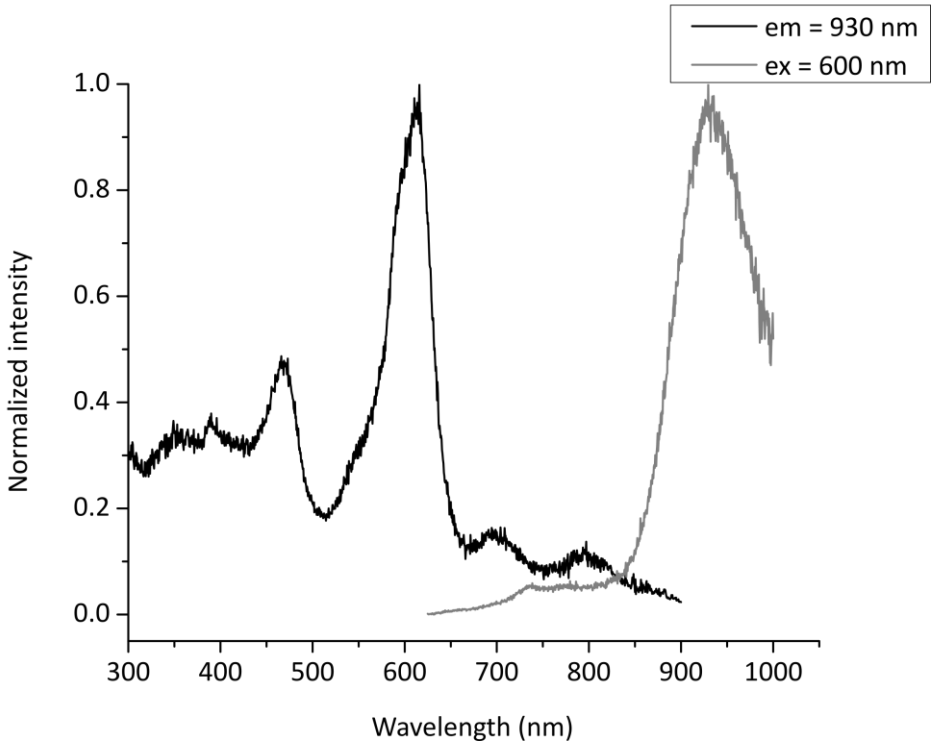

Figure S7. Normalized emission (excited at 600 nm) and excitation spectra (monitored at 930 nm) of compound **2b**-Zn recorded in toluene + 1% pyridine .

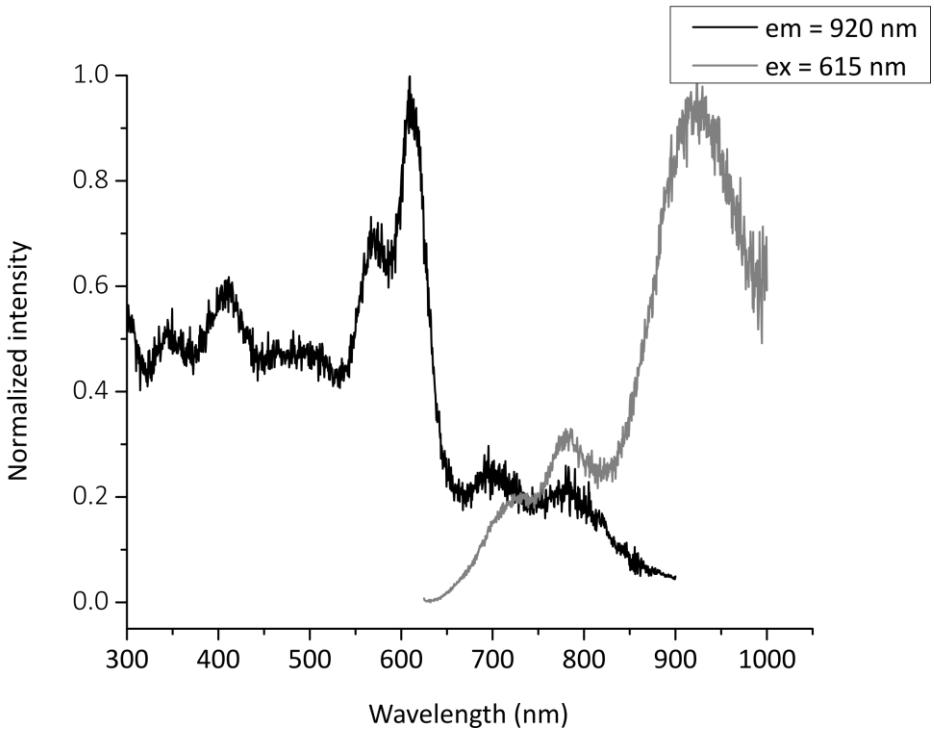

Figure S8. Normalized emission (excited at 615 nm) and excitation spectra (monitored at 920 nm) of compound **3b**-Zn recorded in toluene + 1% pyridine.

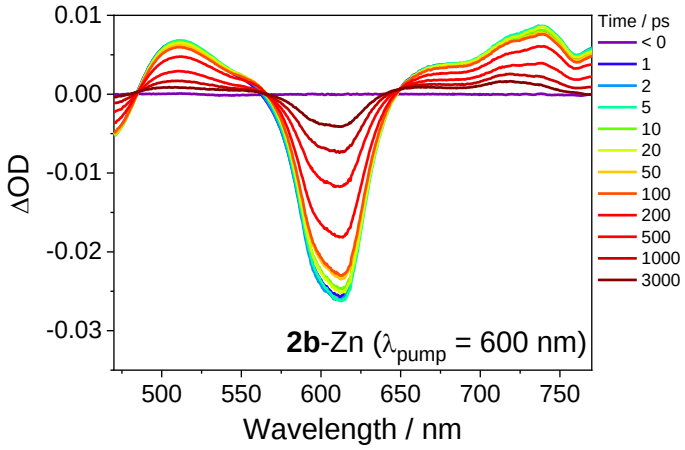

Figure S9. Femtosecond TA spectra of **2b**-Zn in toluene + 1% pyridine obtained following photoexcitation at 600 nm.

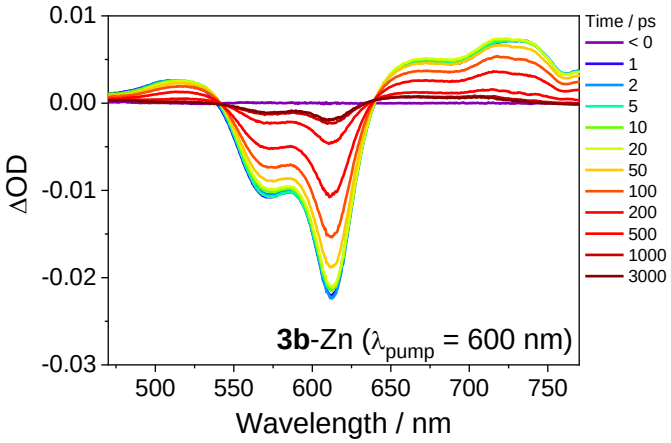

Figure S10. Femtosecond TA spectra of **3b**-Zn in toluene + 1% pyridine obtained following photoexcitation at 600 nm.

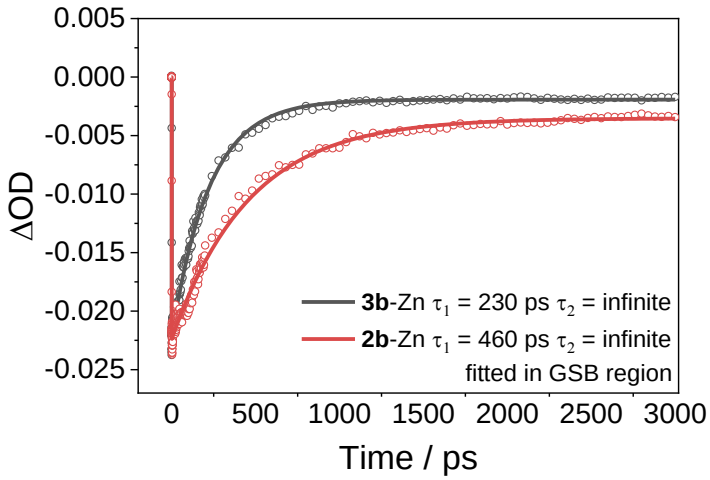

Figure S11. Decay profiles of **2b**-Zn and **3b**-Zn in toluene + 1% pyridine obtained following photoexcitation at 600 nm.

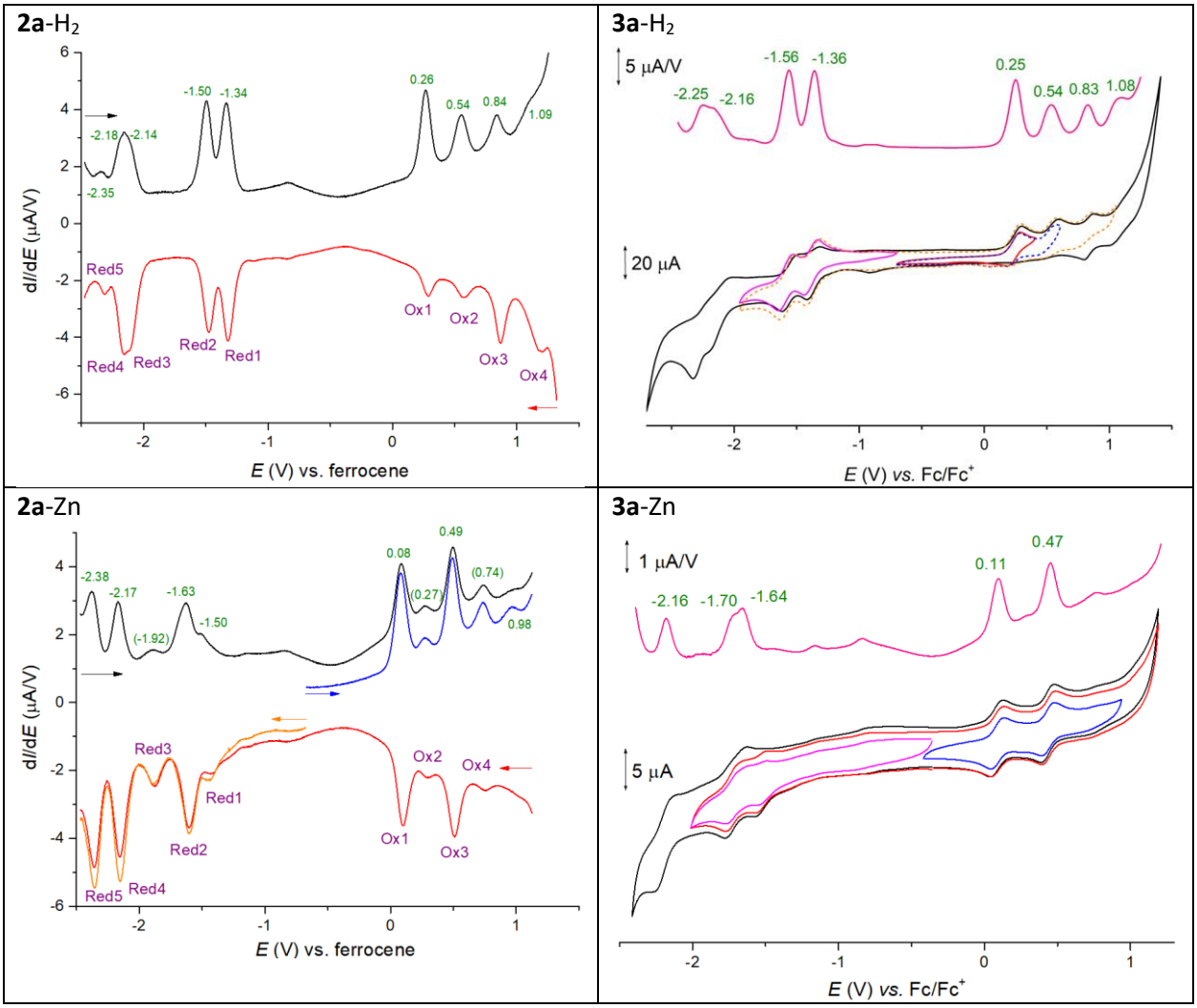

Figure S12. Differential pulse voltammograms and selected cyclic voltammograms for the NDA-fused porphyrins **2a**-M and **3a**-M (M = 2H, Zn). Conditions: dichloromethane, $TBAPF_6$, glassy carbon electrode.

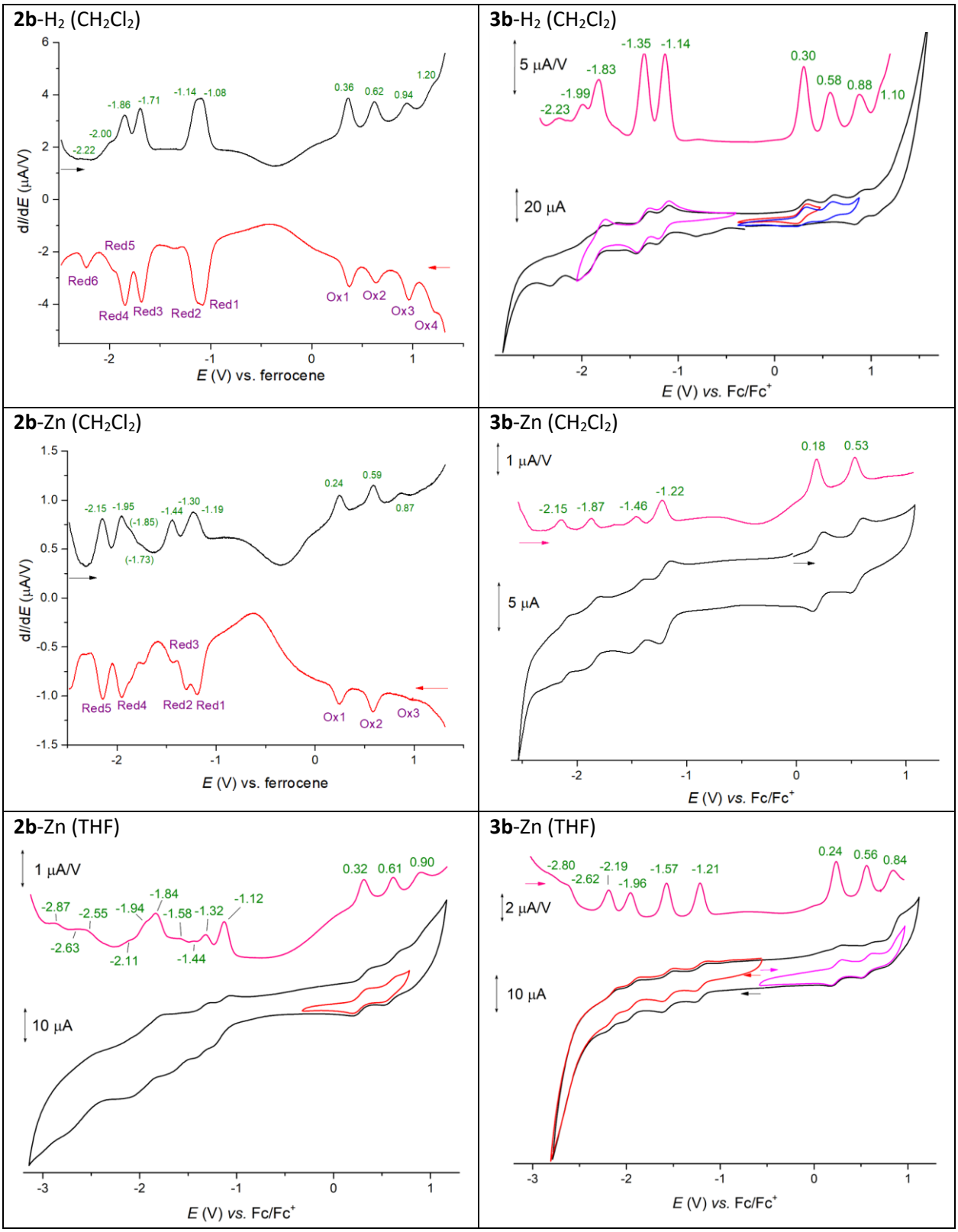

Figure S13. Differential pulse voltammograms and selected cyclic voltammograms for the NMI-fused porphyrins **2b**-M and **3b**-M (M = 2H, Zn). Conditions: solvent (as indicated), $TBAPF_6$, glassy carbon electrode.

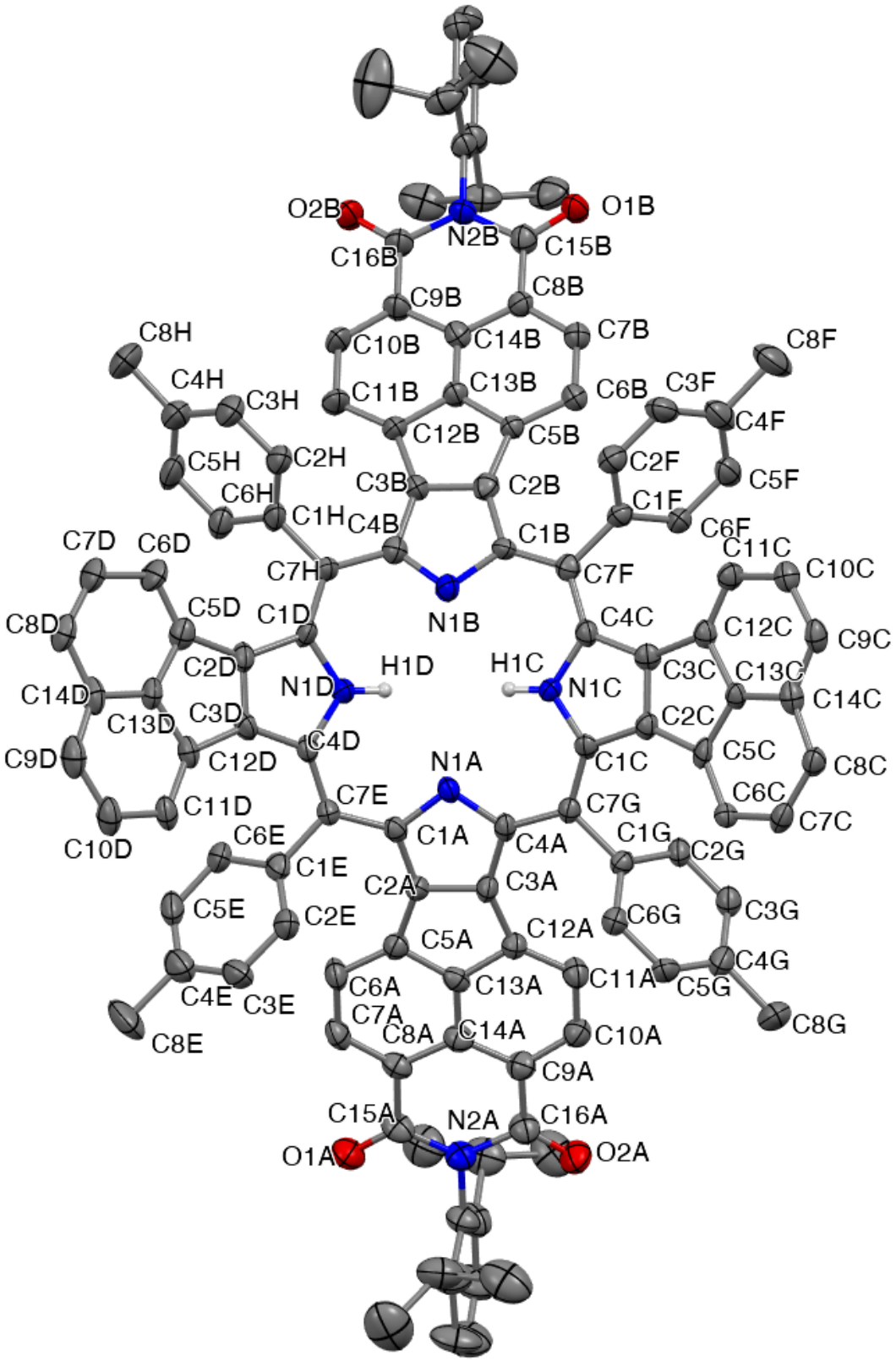

Figure S14. Molecular structure of compound **2b**-H_2. The thermal ellipsoids represents 50% probability. (Hydrogen atoms and solvent molecule are omitted for clarity) .

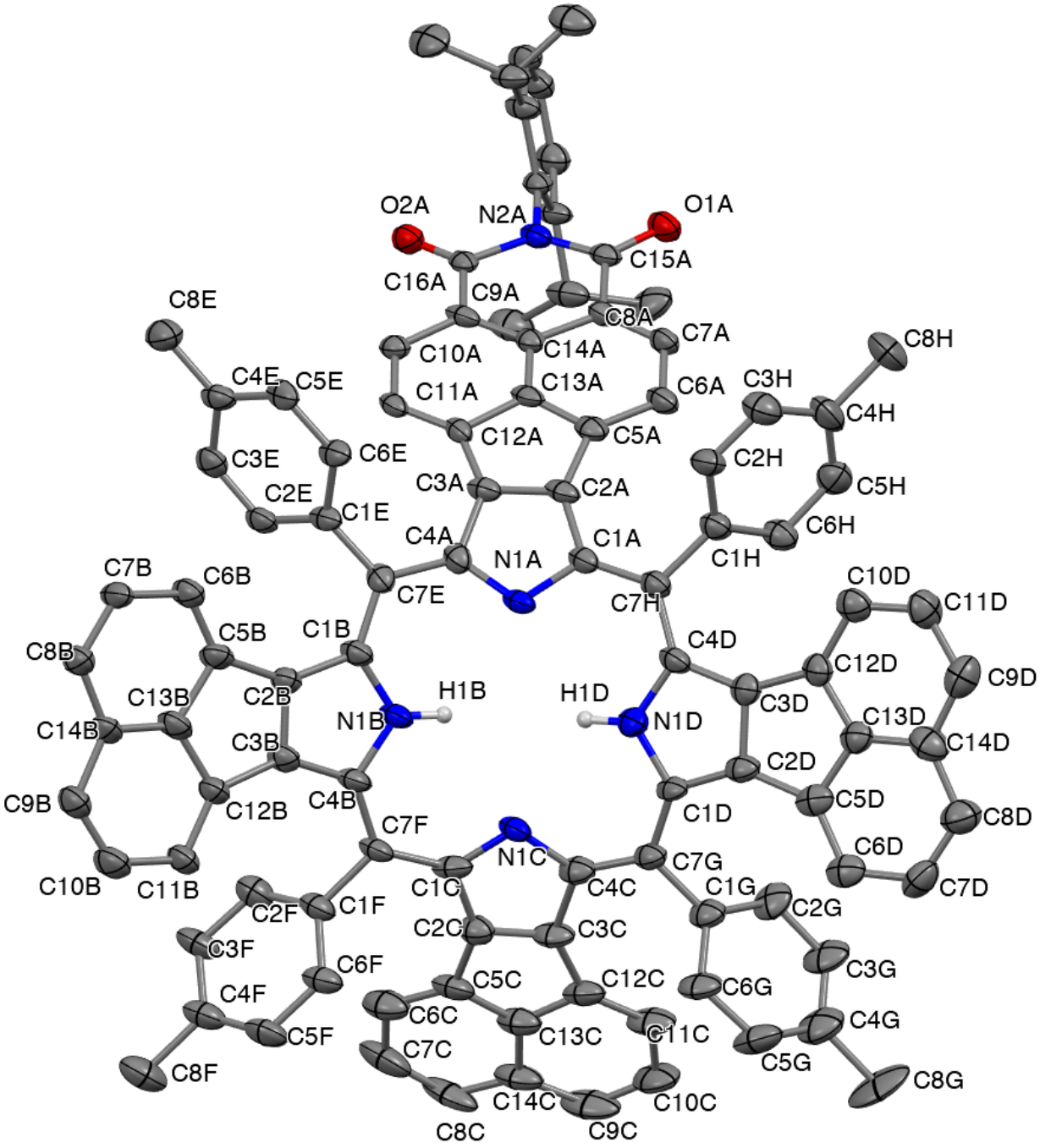

Figure S15. Molecular structure of compound **3b**-H_2. The thermal ellipsoids represents 25% probability. (Hydrogen atoms or solvent molecule are omitted for clarity) .

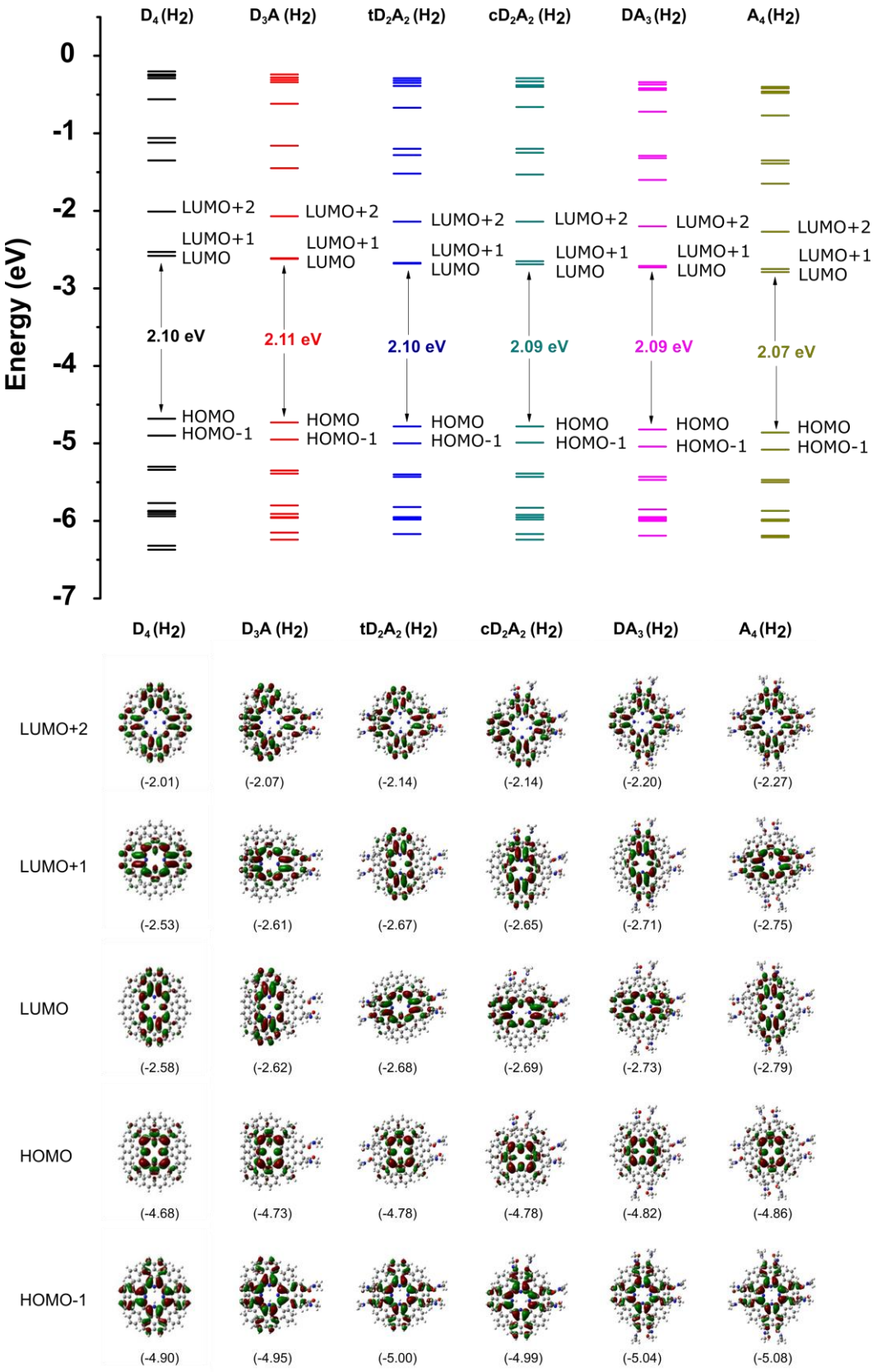

Figure S16. Kohn–Sham frontier orbital energy level diagram for various free base porphyrins containing peripheral naphthalene and napthalenediamide units. The MO diagrams indicate LUMO+2, LUMO+1, LUMO, HOMO and HOMO-1. All calculations were performed at the level of B3LYP/6-31g(d,p) theory.

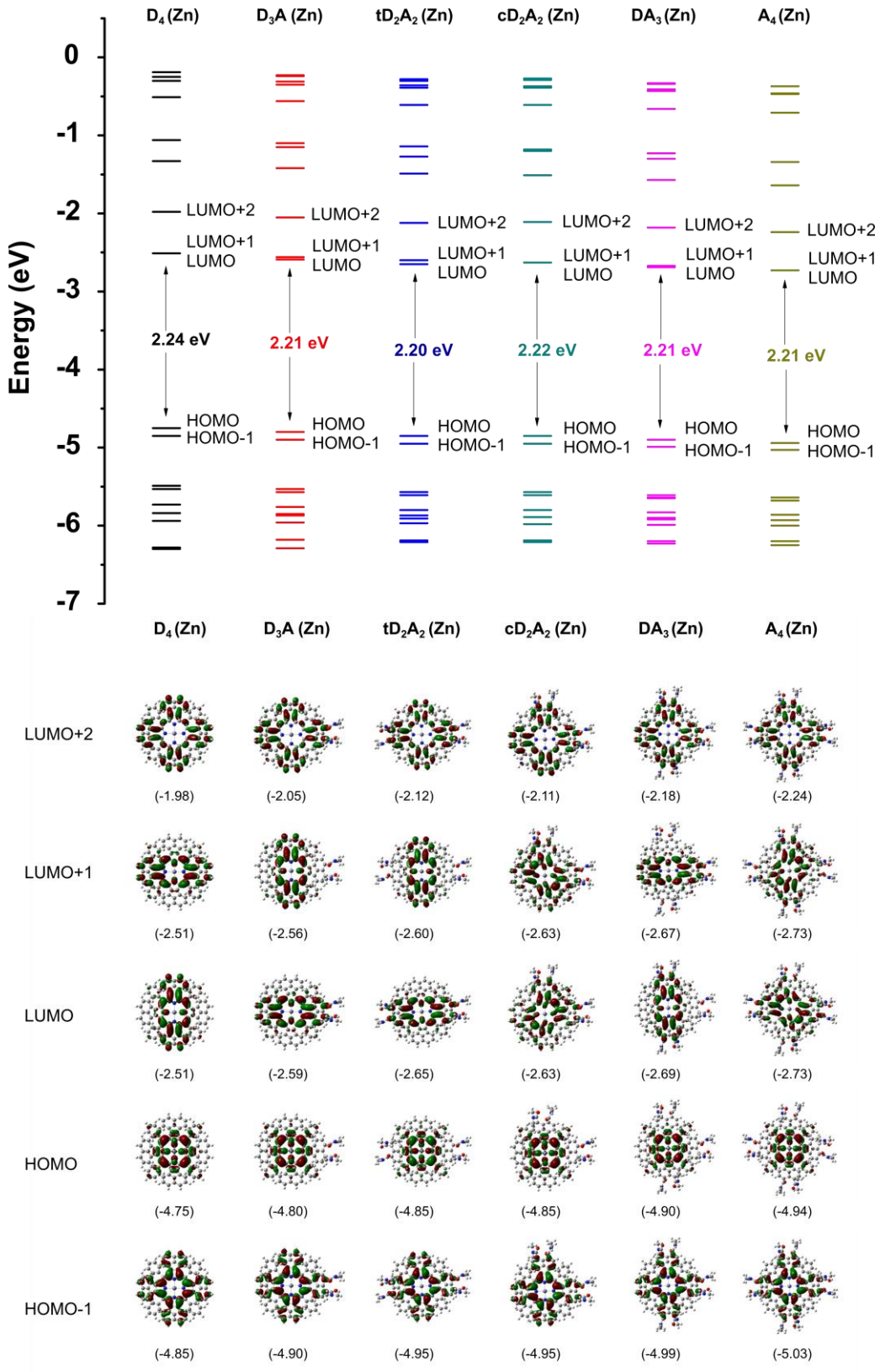

Figure S17. Kohn–Sham frontier orbital energy level diagram for various zinc porphyrins containing peripheral naphthalene and napthalenediamide units. The MO diagrams indicate LUMO+2, LUMO+1, LUMO, HOMO and HOMO-1. All calculations were performed at the level of B3LYP/6-31g(d,p) theory.

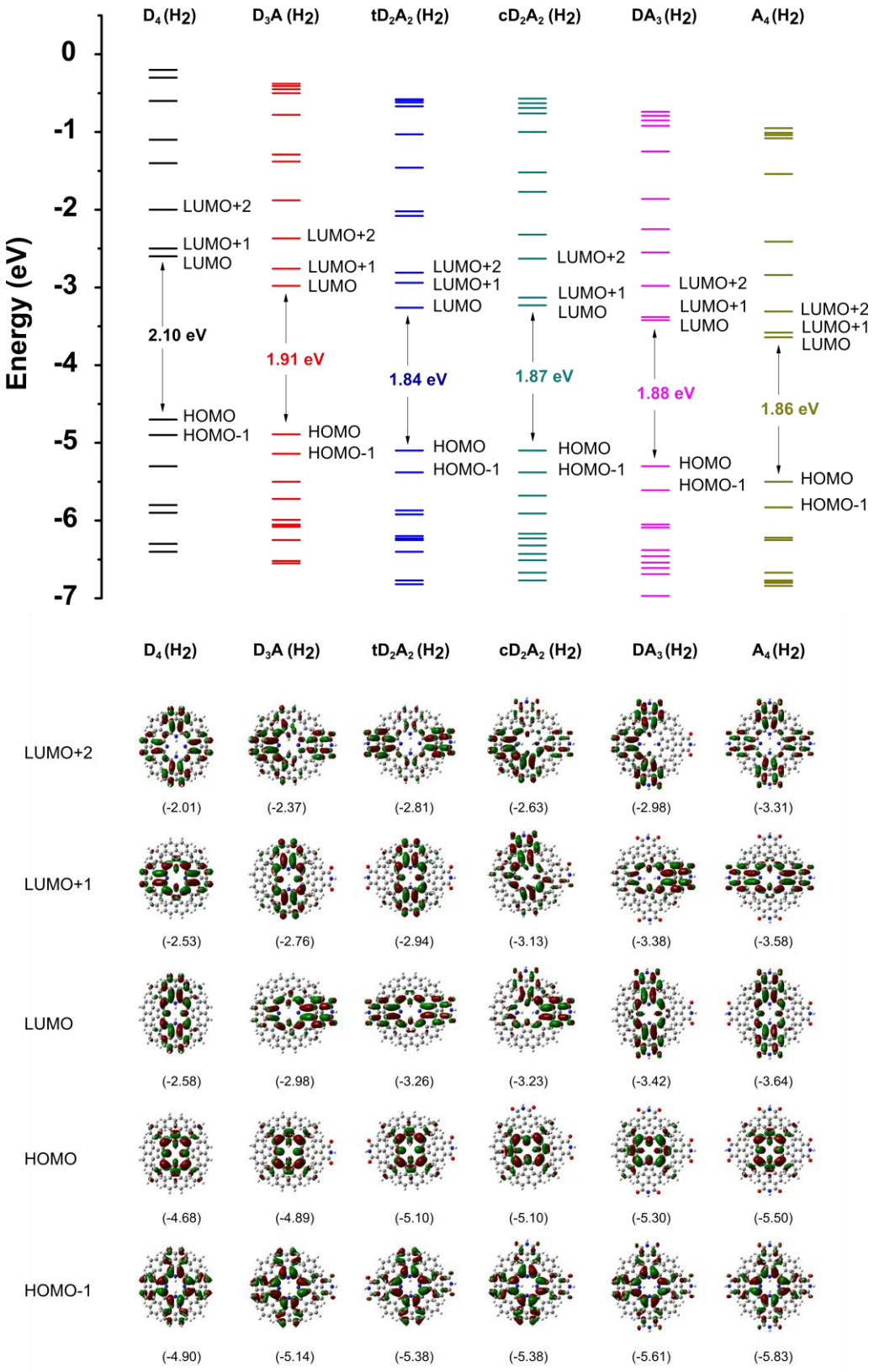

Figure S18. Kohn–Sham frontier orbital energy level diagram for various free base porphyrins containing peripheral naphthalene and napthalenemonoimide units. The MO diagrams indicate LUMO+2, LUMO+1, LUMO, HOMO and HOMO-1. All calculations were performed at the level of B3LYP/6-31g(d,p) theory.

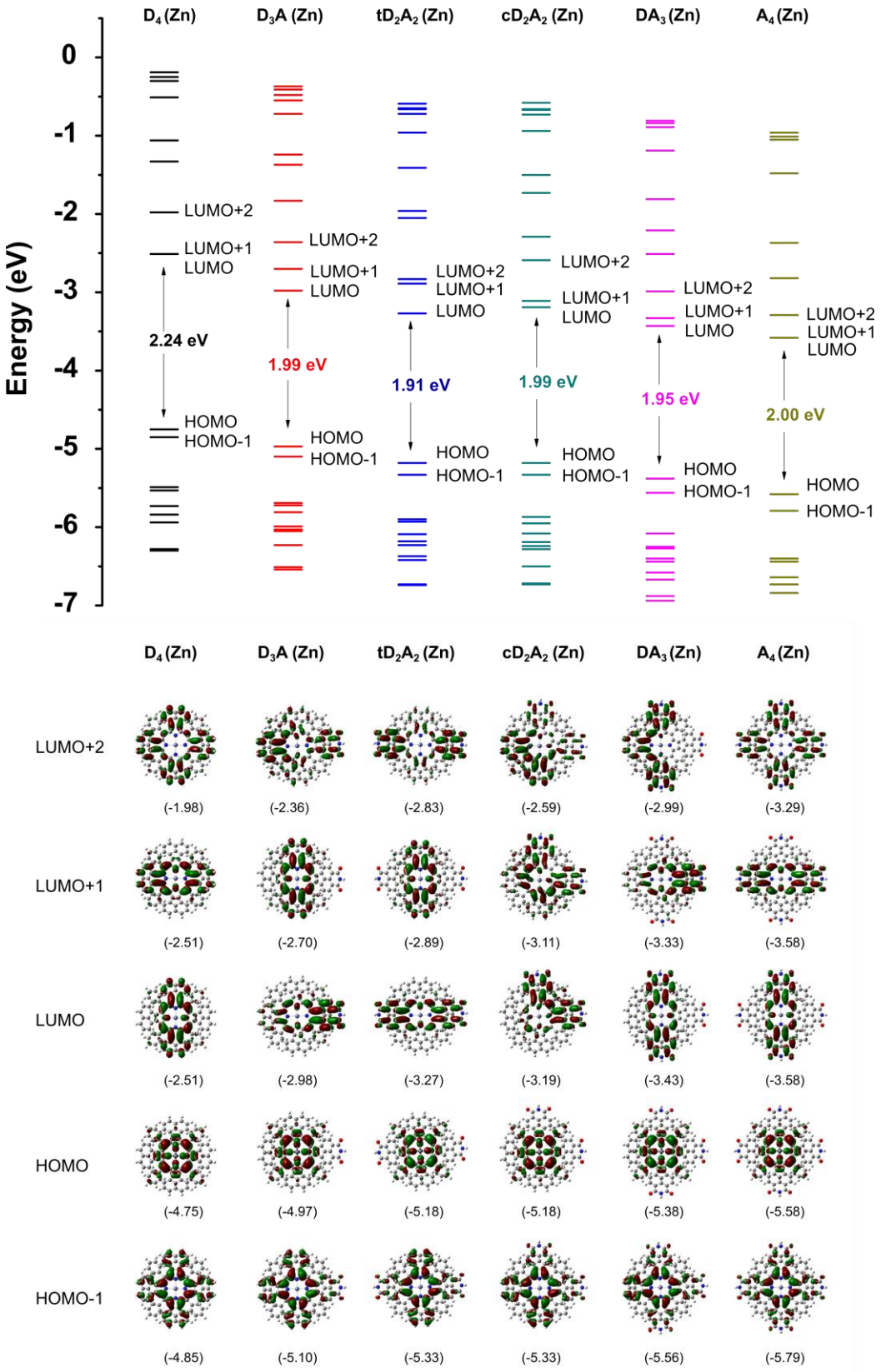

Figure S19. Kohn–Sham frontier orbital energy level diagram for various zinc porphyrins containing peripheral naphthalene and napthalenemonoimide units. The MO diagrams indicate LUMO+2, LUMO+1, LUMO, HOMO and HOMO-1. All calculations were performed at the level of B3LYP/6-31g(d,p) theory.

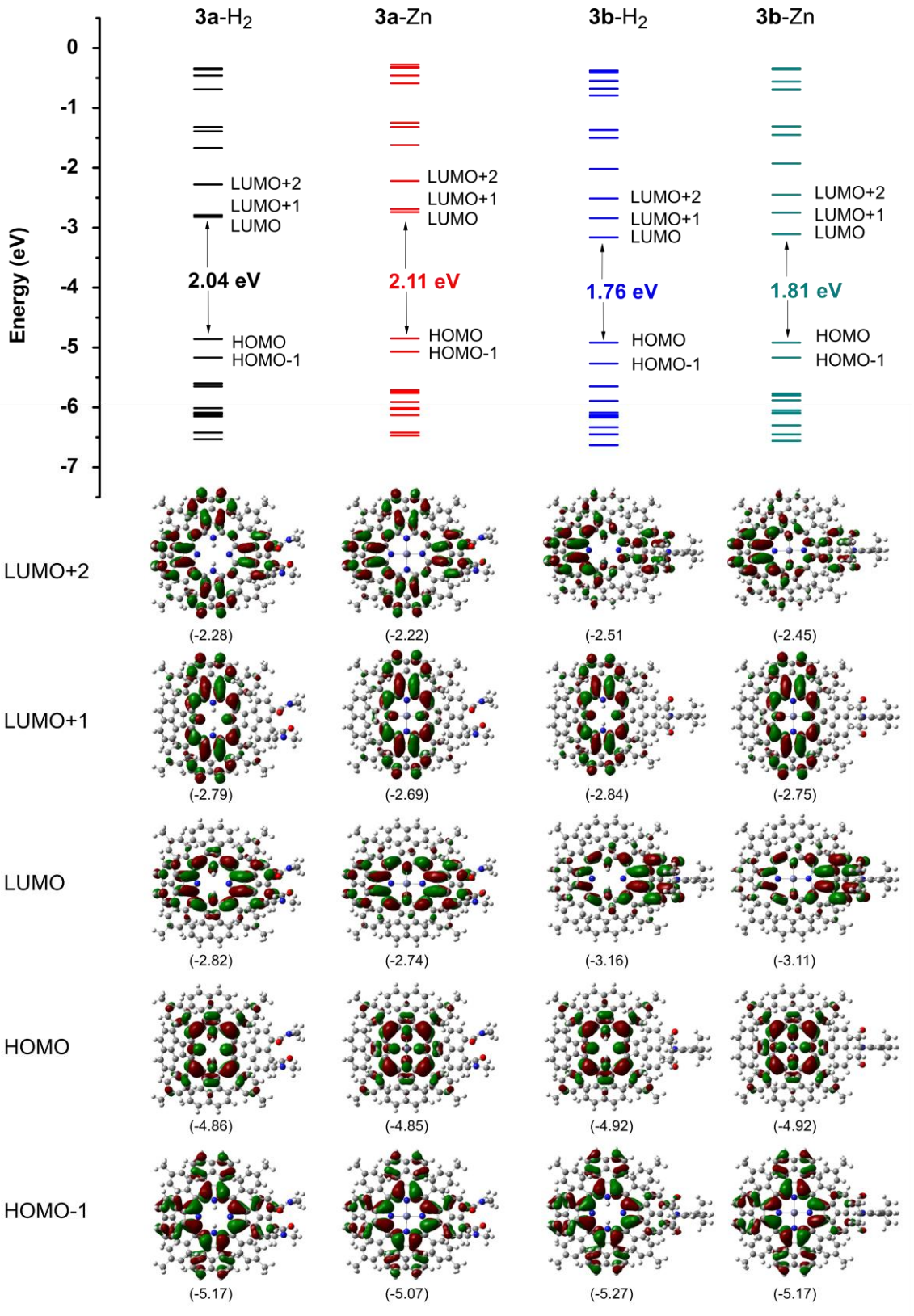

Figure S20. Kohn–Sham frontier orbital energy level diagram for **3a**-H_2, **3a**-Zn**, 3b**-H_2 and **3b**-Zn. The MO diagrams indicate LUMO+2, LUMO+1, LUMO, HOMO and HOMO-1. All calculations were performed at the level of B3LYP/6-31g(d,p) theory with PCM (dichloromethane).

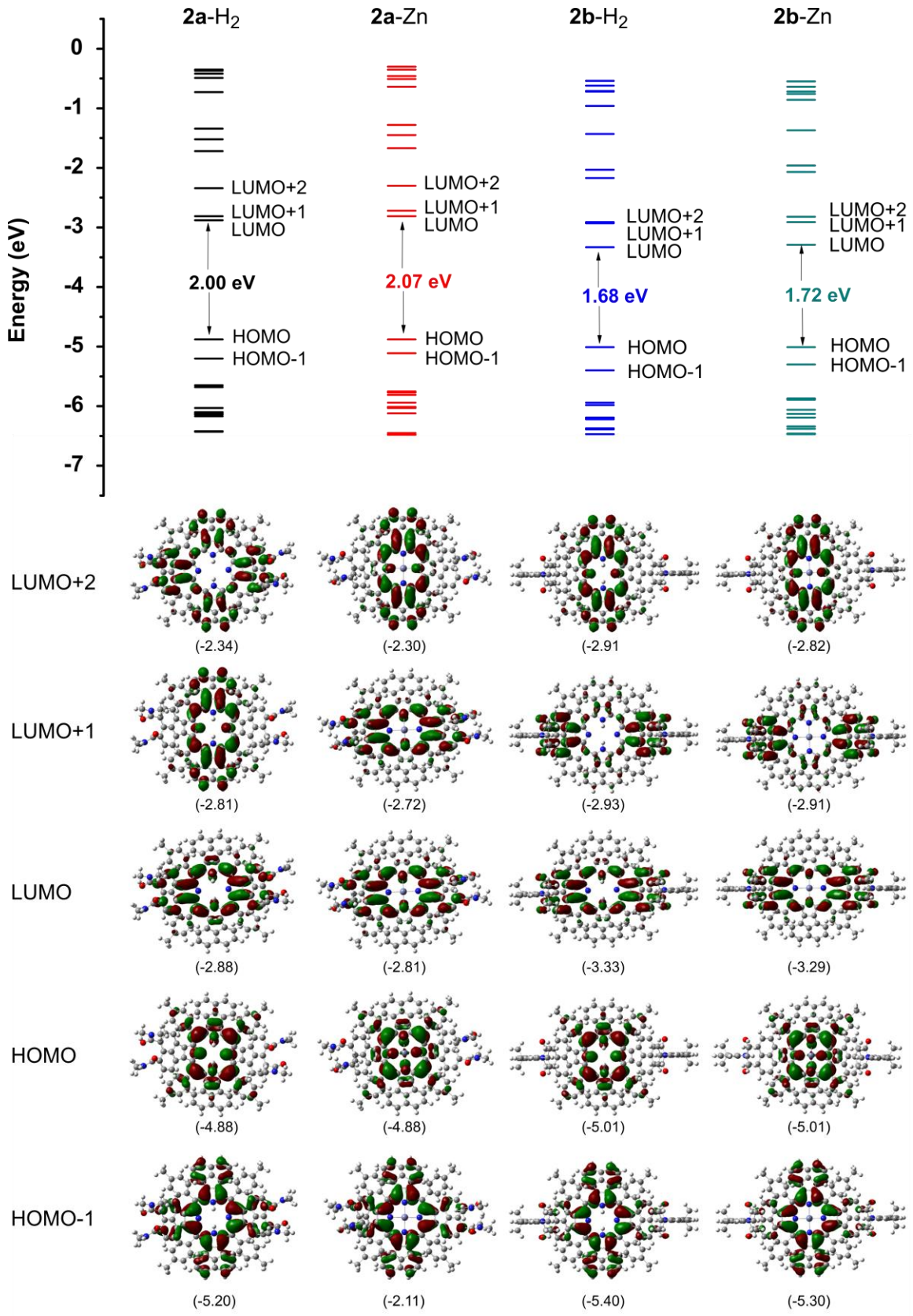

Figure S21. Kohn–Sham frontier orbital energy level diagram for **2a**-H_2, **2a**-Zn**, 2b**-H_2 and **2b**-Zn. The MO diagrams indicate LUMO+2, LUMO+1, LUMO, HOMO and HOMO-1. All calculations were performed at the level of B3LYP/6-31g(d,p) theory with PCM (dichloromethane).

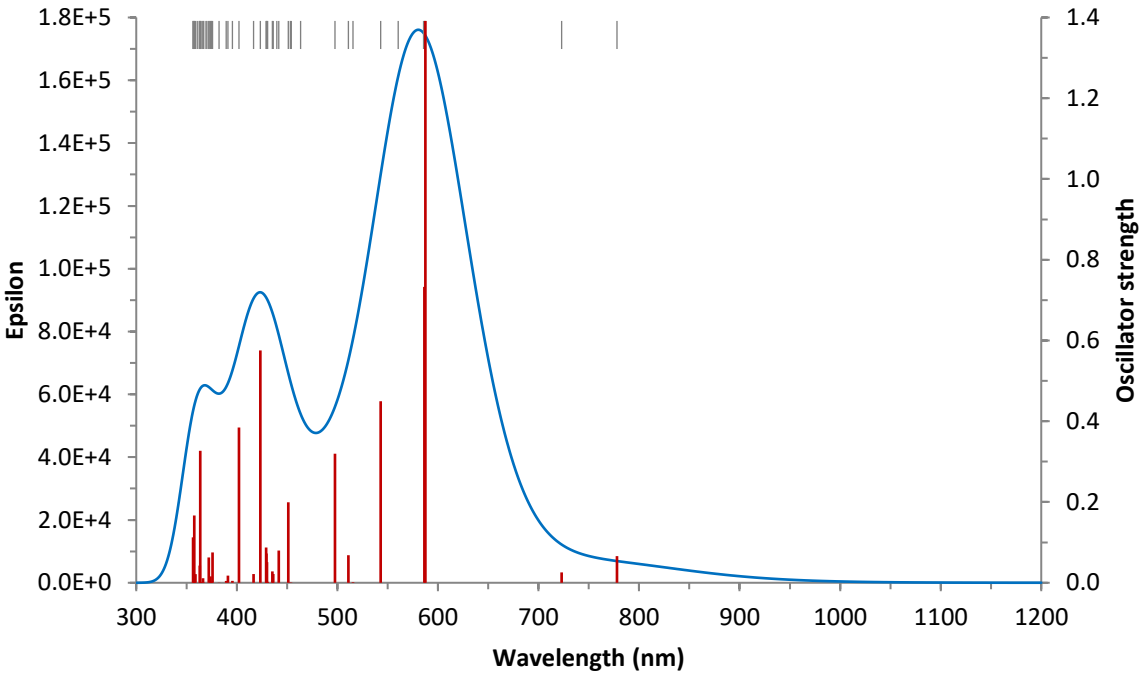

Figure S22. Electronic absorption spectrum of **2a**-H_2 simulated using time-dependent density functional theory (B3LYP/6-31G(d)/PCM(CH_2Cl_2), 50 transitions, linewidth factor 3000 cm^{-1}).

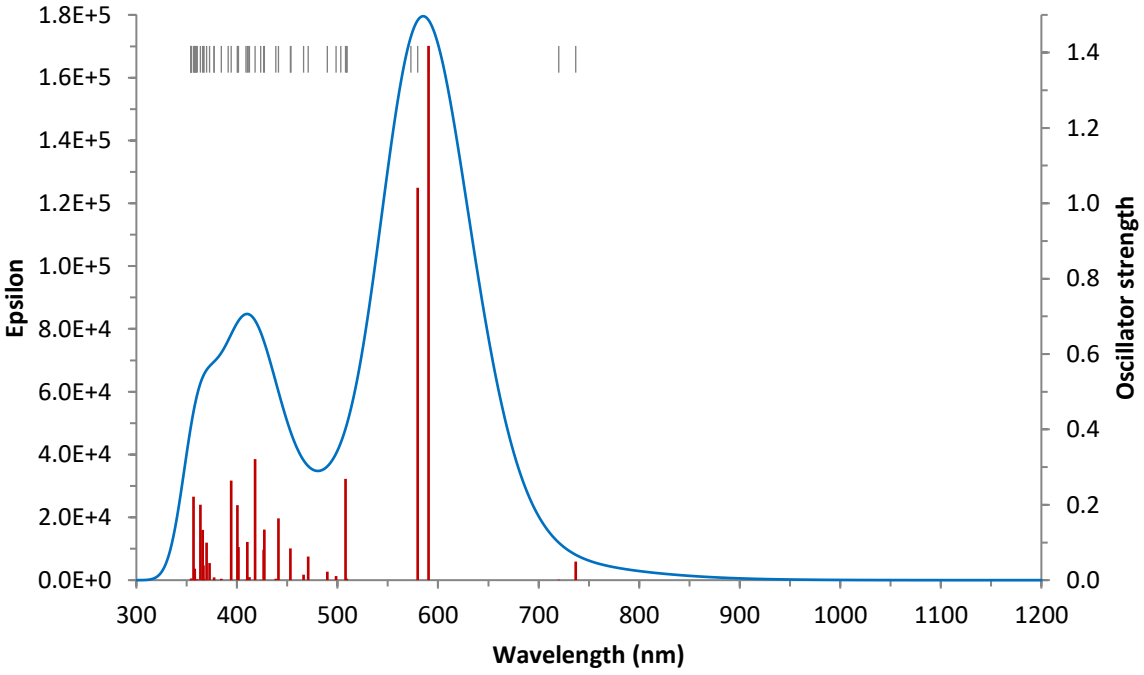

Figure S23. Electronic absorption spectrum of **2a**-Zn simulated using time-dependent density functional theory (B3LYP/6-31G(d)/PCM(CH_2Cl_2), 50 transitions, linewidth factor 3000 cm^{-1}).

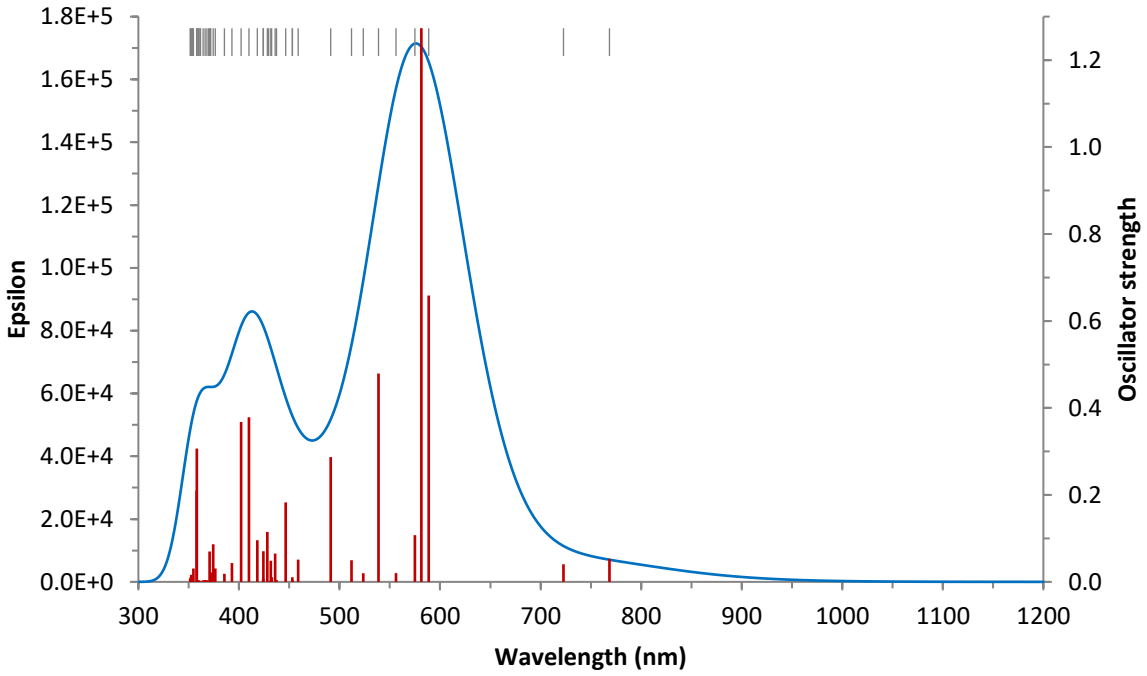

Figure S24. Electronic absorption spectrum of **3a**-H_2 simulated using time-dependent density functional theory (B3LYP/6-31G(d)/PCM(CH_2Cl_2), 50 transitions, linewidth factor 3000 cm^{-1}).

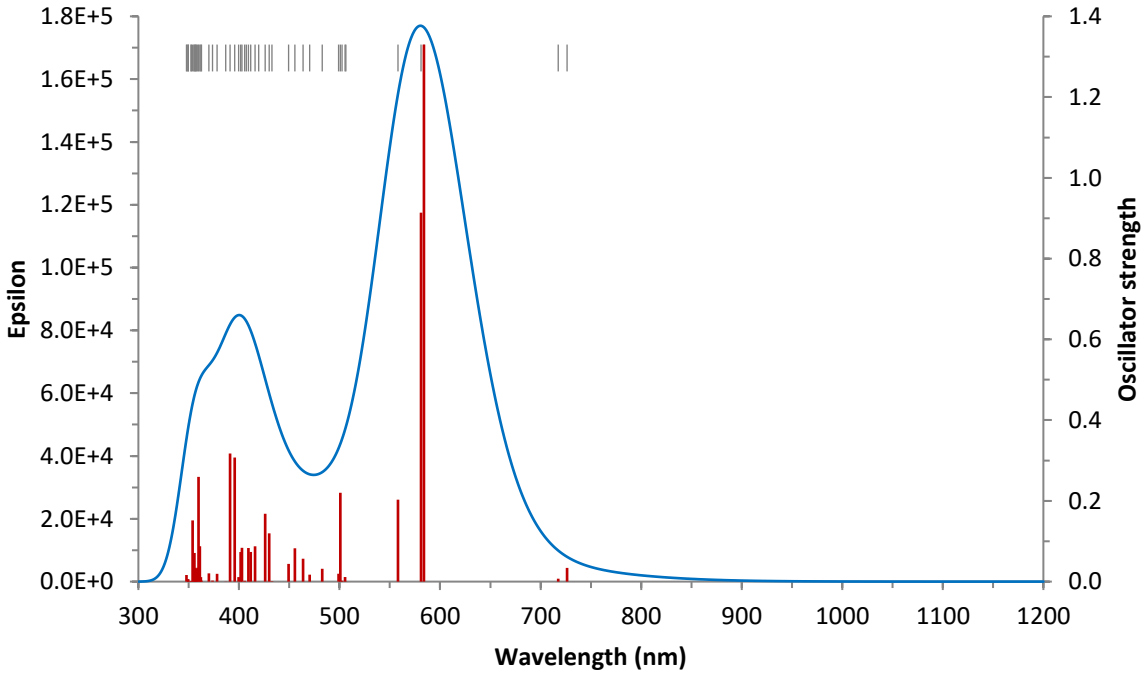

Figure S25. Electronic absorption spectrum of **3a**-Zn simulated using time-dependent density functional theory (B3LYP/6-31G(d)/PCM(CH_2Cl_2), 50 transitions, linewidth factor 3000 cm^{-1}).

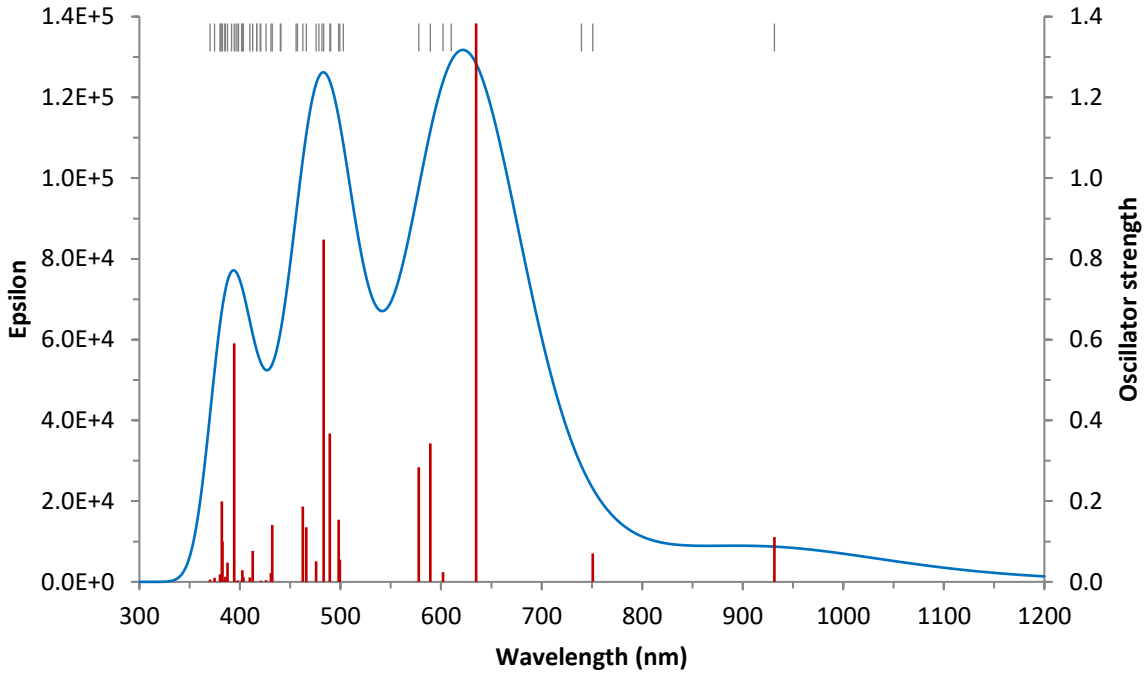

Figure S26. Electronic absorption spectrum of **2b**-H_2 simulated using time-dependent density functional theory (B3LYP/6-31G(d)/PCM(CH_2Cl_2), 50 transitions, linewidth factor 3000 cm^{-1}).

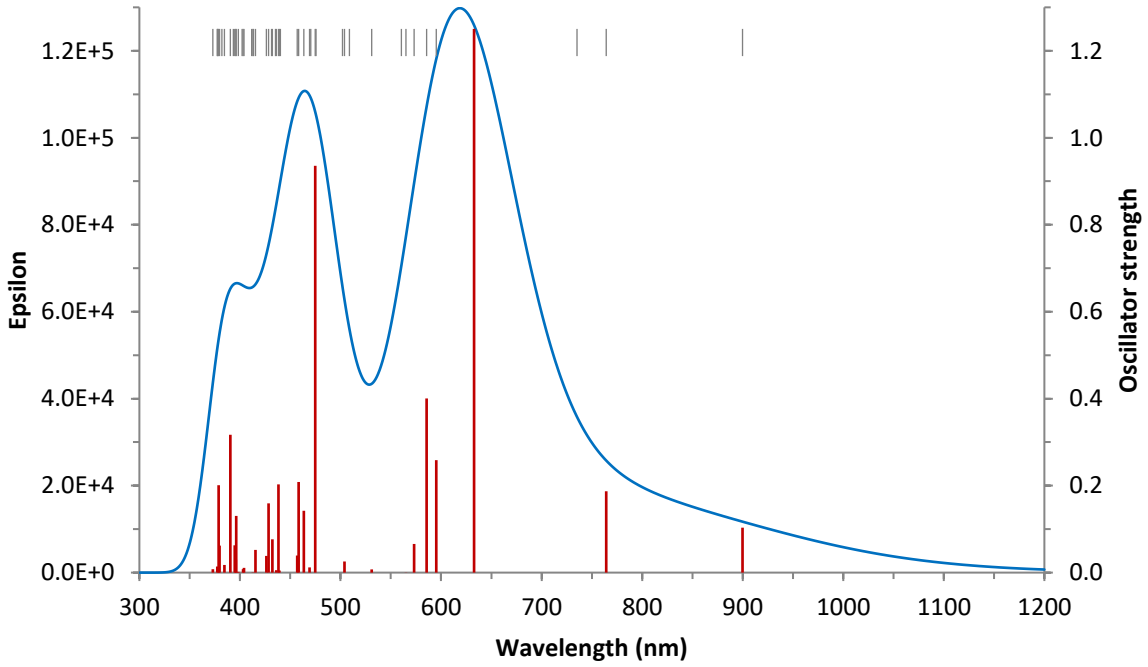

Figure S27. Electronic absorption spectrum of **2b**-Zn simulated using time-dependent density functional theory (B3LYP/6-31G(d)/PCM(CH_2Cl_2), 50 transitions, linewidth factor 3000 cm^{-1}).

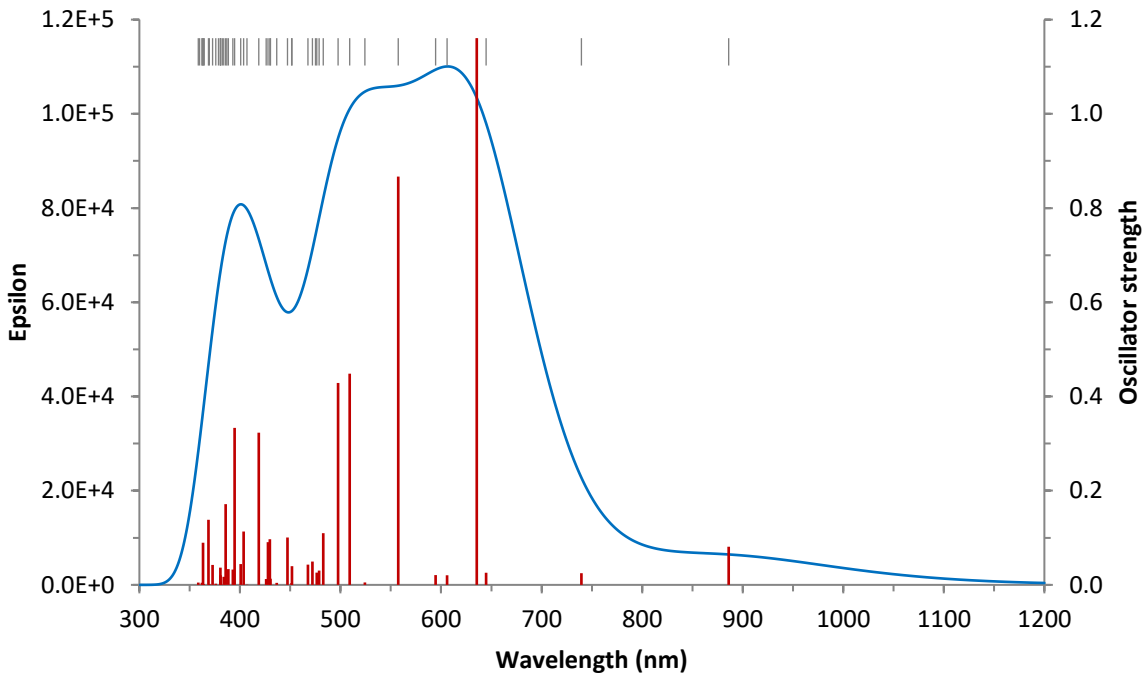

Figure S28. Electronic absorption spectrum of **3b**-H_2 simulated using time-dependent density functional theory (B3LYP/6-31G(d)/PCM(CH_2Cl_2), 50 transitions, linewidth factor 3000 cm^{-1}).

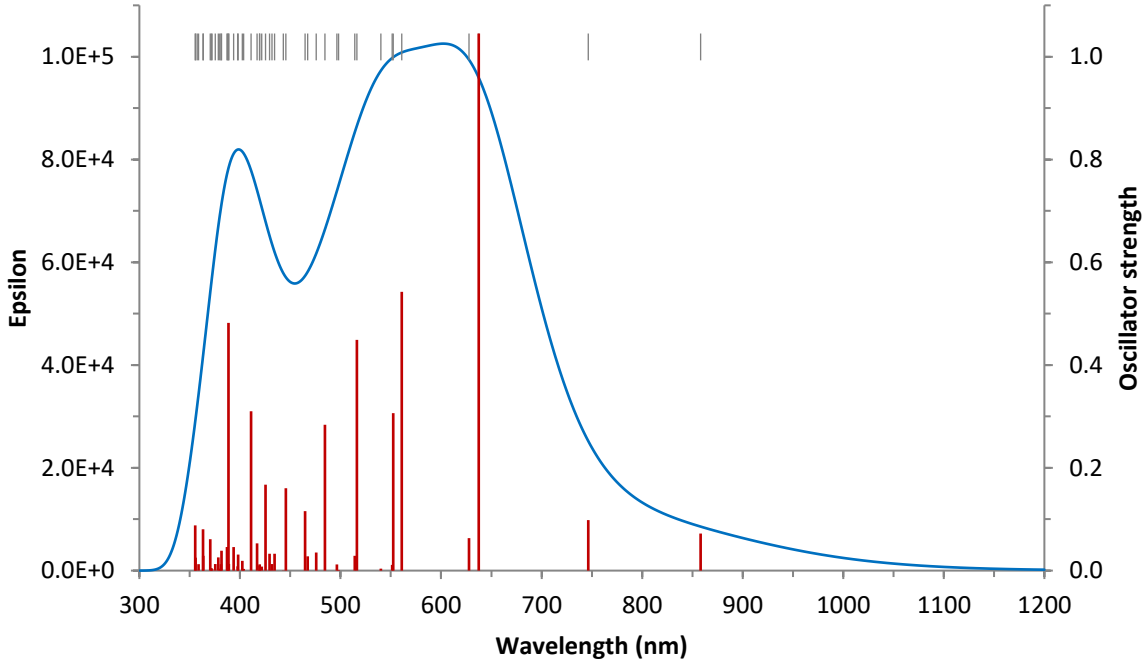

Figure S29. Electronic absorption spectrum of **3b**-Zn simulated using time-dependent density functional theory (B3LYP/6-31G(d)/PCM(CH_2Cl_2), 50 transitions, linewidth factor 3000 cm^{-1}).

Additional Tables

Table S1. Photophysical properties of compounds[a] **2a**-M, **2b**-M, **3a**-M and **3b**-M. (M = 2H; DCM, 5 μM and M = Zn; Toluene + 1% Pyridine, v/v, 5 μM).

Compounds	**λ_{abs} (nm) (logε)**	**λ_{em} (nm)** (ϕ)
2a-H_2	408 (4.60), 568 (5.29), 639 (4.29), 709 (4.17), 778 (4.01)	837 (0.84)
3a-H_2	399 (4.76), 559 (5.37), 639 (4.47), 710 (4.24), 803 (3.73)	833 (1.68)
2b-H_2	462 (4.74), 590 (5.06), 659 (4.37), 716 (4.07), 823 (3.95)	956 (1.09)
3b-H_2	400 (4.71), 499 (4.82), 556 (5.01), 590 (5.07), 652 (4.37), 720 (4.13), 834 (3.84)	950 (0.57)
2a-Zn	415 (4.67), 541 (4.71), 579 (5.35), 704 (4.34), 780 (4.07)	810 (-)
3a-Zn	410 (4.80), 540 (4.85), 577 (5.49), 700 (4.47), 768 (4.09)	815 (-)
2b-Zn	470 (4.73), 597 (4.98), 614 (5.03), 700 (4.22), 800 (4.14), 864 (3.95)	930 (-)
3b-Zn	409 (4.70), 571 (4.95), 613 (5.11), 697 (4.34), 780 (4.13), 852 (3.88)	920 (-)

[a]log (ε/mol^{-1} dm^3 cm^{-1})-molar extinction coefficient, λ_{abs}(absorption maxima), λ_{em}(emission maxima), and ϕ (%)-quantum yield.

Table S2. Electrochemical data for **2a**-M, **2b**-M, **3a**-M and **3b**-M. (M = 2H, Zn).

Compounds	E_{Ox1}	E_{Ox2}	E_{Ox3}	E_{Ox4}	E_{Red1}	E_{Red2}	E_{Red3}	E_{Red4}	E_{Red5}	ΔE
2a-H_2 (DCM)	0.26	0.54[a]	0.84[a]	1.09[a]	–1.34	–1.50	–2.14	–2.18	–2.35[a]	1.60
2b-H_2 (DCM)	0.36	0.62	0.94[a]	1.20[a]	–1.08	–1.14	–1.71	–1.86	–2.00[a] (–2.22)[a]	1.44
3a-H_2 (DCM)	0.25	0.54[a]	0.83[a]	1.08[a]	–1.36	–1.56	–2.16	–2.25[a]		1.61
3b-H_2 (DCM)	0.30	0.58[a]	0.88[a]	1.10[a]	–1.14	–1.35	–1.83	–1.99[a]	–2.23[a]	1.44
2a-Zn (DCM)	0.08	0.49 (0.27)[b]	0.98 (0.74)[b]		–1.63 (–1.50)[b]	(–1.92)[b]	–2.17	–2.38		1.71
2b-Zn (DCM)	0.24	0.59	0.87[a]		–1.19	–1.30	–1.44	–1.95	–2.15	1.43
3a-Zn (DCM)	0.11	0.47	(0.75)[b]		–1.64	–1.70	–2.16	-	-	1.75
3b-Zn (DCM)	0.18	0.53	-		–1.22	–1.46	–1.87	–2.15	-	1.40
2b-Zn (THF)	0.32	0.61	0.91[a]		–1.12	–1.32	–1.44	–1.58	–1.84, –1.94, –2.11, –2.55, –2.63, –2.87	1.44
3b-Zn (THF)	0.24	0.56	0.84		–1.21	–1.57	–1.96	–2.19	–2.62[a], –2.80[a]	1.45

[a] Irreversible couple. [b] Couple due to a minor redox-active component.

Electrode potentials in volts, taken from differential pulse voltammetry (DP) calibrated with Fc^+/Fc couple as internal standard. The values in parentheses are oxidation/reduction potentials of the products of irreversible reduction/oxidation. $\Delta E = E_{Ox1} - E_{Red1}$. All measurements were done in DCM as a solvent, with $[Bu_4N]PF_6$ as supporting electrolyte, glassy carbon working electrode, AgCl/Ag reference electrode, and Pt rod as counter electrode.

Table S3. Computational details (performed at B3LYP/6-31G(d)/PCM(CH_2Cl_2) level of theory).

Code[a]	SCF *E* [b] a.u.	ZPV[c] a.u.	lowest freq.[d] cm^{-1}	SCF *E* + ZPV a.u.	*H*[e] a.u.	*G*[f] a.u.
2a-H_2	-4594.360688	1.483299	4.02	-4592.877389	-4592.781179	-4593.019228
2b-H_2	-5100.681425	1.681037	7.25	-5099.000388	-5098.895799	-5099.15017
3a-H_2	-4099.708778	1.317564	8.23	-4098.391214	-4098.308059	-4098.515596
3b-H_2	-4352.869410	1.416527	6.58	-4351.452883	-4351.365548	-4351.581934
2a-Zn	-6372.386227	1.461276	6.87	-6370.924951	-6370.828316	-6371.065456
2b-Zn	-6878.709759	1.658716	1.20	-6877.051043	-6876.945628	-6877.205977
3a-Zn	-5877.737652	1.295637	8.97	-5876.442015	-5876.358375	-5876.565579
3b-Zn	-6130.898033	1.394502	7.27	-6129.503531	-6129.415609	-6129.632390

[a] Structure code (see the zip file for Cartesian coordinates). [b] SCF electronic energy. [c] Zero-point vibrational energy. [d] Lowest vibrational frequency. [e] Enthalpy. [f] Gibbs free energy.

Table S4. HOMO-LUMO bandgap comparison of various phenyl and tolyl *meso*-substituted free base porphyrins containing peripheral naphthalene and napthalenemonoimide units and their zinc complexes. All calculations were performed at the level of B3LYP/6-31g(d,p) theory.

Code[a]	Formula	HOMO (eV)	LUMO (eV)	HLG (eV)
1b'-H_2_ph	$C_{92}H_{42}N_8O_8$	-5.50	-3.64	1.86
1b'-H_2_tol	$C_{96}H_{50}N_8O_8$	-5.38	-3.58	1.81
2b'- H_2_ph	$C_{88}H_{44}N_6O_4$	-5.10	-3.26	1.84
2b'- H_2_tol	$C_{92}H_{52}N_6O_4$	-4.99	-3.19	1.80
3b'- H_2_ph	$C_{86}H_{45}N_5O_2$	-4.89	-2.98	1.91
3b'- H_2_tol	$C_{90}H_{53}N_5O_2$	-4.79	-2.91	1.88
8b'- H_2_ph	$C_{84}H_{46}N_4$	-4.68	-2.58	2.10
8b'- H_2_tol	$C_{88}H_{54}N_4$	-4.58	-2.51	2.07
1b'-Zn_ph	$C_{92}H_{40}N_8O_8Zn$	-5.58	-3.58	2.00
1b'-Zn_tol	$C_{96}H_{48}N_8O_8Zn$	-5.46	-3.52	1.95
2b'-Zn_ph	$C_{88}H_{42}N_6O_4Zn$	-5.18	-3.27	1.91
2b'-Zn_tol	$C_{92}H_{50}N_6O_4Zn$	-5.07	-3.20	1.87
3b'-Zn_ph	$C_{86}H_{43}N_5O_2Zn$	-4.97	-2.98	1.99
3b'-Zn_tol	$C_{90}H_{51}N_5O_2Zn$	-4.87	-2.92	1.95
8b'-Zn_ph	$C_{84}H_{44}N_4Zn$	-4.75	-2.51	2.24
8b'-Zn_tol	$C_{88}H_{52}N_4Zn$	-4.65	-2.45	2.21

[a] Structure code (see the zip file for Cartesian coordinates).

Table S5. Electronic transitions calculated for **2a**-H_2 using the TD/PCM(DCM)/B3LYP/6-31G(d,p) level of theory.

No.	Energy (cm^{-1})	λ (nm)	f[a]	Major excitations[b]
1	12852	778.1	0.066	H–1»L+1 (17%) HOMO»LUMO (82%)
2	13831	723.0	0.026	H–1»LUMO (27%) HOMO»L+1 (72%)
3	17021	587.5	1.392	H–1»LUMO (71%) HOMO»L+1 (26%)
4	17049	586.5	0.733	H–3»LUMO (16%) H–1»L+1 (70%) HOMO»LUMO (12%)
5	17073	585.7	0.000	HOMO»L+2 (91%)
6	17841	560.5	0.000	H–2»LUMO (87%)
7	18414	543.1	0.450	H–3»LUMO (77%) H–1»L+1 (11%)
8	19398	515.5	0.002	H–2»L+1 (98%)
9	19570	511.0	0.068	H–3»L+1 (99%)
10	20095	497.6	0.320	H–1»L+2 (98%)
11	21578	463.4	0.000	HOMO»L+3 (90%)
12	22018	454.2	0.000	H–7»L+1 (44%) H–4»L+1 (35%)
13	22063	453.2	0.001	H–6»L+1 (92%)
14	22163	451.2	0.199	H–4»LUMO (96%)
15	22638	441.7	0.080	H–6»LUMO (95%)
16	22738	439.8	0.000	H–7»L+1 (20%) H–5»LUMO (70%)
17	22924	436.2	0.022	H–7»LUMO (89%)
18	22969	435.4	0.028	H–2»L+2 (86%)
19	23221	430.7	0.002	H–5»LUMO (15%) H–3»L+2 (62%)
20	23255	430.0	0.051	H–7»L+1 (11%) H–5»L+1 (29%) H–4»L+1 (32%) H–3»L+2 (19%)
21	23284	429.5	0.073	H–8»LUMO (94%)
22	23301	429.2	0.087	H–7»L+1 (11%) H–5»L+1 (60%) H–4»L+1 (16%)
23	23618	423.4	0.575	H–8»L+1 (14%) HOMO»L+4 (76%)
24	24001	416.7	0.022	H–8»L+1 (82%) HOMO»L+4 (13%)
25	24867	402.1	0.385	HOMO»L+5 (81%)
26	25277	395.6	0.005	H–1»L+3 (89%)
27	25564	391.2	0.018	H–9»LUMO (88%)
28	25677	389.5	0.005	H–10»LUMO (93%)
29	26155	382.3	0.001	H–11»LUMO (60%) H–1»L+4 (29%)
30	26606	375.9	0.075	H–11»L+1 (29%) H–9»L+1 (45%)
31	26672	374.9	0.002	H–7»L+2 (12%) H–4»L+2 (61%)
32	26711	374.4	0.001	H–12»LUMO (82%)
33	26751	373.8	0.016	H–13»LUMO (73%)
34	26846	372.5	0.000	H–6»L+2 (44%) H–3»L+3 (15%) H–2»L+4 (11%)
35	26872	372.1	0.063	H–3»L+4 (24%) H–2»L+3 (45%)
36	27006	370.3	0.000	H–6»L+2 (38%) H–3»L+3 (21%) H–2»L+4 (16%)
37	27076	369.3	0.000	H–10»L+1 (83%)
38	27241	367.1	0.001	H–7»L+2 (61%) H–4»L+2 (16%)
39	27294	366.4	0.011	H–11»L+1 (23%) H–9»L+1 (41%) H–5»L+2 (12%)
40	27363	365.5	0.001	H–14»LUMO (85%)
41	27453	364.3	0.001	H–15»LUMO (36%) H–11»L+1 (19%) H–5»L+2 (29%)
42	27499	363.6	0.327	H–18»LUMO (14%) H–11»LUMO (19%) H–1»L+4 (38%)
43	27537	363.2	0.043	H–15»LUMO (37%) H–5»L+2 (33%)
44	27582	362.6	0.000	H–17»LUMO (75%)
45	27729	360.6	0.000	H–14»L+1 (74%)
46	27866	358.9	0.021	H–18»LUMO (66%)
47	27946	357.8	0.002	H–16»LUMO (87%)
48	27956	357.7	0.167	H–18»L+1 (26%) H–11»L+1 (10%) H–1»L+5 (43%)
49	28044	356.6	0.001	H–8»L+2 (68%)
50	28051	356.5	0.112	H–15»L+1 (78%)

[a] Oscillator strength. [b] Contributions smaller than 10% are not included. H = HOMO, L = LUMO. Orbitals are numbered consecutively regardless of possible degeneracies.

Table S6. Electronic transitions calculated for **2a**-Zn using the TD/PCM(DCM)/B3LYP/6-31G(d,p) level of theory.

No.	Energy (cm^{-1})	λ (nm)	f[a]	Major excitations[b]
1	13570	736.9	0.049	H–1»L+1 (19%) HOMO»LUMO (80%)
2	13888	720.0	0.001	H–1»LUMO (35%) HOMO»L+1 (64%)
3	16934	590.5	1.418	H–1»LUMO (64%) HOMO»L+1 (33%)
4	17249	579.7	1.041	H–1»L+1 (79%) HOMO»LUMO (18%)
5	17452	573.0	0.000	HOMO»L+2 (99%)
6	19624	509.6	0.002	H–4»LUMO (93%)
7	19652	508.9	0.004	H–2»LUMO (85%)
8	19685	508.0	0.269	H–1»L+2 (95%)
9	19869	503.3	0.000	H–3»L+1 (94%)
10	20057	498.6	0.011	H–2»L+1 (86%)
11	20413	489.9	0.023	H–3»LUMO (96%)
12	21238	470.8	0.063	H–5»LUMO (84%) H–2»LUMO (12%)
13	21446	466.3	0.015	H–4»L+1 (97%)
14	22041	453.7	0.000	HOMO»L+3 (95%)
15	22067	453.2	0.084	H–5»L+1 (87%)
16	22662	441.3	0.164	H–6»LUMO (97%)
17	22796	438.7	0.004	H–7»LUMO (85%)
18	23406	427.2	0.134	H–7»L+1 (91%)
19	23444	426.5	0.081	H–8»LUMO (92%)
20	23607	423.6	0.001	H–7»LUMO (10%) H–6»L+1 (82%)
21	23921	418.0	0.321	H–12»LUMO (19%) H–8»L+1 (19%) HOMO»L+4 (49%)
22	24247	412.4	0.008	H–12»LUMO (17%) H–8»L+1 (63%)
23	24318	411.2	0.000	H–2»L+2 (88%)
24	24372	410.3	0.101	H–4»L+2 (51%) HOMO»L+4 (19%)
25	24454	408.9	0.001	H–12»L+1 (11%) H–3»L+2 (67%)
26	24906	401.5	0.088	H–12»L+1 (27%) HOMO»L+5 (29%)
27	24964	400.6	0.003	H–1»L+3 (93%)
28	24972	400.5	0.199	H–12»LUMO (29%) H–12»L+1 (10%) H–4»L+2 (21%) HOMO»L+4 (13%) HOMO»L+5 (11%)
29	25363	394.3	0.264	H–12»L+1 (28%) H–1»L+4 (15%) HOMO»L+5 (37%)
30	25556	391.3	0.000	H–5»L+2 (84%)
31	26011	384.4	0.004	H–9»LUMO (56%) H–1»L+4 (30%)
32	26505	377.3	0.007	H–10»LUMO (91%)
33	26510	377.2	0.000	H–11»LUMO (91%)
34	26827	372.8	0.045	H–9»L+1 (48%) H–7»L+2 (18%) H–1»L+5 (17%)
35	27041	369.8	0.100	H–6»L+2 (73%)
36	27233	367.2	0.003	H–13»LUMO (89%)
37	27272	366.7	0.039	H–9»L+1 (15%) H–7»L+2 (62%)
38	27328	365.9	0.133	H–14»LUMO (19%) H–7»L+2 (11%) H–1»L+4 (24%) HOMO»L+5 (10%)
39	27498	363.7	0.200	H–19»LUMO (21%) H–14»LUMO (60%)
40	27737	360.5	0.003	H–17»LUMO (22%) H–15»LUMO (35%) H–8»L+2 (33%)
41	27805	359.6	0.000	H–18»LUMO (87%)
42	27854	359.0	0.000	H–16»LUMO (90%)
43	27902	358.4	0.000	H–15»L+1 (68%)
44	27929	358.0	0.031	H–16»L+1 (53%) H–10»L+1 (12%) H–3»L+3 (18%)
45	27975	357.5	0.000	H–15»LUMO (56%) H–8»L+2 (28%)
46	28025	356.8	0.222	H–19»L+1 (23%) H–9»L+1 (11%) H–1»L+5 (41%)
47	28188	354.8	0.000	H–17»LUMO (20%) H–11»L+1 (60%)
48	28206	354.5	0.005	H–19»LUMO (64%)
49	28234	354.2	0.001	H–17»LUMO (17%) H–17»L+1 (12%) H–13»L+1 (10%) H–11»L+1 (33%)
50	28238	354.1	0.000	H–10»L+1 (83%)

[a] Oscillator strength. [b] Contributions smaller than 10% are not included. H = HOMO, L = LUMO. Orbitals are numbered consecutively regardless of possible degeneracies.

Table S7. Electronic transitions calculated for **2b**-H_2 using the TD/PCM(DCM)/B3LYP/6-31G(d,p) level of theory.

No.	Energy (cm^{-1})	λ (nm)	f[a]	Major excitations[b]
1	10735	931.5	0.111	HOMO»LUMO (95%)
2	13318	750.9	0.070	H–1»LUMO (61%) HOMO»L+2 (38%)
3	13520	739.6	0.000	HOMO»L+1 (99%)
4	15751	634.9	1.383	H–1»LUMO (39%) HOMO»L+2 (58%)
5	16390	610.1	0.000	H–2»LUMO (89%)
6	16613	602.0	0.024	H–3»LUMO (71%) H–2»L+1 (10%) H–1»L+2 (17%)
7	16968	589.3	0.343	H–3»LUMO (14%) H–1»L+2 (60%) HOMO»L+3 (21%)
8	17306	577.8	0.284	H–1»L+1 (99%)
9	19888	502.8	0.000	H–4»LUMO (73%) HOMO»L+4 (13%)
10	20026	499.4	0.055	H–5»LUMO (98%)
11	20073	498.2	0.154	H–6»LUMO (84%)
12	20396	490.3	0.000	HOMO»L+4 (84%)
13	20435	489.4	0.368	H–6»LUMO (14%) H–2»L+1 (49%) HOMO»L+3 (22%)
14	20694	483.2	0.848	H–2»L+1 (25%) H–1»L+2 (12%) HOMO»L+3 (50%)
15	20768	481.5	0.000	H–4»LUMO (17%) H–3»L+1 (70%)
16	20897	478.5	0.000	H–2»L+2 (97%)
17	21020	475.7	0.051	H–3»L+2 (94%)
18	21461	466.0	0.135	H–7»LUMO (94%)
19	21620	462.5	0.187	H–8»LUMO (93%)
20	21874	457.2	0.000	H–6»L+1 (15%) H–5»L+2 (78%)
21	21937	455.8	0.000	H–6»L+2 (74%) H–5»L+1 (15%)
22	22690	440.7	0.000	H–9»LUMO (90%)
23	22717	440.2	0.001	H–10»LUMO (88%)
24	23142	432.1	0.141	H–4»L+2 (95%)
25	23213	430.8	0.022	H–1»L+3 (79%)
26	23479	425.9	0.004	H–4»L+1 (89%)
27	23767	420.8	0.003	H–6»L+2 (17%) H–5»L+1 (81%)
28	23803	420.1	0.000	H–6»L+1 (82%) H–5»L+2 (16%)
29	23996	416.7	0.000	H–12»L+1 (12%) H–11»LUMO (82%)
30	24000	416.7	0.000	H–12»LUMO (83%) H–11»L+1 (12%)
31	24232	412.7	0.077	H–1»L+4 (87%)
32	24401	409.8	0.011	H–13»LUMO (65%) H–8»L+1 (10%) HOMO»L+5 (18%)
33	24785	403.5	0.011	H–15»LUMO (63%) H–7»L+1 (23%)
34	24835	402.7	0.000	H–8»L+2 (87%)
35	24851	402.4	0.029	H–7»L+2 (87%)
36	24897	401.7	0.003	H–14»LUMO (94%)
37	25090	398.6	0.000	H–16»LUMO (95%)
38	25123	398.0	0.003	H–17»LUMO (18%) H–13»LUMO (14%) H–8»L+1 (60%)
39	25243	396.2	0.002	H–15»LUMO (30%) H–7»L+1 (58%)
40	25362	394.3	0.591	H–17»LUMO (53%) H–8»L+1 (10%) HOMO»L+5 (27%)
41	25534	391.6	0.000	H–3»L+4 (11%) H–2»L+3 (78%)
42	25798	387.6	0.048	H–3»L+3 (72%) H–2»L+4 (15%)
43	25940	385.5	0.013	H–18»LUMO (75%) H–7»L+1 (14%)
44	25978	384.9	0.000	H–19»LUMO (87%)
45	26136	382.6	0.100	H–20»LUMO (86%)
46	26178	382.0	0.199	H–17»LUMO (17%) H–8»L+1 (13%) H–1»L+3 (10%) HOMO»L+5 (35%)
47	26261	380.8	0.000	H–9»L+1 (90%)
48	26303	380.2	0.019	H–10»L+1 (81%)
49	26685	374.7	0.010	H–21»LUMO (74%)
50	27010	370.2	0.006	H–9»L+2 (96%)

[a] Oscillator strength. [b] Contributions smaller than 10% are not included. H = HOMO, L = LUMO. Orbitals are numbered consecutively regardless of possible degeneracies.

Table S8. Electronic transitions calculated for **2b**-Zn using the TD/PCM(DCM)/B3LYP/6-31G(d,p) level of theory.

No.	Energy (cm^{-1})	λ (nm)	f[a]	Major excitations[b]
1	11114	899.8	0.103	HOMO»LUMO (96%)
2	13085	764.2	0.187	H–1»LUMO (72%) HOMO»L+2 (27%)
3	13602	735.2	0.000	HOMO»L+1 (100%)
4	15802	632.8	1.250	H–1»LUMO (28%) HOMO»L+2 (69%)
5	16800	595.2	0.259	H–1»L+1 (99%)
6	17076	585.6	0.401	H–1»L+2 (79%) HOMO»L+3 (12%)
7	17446	573.2	0.066	H–6»LUMO (10%) H–3»LUMO (78%)
8	17697	565.1	0.000	H–2»LUMO (99%)
9	17839	560.6	0.000	H–5»LUMO (21%) H–4»LUMO (67%)
10	18831	531.0	0.007	H–6»LUMO (70%) H–3»LUMO (14%)
11	19651	508.9	0.000	H–5»LUMO (13%) H–4»LUMO (10%) H–3»L+1 (18%) H–2»L+2 (56%)
12	19843	504.0	0.026	H–3»L+2 (66%) H–2»L+1 (29%)
13	19921	502.0	0.000	H–5»LUMO (55%) H–4»LUMO (17%) H–2»L+2 (21%)
14	21024	475.7	0.000	HOMO»L+4 (96%)
15	21059	474.9	0.936	HOMO»L+3 (73%)
16	21257	470.4	0.000	H–3»L+1 (72%) H–2»L+2 (18%)
17	21312	469.2	0.012	H–3»L+2 (30%) H–2»L+1 (69%)
18	21574	463.5	0.142	H–7»LUMO (96%)
19	21816	458.4	0.208	H–8»LUMO (93%)
20	21884	456.9	0.039	H–6»LUMO (17%) H–5»L+1 (14%) H–4»L+1 (57%)
21	22716	440.2	0.000	H–6»L+1 (83%)
22	22767	439.2	0.005	H–4»L+2 (88%)
23	22814	438.3	0.203	H–11»LUMO (78%)
24	22927	436.2	0.006	H–9»LUMO (85%)
25	22971	435.3	0.000	H–10»LUMO (87%)
26	23134	432.3	0.077	H–6»L+2 (13%) H–1»L+3 (65%)
27	23179	431.4	0.000	H–5»L+1 (75%) H–4»L+1 (19%)
28	23338	428.5	0.159	H–5»L+2 (87%)
29	23459	426.3	0.038	H–6»L+2 (81%) H–1»L+3 (11%)
30	24070	415.5	0.052	H–1»L+4 (89%)
31	24187	413.4	0.000	H–12»LUMO (78%)
32	24219	412.9	0.001	H–13»LUMO (81%) H–12»L+1 (11%)
33	24291	411.7	0.000	H–14»LUMO (77%)
34	24751	404.0	0.011	H–15»LUMO (74%) H–7»L+1 (15%)
35	24805	403.1	0.008	H–16»LUMO (91%)
36	24866	402.2	0.000	H–17»LUMO (96%)
37	25102	398.4	0.002	H–15»LUMO (22%) H–7»L+1 (65%)
38	25234	396.3	0.130	H–14»LUMO (10%) H–11»L+2 (11%) H–8»L+1 (59%)
39	25261	395.9	0.030	H–7»L+2 (90%)
40	25327	394.8	0.063	H–18»LUMO (22%) H–11»L+2 (40%) H–8»L+1 (11%) HOMO»L+5 (20%)
41	25416	393.5	0.000	H–8»L+2 (89%)
42	25611	390.5	0.317	H–18»LUMO (47%) H–11»L+2 (28%)
43	26003	384.6	0.018	H–19»LUMO (77%) H–7»L+1 (13%)
44	26175	382.0	0.000	H–20»LUMO (84%)
45	26336	379.7	0.062	H–21»LUMO (87%)
46	26399	378.8	0.201	H–18»LUMO (14%) H–2»L+4 (15%) HOMO»L+5 (29%)
47	26448	378.1	0.000	H–9»L+1 (89%)
48	26478	377.7	0.000	H–11»L+1 (87%)
49	26491	377.5	0.014	H–10»L+1 (81%)
50	26806	373.1	0.008	H–22»LUMO (62%) H–17»L+1 (11%) H–3»L+3 (13%)

[a] Oscillator strength. [b] Contributions smaller than 10% are not included. H = HOMO, L = LUMO. Orbitals are numbered consecutively regardless of possible degeneracies.

Table S9. Electronic transitions calculated for **3a**-H_2 using the TD/PCM(DCM)/B3LYP/6-31G(d,p) level of theory.

No.	Energy (cm^{-1})	λ (nm)	f[a]	Major excitations[b]
1	13013	768.5	0.053	H–1»L+1 (19%) HOMO»LUMO (79%)
2	13836	722.7	0.041	H–1»LUMO (25%) HOMO»L+1 (74%)
3	16986	588.7	0.659	H–3»LUMO (10%) H–1»L+1 (59%) HOMO»LUMO (13%) HOMO»L+2 (15%)
4	17200	581.4	1.273	H–1»LUMO (73%) HOMO»L+1 (24%)
5	17392	575.0	0.108	H–2»LUMO (23%) HOMO»L+2 (66%)
6	17979	556.2	0.020	H–3»LUMO (18%) H–2»LUMO (60%) HOMO»L+2 (17%)
7	18560	538.8	0.479	H–3»LUMO (66%) H–2»LUMO (10%) H–1»L+1 (10%)
8	19097	523.6	0.020	H–2»L+1 (98%)
9	19533	512.0	0.050	H–3»L+1 (98%)
10	20356	491.3	0.287	H–1»L+2 (98%)
11	21791	458.9	0.051	H–7»L+1 (10%) H–4»L+1 (11%) HOMO»L+3 (73%)
12	22067	453.2	0.003	H–6»L+1 (82%)
13	22069	453.1	0.011	H–7»L+1 (36%) H–4»L+1 (25%) HOMO»L+3 (22%)
14	22397	446.5	0.183	H–4»LUMO (95%)
15	22864	437.4	0.004	H–7»L+1 (28%) H–6»LUMO (17%) H–5»LUMO (27%) H–4»L+1 (23%)
16	22935	436.0	0.065	H–6»LUMO (75%)
17	23121	432.5	0.011	H–2»L+2 (81%)
18	23166	431.7	0.049	H–7»LUMO (69%) H–5»L+1 (25%)
19	23280	429.6	0.001	H–5»LUMO (58%) H–4»L+1 (32%)
20	23351	428.2	0.115	H–7»LUMO (23%) H–5»L+1 (70%)
21	23568	424.3	0.071	H–8»LUMO (91%)
22	23578	424.1	0.008	H–3»L+2 (84%)
23	23908	418.3	0.096	H–8»L+1 (90%)
24	24393	410.0	0.379	HOMO»L+4 (84%)
25	24866	402.2	0.368	H–1»L+3 (10%) HOMO»L+5 (77%)
26	25444	393.0	0.043	H–1»L+3 (77%)
27	25938	385.5	0.019	H–9»LUMO (91%)
28	26561	376.5	0.031	H–10»LUMO (70%) H–1»L+4 (24%)
29	26709	374.4	0.087	H–10»L+1 (48%) H–9»L+1 (29%) H–1»L+5 (10%)
30	26891	371.9	0.022	H–11»LUMO (10%) H–3»L+3 (47%)
31	26910	371.6	0.004	H–7»L+2 (16%) H–4»L+2 (60%)
32	26967	370.8	0.070	H–12»LUMO (47%) H–2»L+3 (14%) H–2»L+4 (15%)
33	27033	369.9	0.002	H–11»LUMO (79%)
34	27162	368.2	0.004	H–6»L+2 (70%)
35	27296	366.4	0.004	H–13»L+1 (10%) H–10»L+1 (23%) H–9»L+1 (58%)
36	27443	364.4	0.004	H–7»L+2 (50%) H–4»L+2 (23%)
37	27641	361.8	0.000	H–13»L+1 (18%) H–12»LUMO (23%) H–5»L+2 (18%)
38	27678	361.3	0.002	H–13»LUMO (78%)
39	27771	360.1	0.002	H–13»L+1 (53%) H–5»L+2 (15%)
40	27794	359.8	0.003	H–12»L+1 (67%)
41	27805	359.6	0.004	H–16»LUMO (10%) H–14»LUMO (48%) H–12»L+1 (10%)
42	27829	359.3	0.003	H–5»L+2 (41%) H–2»L+3 (15%) H–2»L+4 (13%)
43	27925	358.1	0.307	H–17»LUMO (25%) H–10»LUMO (11%) H–1»L+4 (33%)
44	27941	357.9	0.210	H–17»L+1 (18%) H–10»L+1 (10%) H–1»L+5 (43%)
45	28191	354.7	0.031	H–17»LUMO (12%) H–15»LUMO (33%) H–14»L+1 (19%)
46	28252	354.0	0.010	H–17»LUMO (19%) H–14»L+1 (30%) H–8»L+2 (11%) H–1»L+4 (10%)
47	28274	353.7	0.003	H–18»LUMO (38%) H–16»LUMO (32%)
48	28358	352.6	0.016	H–11»L+1 (47%)
49	28410	352.0	0.010	H–11»L+1 (31%) H–8»L+2 (29%)
50	28450	351.5	0.007	H–15»L+1 (73%)

[a] Oscillator strength. [b] Contributions smaller than 10% are not included. H = HOMO, L = LUMO. Orbitals are numbered consecutively regardless of possible degeneracies.

Table S10. Electronic transitions calculated for **3a**-Zn using the TD/PCM(DCM)/B3LYP/6-31G(d,p) level of theory.

No.	Energy (cm^{-1})	λ (nm)	f[a]	Major excitations[b]
1	13768	726.3	0.034	H–1»L+1 (23%) HOMO»LUMO (76%)
2	13937	717.5	0.007	H–1»LUMO (31%) HOMO»L+1 (67%)
3	17124	584.0	1.330	H–1»LUMO (67%) HOMO»L+1 (30%)
4	17209	581.1	0.914	H–1»L+1 (66%) HOMO»LUMO (19%) HOMO»L+2 (12%)
5	17916	558.2	0.203	HOMO»L+2 (87%)
6	19750	506.3	0.000	H–4»LUMO (90%)
7	19781	505.5	0.011	H–2»LUMO (80%)
8	19899	502.5	0.002	H–3»L+1 (83%)
9	19967	500.8	0.220	H–1»L+2 (88%)
10	20036	499.1	0.020	H–2»L+1 (80%)
11	20712	482.8	0.032	H–3»LUMO (92%)
12	21262	470.3	0.017	H–4»L+1 (89%)
13	21562	463.8	0.057	H–5»LUMO (85%)
14	21948	455.6	0.083	H–5»L+1 (84%)
15	22253	449.4	0.044	HOMO»L+3 (95%)
16	23105	432.8	0.001	H–7»L+1 (14%) H–6»LUMO (80%)
17	23251	430.1	0.120	H–7»LUMO (94%)
18	23469	426.1	0.168	H–6»L+1 (95%)
19	23830	419.6	0.000	H–7»L+1 (81%) H–6»LUMO (15%)
20	24036	416.0	0.087	H–8»LUMO (93%)
21	24289	411.7	0.073	H–10»LUMO (37%) H–8»L+1 (24%) H–4»L+2 (13%) HOMO»L+4 (16%)
22	24424	409.4	0.083	H–8»L+1 (41%) H–2»L+2 (33%)
23	24550	407.3	0.000	H–10»LUMO (18%) H–8»L+1 (24%) H–2»L+2 (44%)
24	24649	405.7	0.002	H–10»L+1 (39%) H–3»L+2 (47%)
25	24814	403.0	0.084	H–4»L+2 (46%) HOMO»L+4 (31%)
26	24894	401.7	0.073	H–10»L+1 (14%) H–3»L+2 (28%) H–1»L+3 (11%) HOMO»L+5 (36%)
27	25019	399.7	0.011	H–10»L+1 (16%) H–1»L+3 (70%)
28	25265	395.8	0.307	H–10»LUMO (26%) H–4»L+2 (22%) HOMO»L+4 (34%)
29	25564	391.2	0.317	H–10»L+1 (20%) H–1»L+3 (11%) HOMO»L+5 (43%)
30	25849	386.9	0.000	H–5»L+2 (83%)
31	26436	378.3	0.019	H–9»LUMO (82%)
32	26758	373.7	0.003	H–11»LUMO (61%) H–1»L+4 (27%)
33	27020	370.1	0.020	H–11»L+1 (41%) H–9»L+1 (21%) H–1»L+5 (28%)
34	27569	362.7	0.002	H–12»LUMO (85%)
35	27615	362.1	0.011	H–6»L+2 (82%)
36	27692	361.1	0.088	H–11»LUMO (11%) H–7»L+2 (74%)
37	27791	359.8	0.259	H–18»LUMO (24%) H–11»LUMO (15%) H–1»L+4 (32%)
38	27853	359.0	0.034	H–15»LUMO (17%) H–13»LUMO (70%)
39	27950	357.8	0.028	H–16»LUMO (11%) H–15»LUMO (17%) H–9»L+1 (37%) H–1»L+5 (10%)
40	27997	357.2	0.031	H–15»LUMO (12%) H–14»L+1 (42%) H–9»L+1 (12%)
41	28038	356.7	0.034	H–13»L+1 (62%)
42	28113	355.7	0.071	H–16»LUMO (18%) H–15»LUMO (13%) H–14»L+1 (29%)
43	28155	355.2	0.004	H–17»LUMO (22%) H–14»LUMO (49%) H–8»L+2 (10%)
44	28254	353.9	0.152	H–11»L+1 (39%) H–9»L+1 (10%) H–1»L+5 (20%)
45	28358	352.6	0.002	H–17»LUMO (15%) H–14»LUMO (30%)
46	28385	352.3	0.001	H–19»LUMO (11%) H–16»LUMO (27%) H–2»L+3 (14%)
47	28596	349.7	0.002	H–17»L+1 (15%) H–16»LUMO (26%) H–15»LUMO (14%) H–4»L+3 (13%) H–2»L+3 (10%)
48	28615	349.5	0.006	H–18»LUMO (30%) H–15»L+1 (19%) H–8»L+2 (10%)
49	28700	348.4	0.000	H–18»LUMO (21%) H–17»LUMO (13%) H–15»L+1 (20%) H–8»L+2 (10%)
50	28750	347.8	0.016	H–17»LUMO (25%) H–16»L+1 (20%) H–13»L+1 (12%) H–3»L+3 (19%)

[a] Oscillator strength. [b] Contributions smaller than 10% are not included. H = HOMO, L = LUMO. Orbitals are numbered consecutively regardless of possible degeneracies.

Table S11. Electronic transitions calculated for **3b**-H_2 using the TD/PCM(DCM)/B3LYP/6-31G(d,p) level of theory.

No.	Energy (cm^{-1})	λ (nm)	f[a]	Major excitations[b]
1	11286	886.0	0.081	HOMO»LUMO (94%)
2	13521	739.6	0.025	H–1»LUMO (49%) HOMO»L+1 (49%)
3	15508	644.8	0.026	H–1»L+1 (33%) HOMO»L+2 (63%)
4	15735	635.5	1.161	H–1»LUMO (50%) HOMO»L+1 (45%)
5	16502	606.0	0.020	H–2»LUMO (81%)
6	16818	594.6	0.021	H–3»LUMO (83%)
7	17940	557.4	0.867	H–1»L+1 (43%) HOMO»L+2 (31%)
8	19074	524.3	0.005	H–2»L+1 (95%)
9	19641	509.1	0.448	H–1»L+2 (89%)
10	20096	497.6	0.429	HOMO»L+3 (86%)
11	20710	482.9	0.110	H–7»LUMO (15%) H–4»LUMO (76%)
12	20888	478.7	0.030	H–6»LUMO (68%) H–5»LUMO (18%)
13	20991	476.4	0.026	H–3»L+1 (89%)
14	21047	475.1	0.000	H–6»LUMO (23%) H–5»LUMO (70%)
15	21183	472.1	0.050	H–2»L+2 (84%)
16	21385	467.6	0.043	H–7»LUMO (75%) H–4»LUMO (14%)
17	22137	451.7	0.040	H–8»LUMO (19%) H–6»L+1 (68%)
18	22153	451.4	0.004	H–7»L+1 (48%) H–4»L+1 (37%)
19	22357	447.3	0.101	H–8»LUMO (74%) H–6»L+1 (19%)
20	22905	436.6	0.004	H–3»L+2 (81%)
21	23237	430.4	0.013	H–7»L+1 (41%) H–4»L+1 (55%)
22	23269	429.8	0.097	H–5»L+1 (86%)
23	23371	427.9	0.091	H–1»L+3 (75%)
24	23470	426.1	0.012	H–9»LUMO (91%)
25	23881	418.7	0.323	HOMO»L+4 (84%)
26	24572	407.0	0.001	H–12»LUMO (88%)
27	24773	403.7	0.113	H–10»LUMO (51%) HOMO»L+5 (35%)
28	24954	400.7	0.044	H–8»L+1 (80%)
29	25336	394.7	0.333	H–10»LUMO (33%) H–4»L+2 (25%) HOMO»L+5 (29%)
30	25448	393.0	0.033	H–11»LUMO (90%)
31	25742	388.5	0.034	H–17»LUMO (16%) H–13»LUMO (48%) H–4»L+2 (20%)
32	25842	387.0	0.000	H–16»LUMO (30%) H–14»LUMO (52%)
33	25920	385.8	0.171	H–13»LUMO (30%) H–4»L+2 (37%) HOMO»L+5 (14%)
34	26048	383.9	0.017	H–6»L+2 (81%)
35	26148	382.4	0.000	H–16»LUMO (21%) H–5»L+2 (46%)
36	26265	380.7	0.020	H–7»L+2 (83%)
37	26273	380.6	0.009	H–16»LUMO (31%) H–14»LUMO (21%) H–5»L+2 (30%)
38	26278	380.6	0.037	H–17»LUMO (18%) H–15»LUMO (59%)
39	26409	378.7	0.000	H–2»L+3 (85%)
40	26598	376.0	0.003	H–17»LUMO (52%) H–15»LUMO (27%)
41	26824	372.8	0.042	H–18»LUMO (76%) H–14»LUMO (10%)
42	27059	369.6	0.002	H–10»L+1 (19%) H–3»L+3 (57%)
43	27122	368.7	0.138	H–10»L+1 (59%) H–3»L+3 (17%)
44	27437	364.5	0.000	H–26»LUMO (14%) H–19»LUMO (45%) H–9»L+1 (20%)
45	27486	363.8	0.002	H–19»LUMO (14%) H–9»L+1 (68%)
46	27527	363.3	0.090	H–1»L+4 (60%)
47	27584	362.5	0.001	H–2»L+4 (74%)
48	27603	362.3	0.005	H–11»L+1 (80%)
49	27791	359.8	0.000	H–25»LUMO (83%)
50	27889	358.6	0.005	H–26»LUMO (11%) H–15»L+1 (15%) H–13»L+1 (37%) H–1»L+5 (18%)

[a] Oscillator strength. [b] Contributions smaller than 10% are not included. H = HOMO, L = LUMO. Orbitals are numbered consecutively regardless of possible degeneracies.

Table S12. Electronic transitions calculated for **3b**-Zn using the TD/PCM(DCM)/B3LYP/6-31G(d,p) level of theory.

No.	Energy (cm^{-1})	λ (nm)	f[a]	Major excitations[b]
1	11653	858.1	0.072	HOMO»LUMO (96%)
2	13398	746.4	0.098	H–1»LUMO (62%) HOMO»L+1 (36%)
3	15687	637.5	1.045	H–1»LUMO (37%) HOMO»L+1 (56%)
4	15929	627.8	0.063	H–1»L+1 (45%) HOMO»L+2 (52%)
5	17828	560.9	0.543	H–6»LUMO (12%) H–4»LUMO (11%) H–2»LUMO (14%) H–1»L+1 (32%) HOMO»L+2 (24%)
6	18102	552.4	0.306	H–4»LUMO (16%) H–2»LUMO (30%) H–1»L+1 (14%) HOMO»L+2 (22%)
7	18136	551.4	0.011	H–6»LUMO (11%) H–4»LUMO (30%) H–2»LUMO (49%)
8	18514	540.1	0.004	H–3»LUMO (96%)
9	19369	516.3	0.449	H–1»L+2 (91%)
10	19448	514.2	0.029	H–6»LUMO (33%) H–5»LUMO (16%) H–4»LUMO (31%) H–3»L+1 (13%)
11	20077	498.1	0.001	H–3»L+1 (79%)
12	20145	496.4	0.012	H–4»L+1 (15%) H–2»L+1 (75%)
13	20639	484.5	0.284	H–5»LUMO (27%) HOMO»L+3 (62%)
14	21016	475.8	0.035	H–6»LUMO (23%) H–5»LUMO (45%) HOMO»L+3 (28%)
15	21396	467.4	0.028	H–7»LUMO (24%) H–4»L+1 (58%) H–2»L+1 (14%)
16	21515	464.8	0.116	H–7»LUMO (73%) H–4»L+1 (17%)
17	22439	445.6	0.160	H–8»LUMO (88%)
18	22567	443.1	0.000	H–4»L+2 (11%) H–2»L+2 (74%)
19	23018	434.4	0.033	H–6»L+1 (28%) H–5»L+1 (43%) H–1»L+3 (21%)
20	23155	431.9	0.013	H–10»LUMO (82%)
21	23285	429.5	0.033	H–5»L+1 (12%) H–3»L+2 (15%) H–1»L+3 (55%)
22	23505	425.4	0.167	H–6»L+1 (57%) H–5»L+1 (36%)
23	23717	421.6	0.008	H–9»LUMO (94%)
24	23830	419.6	0.012	H–3»L+2 (75%)
25	23839	419.5	0.010	H–7»L+1 (95%)
26	23979	417.0	0.053	H–4»L+2 (76%) H–2»L+2 (10%)
27	24326	411.1	0.310	HOMO»L+4 (77%)
28	24773	403.7	0.003	H–14»LUMO (64%) H–11»LUMO (20%)
29	24853	402.4	0.019	H–14»LUMO (24%) H–11»LUMO (48%) HOMO»L+5 (16%)
30	25113	398.2	0.031	H–11»LUMO (14%) H–10»L+1 (64%) HOMO»L+5 (12%)
31	25143	397.7	0.008	H–6»L+2 (51%) H–5»L+2 (30%)
32	25399	393.7	0.046	H–8»L+1 (69%)
33	25711	388.9	0.013	H–17»LUMO (14%) H–15»LUMO (30%) H–12»LUMO (45%)
34	25733	388.6	0.482	H–18»LUMO (10%) H–10»L+1 (18%) HOMO»L+5 (43%)
35	25796	387.7	0.008	H–17»LUMO (35%) H–15»LUMO (11%) H–12»LUMO (43%)
36	25831	387.1	0.046	H–13»LUMO (84%)
37	26201	381.7	0.039	H–16»LUMO (18%) H–7»L+2 (63%)
38	26240	381.1	0.013	H–17»LUMO (10%) H–15»LUMO (11%) H–8»L+1 (13%) H–6»L+2 (21%) H–5»L+2 (33%)
39	26324	379.9	0.004	H–17»LUMO (24%) H–15»LUMO (36%) H–5»L+2 (19%)
40	26421	378.5	0.026	H–18»LUMO (15%) H–16»LUMO (37%) H–7»L+2 (19%) H–1»L+4 (19%)
41	26634	375.5	0.013	H–18»LUMO (52%) H–16»LUMO (26%)
42	26861	372.3	0.003	H–3»L+3 (68%)
43	26916	371.5	0.005	H–19»LUMO (34%) H–4»L+3 (13%) H–2»L+3 (33%)
44	26993	370.5	0.061	H–19»LUMO (50%) H–2»L+3 (16%)
45	27508	363.5	0.029	H–11»L+1 (62%) H–1»L+5 (18%)
46	27526	363.3	0.080	H–1»L+4 (55%)
47	27867	358.8	0.013	H–20»LUMO (63%) H–11»L+1 (11%)
48	27973	357.5	0.000	H–25»LUMO (84%)
49	28101	355.9	0.025	H–16»L+1 (10%) H–13»L+1 (59%)
50	28127	355.5	0.088	H–12»L+1 (83%)

[a] Oscillator strength. [b] Contributions smaller than 10% are not included. H = HOMO, L = LUMO. Orbitals are numbered consecutively regardless of possible degeneracies.

Table S13. Crystal data and structure refinement for **2b**-H_2 and **3b**-H_2.

Identification code	**2b**-H_2 (2015790)	**3b**-H_2 (2015791)
Empirical formula	$C_{135.3}H_{117.3}Cl_{26.4}N_6O_4$	$C_{121.9}H_{111.3}Cl_{9.3}N_5O_2$
Formula weight	2835.98	2011.06
Temperature/K	100(2)	100(2)
Crystal system	triclinic	monoclinic
Space group	P-1	I2/a
a/Å	16.064(5)	35.41(2)
b/Å	20.140(6)	16.245(7)
c/Å	21.720(9)	42.180(3)
α/°	91.95(3)	90
β/°	97.51(3)	111.65(5)
γ/°	93.50(3)	90
Volume/Å^3	6948(4)	22552(18)
Z	2	8
D_{calc}g/cm^3	1.356	1.185
μ/mm^{-1}	5.160	2.502
F(000)	2904.0	8414.0
Crystal size/mm^3	0.700 × 0.090 × 0.040	0.460 × 0.190 × 0.080
Radiation	CuKα (λ = 1.54184)	Cu Kα (λ = 1.54184)
2θ range for data collection/°	7.318 to 136.39	6.944 to 136.274
Index ranges	-17 ≤ h ≤ 19, -23 ≤ k ≤ 15, -25 ≤ l ≤ 24	-42 ≤ h ≤ 42, -19 ≤ k ≤ 12, -50 ≤ l ≤ 48
Reflections collected	44082	47946
Independent reflections	24468 [R_{int} = 0.1082, R_{sigma} = 0.1757]	20155 [R_{int} = 0.1421, R_{sigma} = 0.2001]
Data/restraints/parameters	24468/102/1778	20155/67/1300
Goodness-of-fit on F^2	1.161	1.075
Final *R* indexes [I>=2σ (I)]	R_1 = 0.1182, wR_2 = 0.2904	R_1 = 0.1240, wR_2 = 0.2718
Final R indexes [all data]	R_1 = 0.1918, wR_2 = 0.3513	R_1 = 0.2826, wR_2 = 0.3992
Largest diff. peak/hole / e Å^{-3}	1.11/-0.71	0.60/-0.38

Table S14. Dihedral angles [a] between opposing naphthalene/NMI moieties in **2b**-H_2, **2b**-Zn, **3b**-H_2 and **3b**-Zn obtained from experimental (XRD) and calculated (DFT) geometries.

Compounds	naphthalene/naphthalene angle (deg)	NMI/NMI angle (deg)	NMI/naphthalene angle (deg)
2b-H_2 (XRD)	109.13	117.52	-
3b-H_2 (XRD)	128.81	-	90.18
2b-H_2 (DFT)	104.00	98.32	-
3b-H_2 (DFT)	103.60	-	99.30
2b-Zn (DFT)	106.85	102.40	-
3b-Zn (DFT)	106.19	-	105.19

[a] For both NMI (naphthalenemonoimide) and naphthalene units the mean plane was calculated using the 10 carbon atoms of the two naphthalene rings.

NMR Spectra

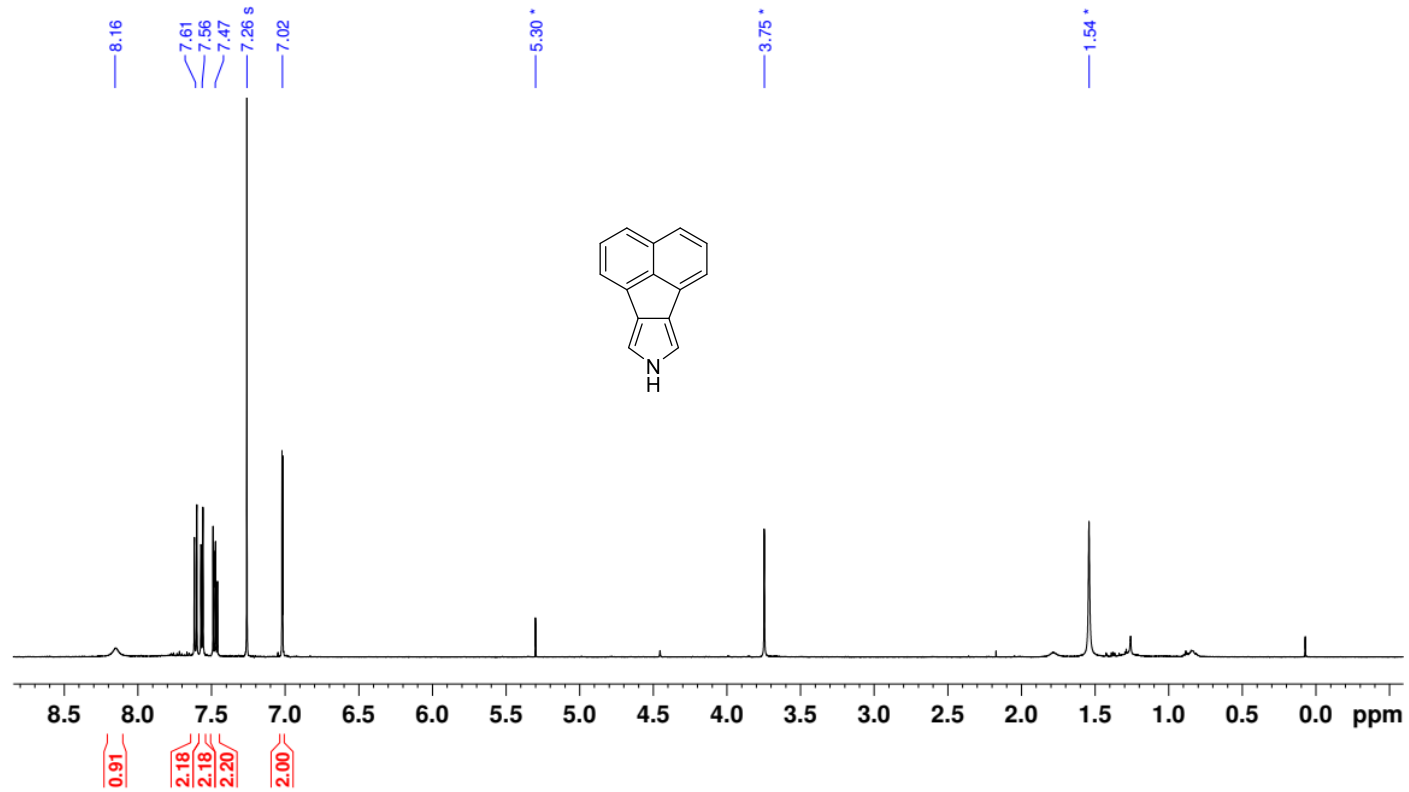

Figure S30. ^{1}H NMR spectrum of **4** (500 MHz, chloroform-*d* , 300 K).

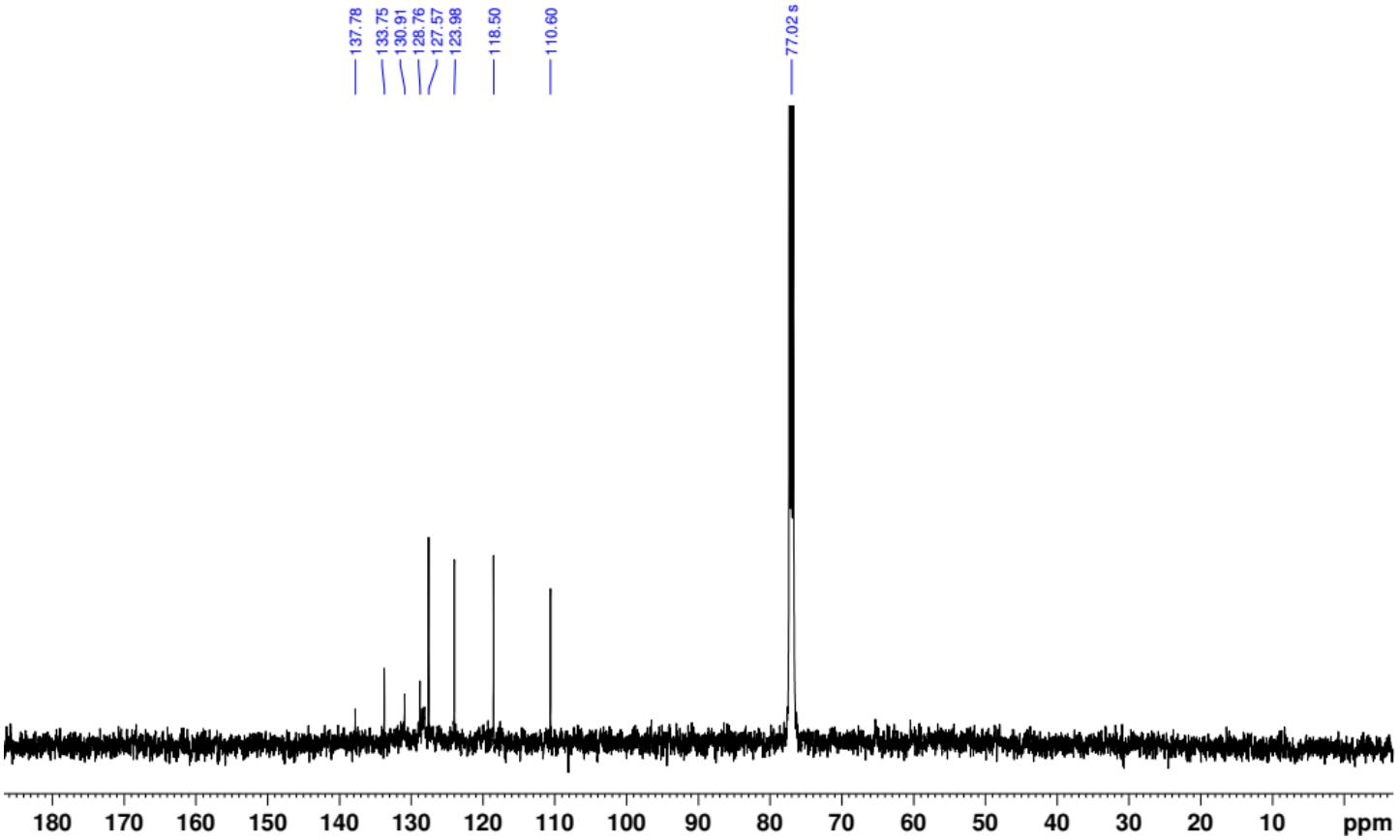

Figure S31. ^{13}C NMR spectrum of **4** (125 MHz, chloroform-*d* , 300 K).

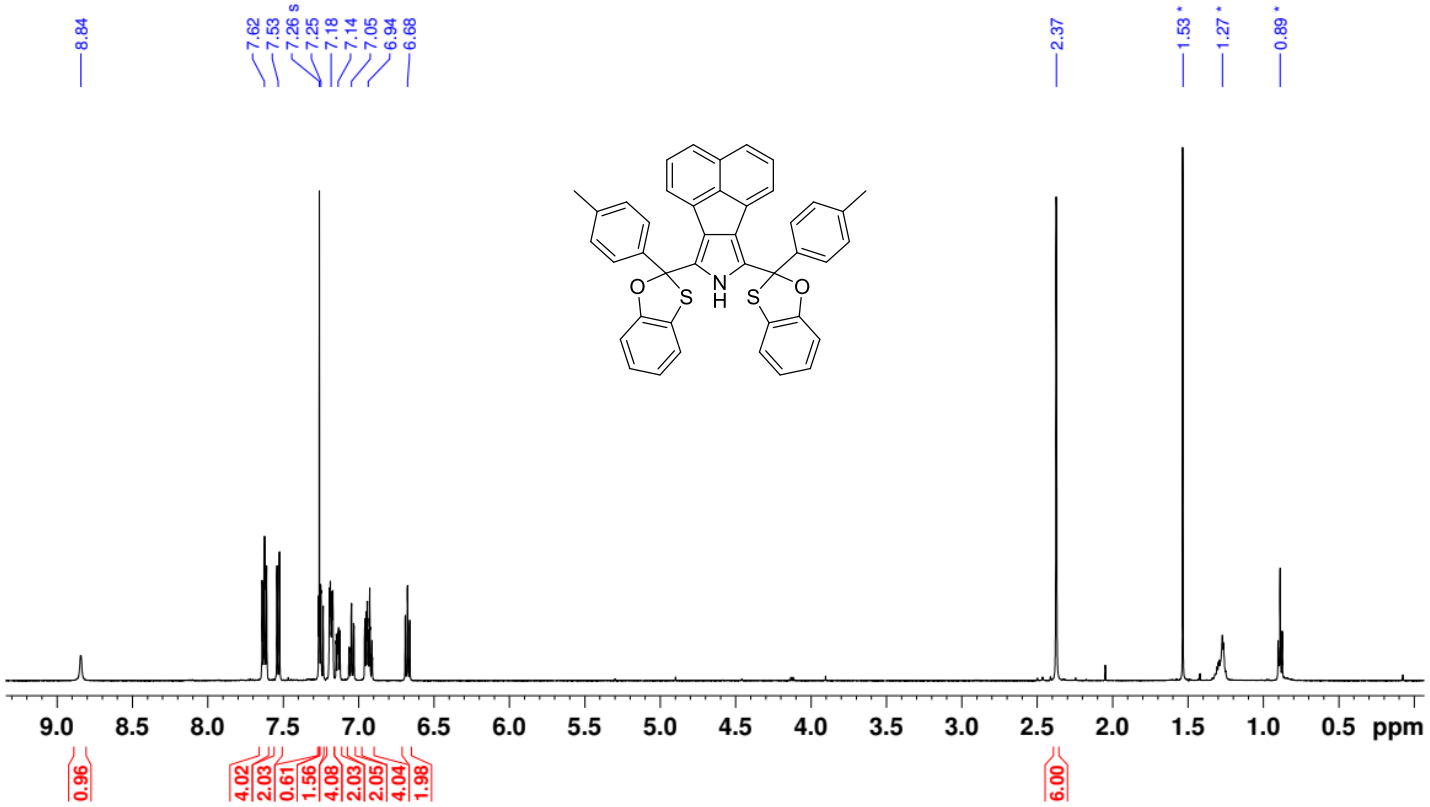

Figure S32. ^{1}H NMR spectrum of **5** (500 MHz, chloroform-*d* , 300 K).

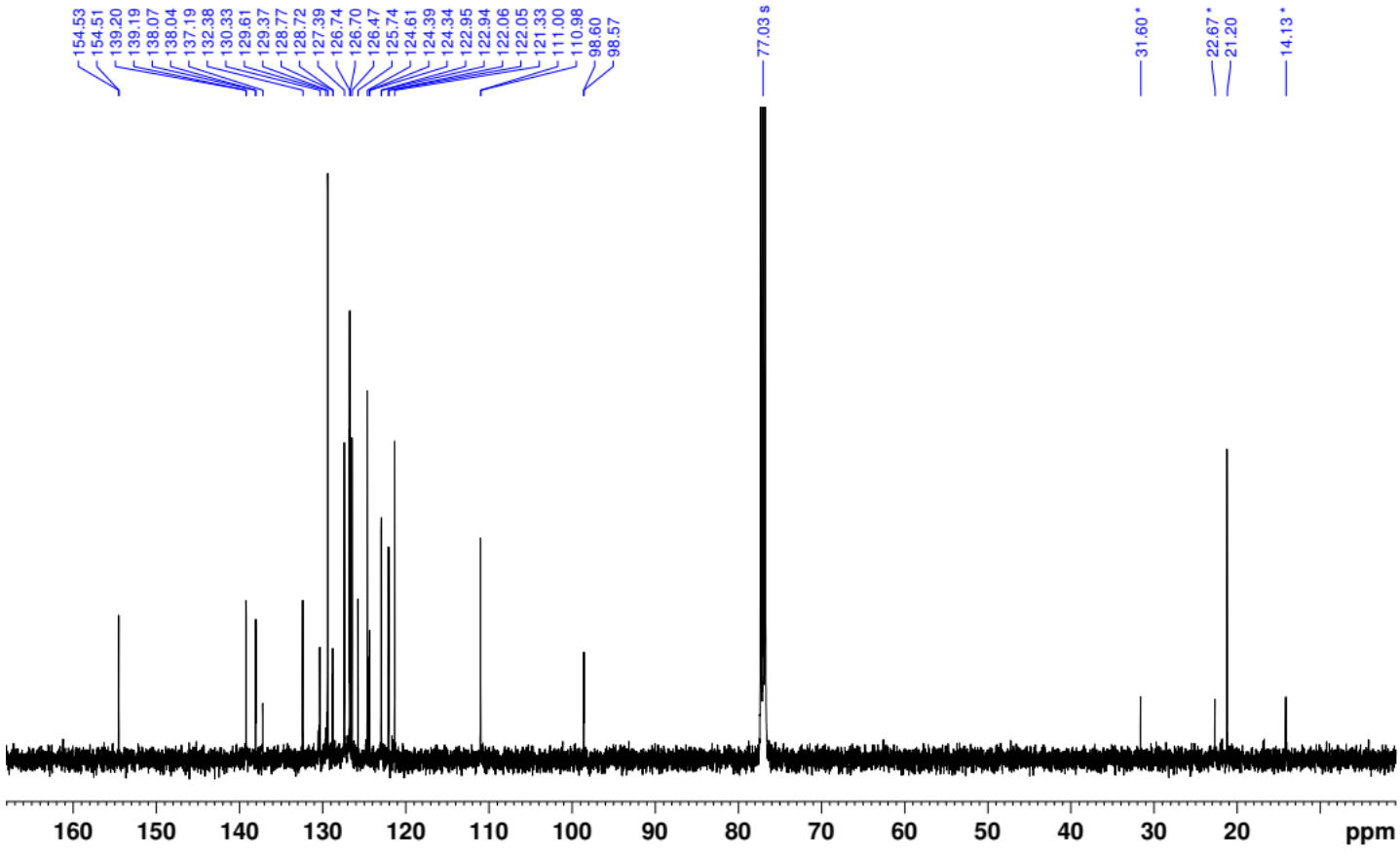

Figure S33. ^{13}C NMR spectrum of **5** (125 MHz, chloroform-*d* , 300 K).

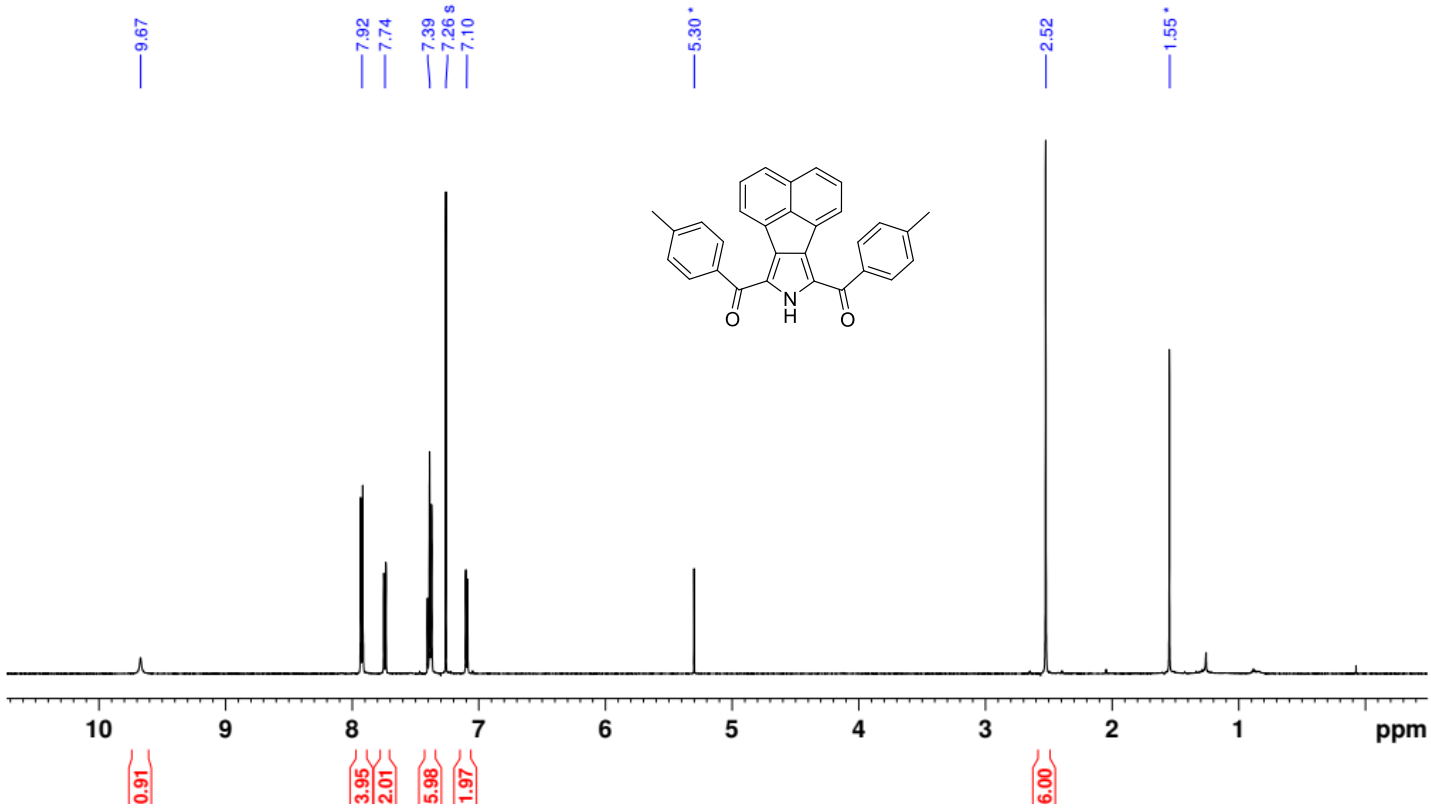

Figure S34. ^{1}H NMR spectrum of **6** (500 MHz, chloroform-*d* , 300 K).

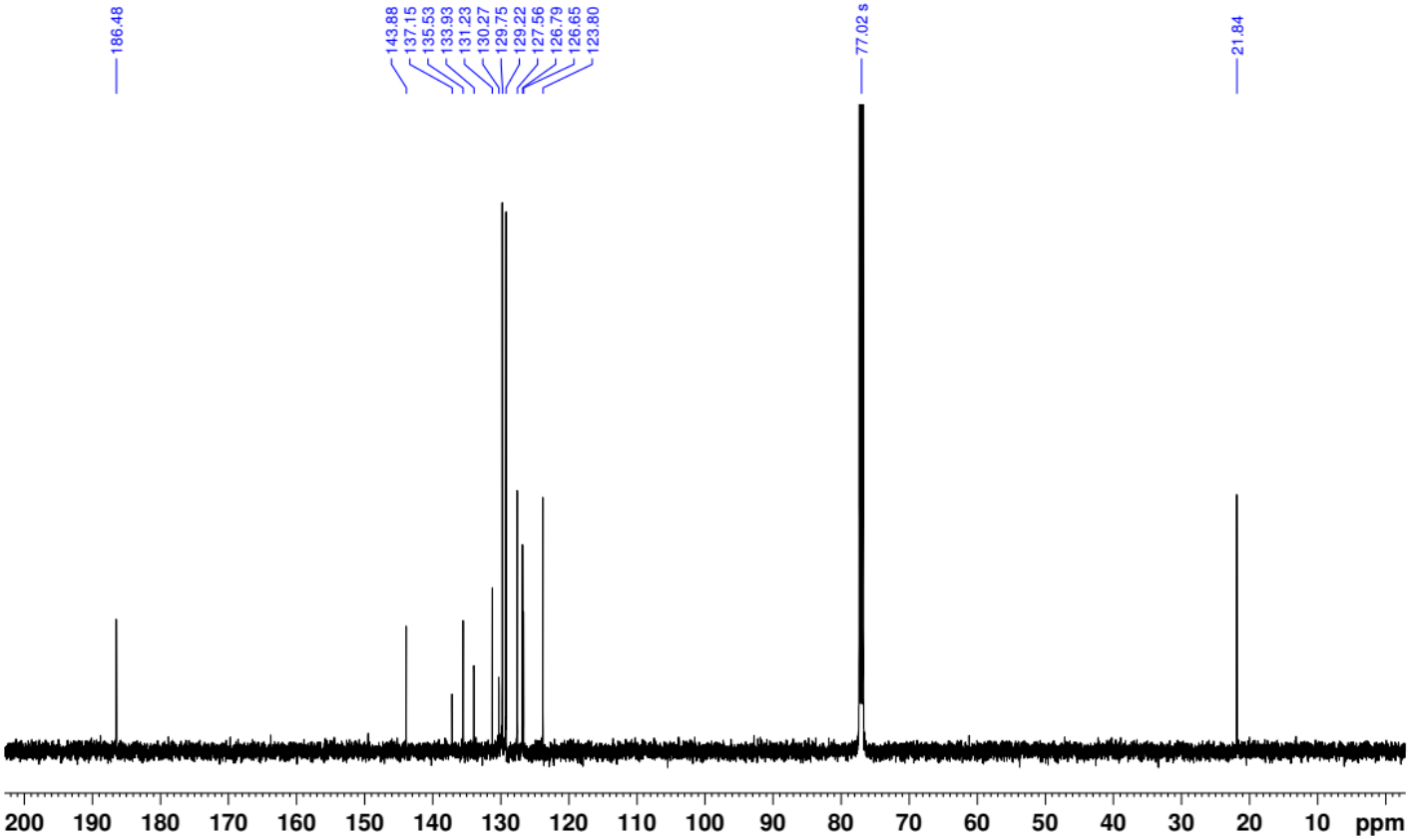

Figure S35. ^{13}C NMR spectrum of **6** (125 MHz, chloroform-*d* , 300 K).

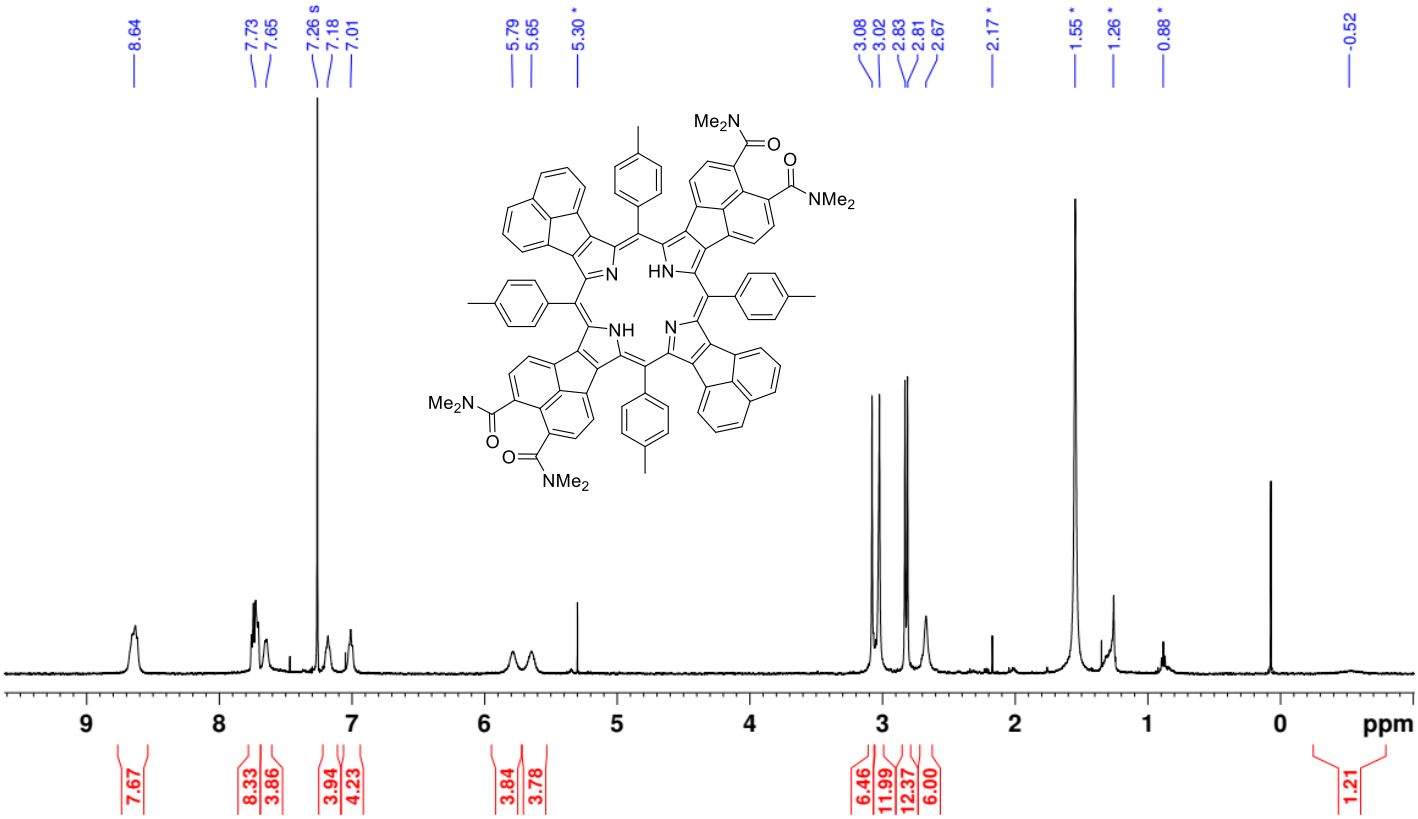

Figure S36. ^{1}H NMR spectrum of **2a**-H_2 (500 MHz, chloroform-*d* , 300 K).

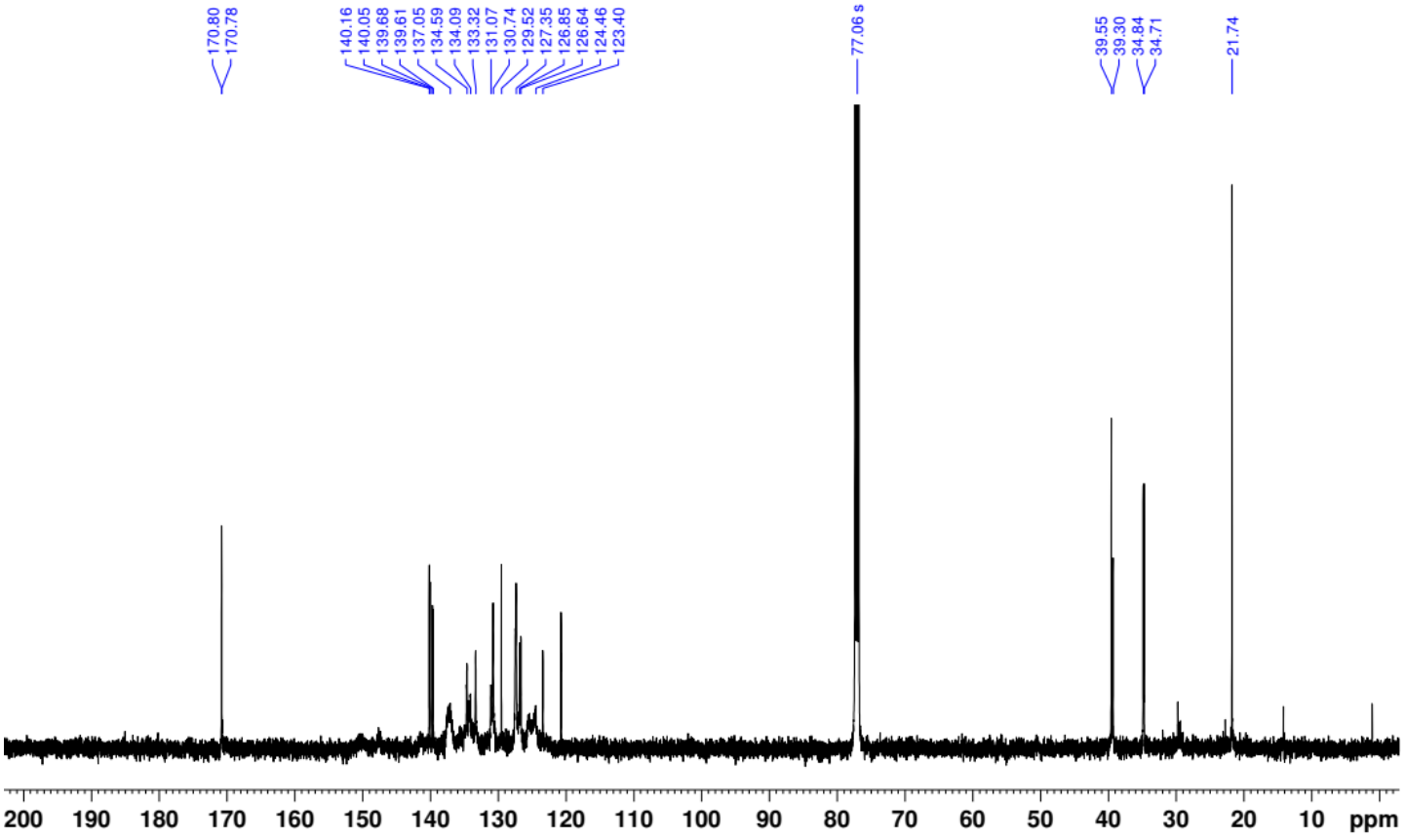

Figure S37. ^{13}C NMR spectrum of **2a**-H_2 (151 MHz, chloroform-*d* , 300 K).

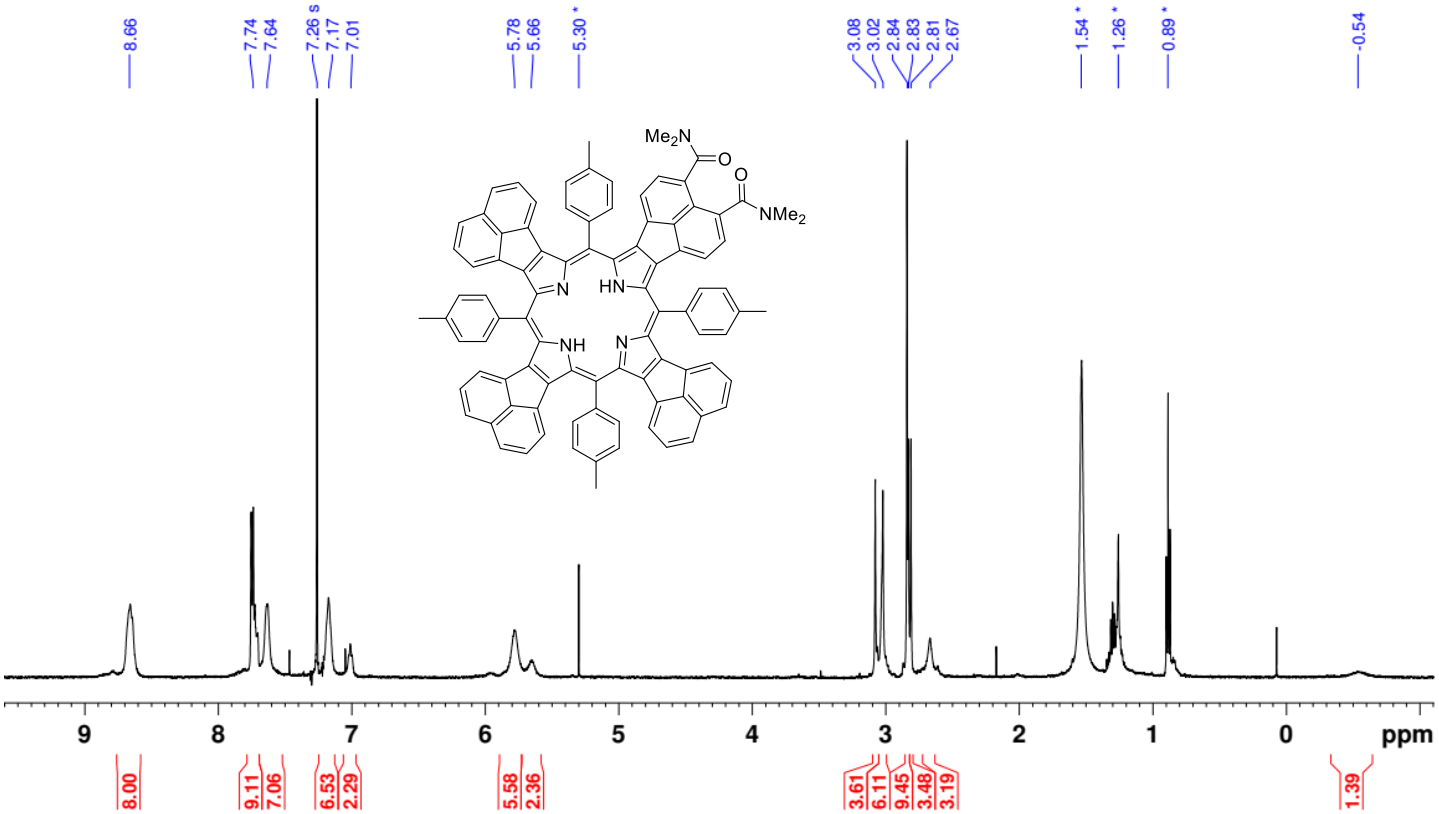

Figure S38. ^{1}H NMR spectrum of **3a**-H_2 (500 MHz, chloroform-*d* , 300 K).

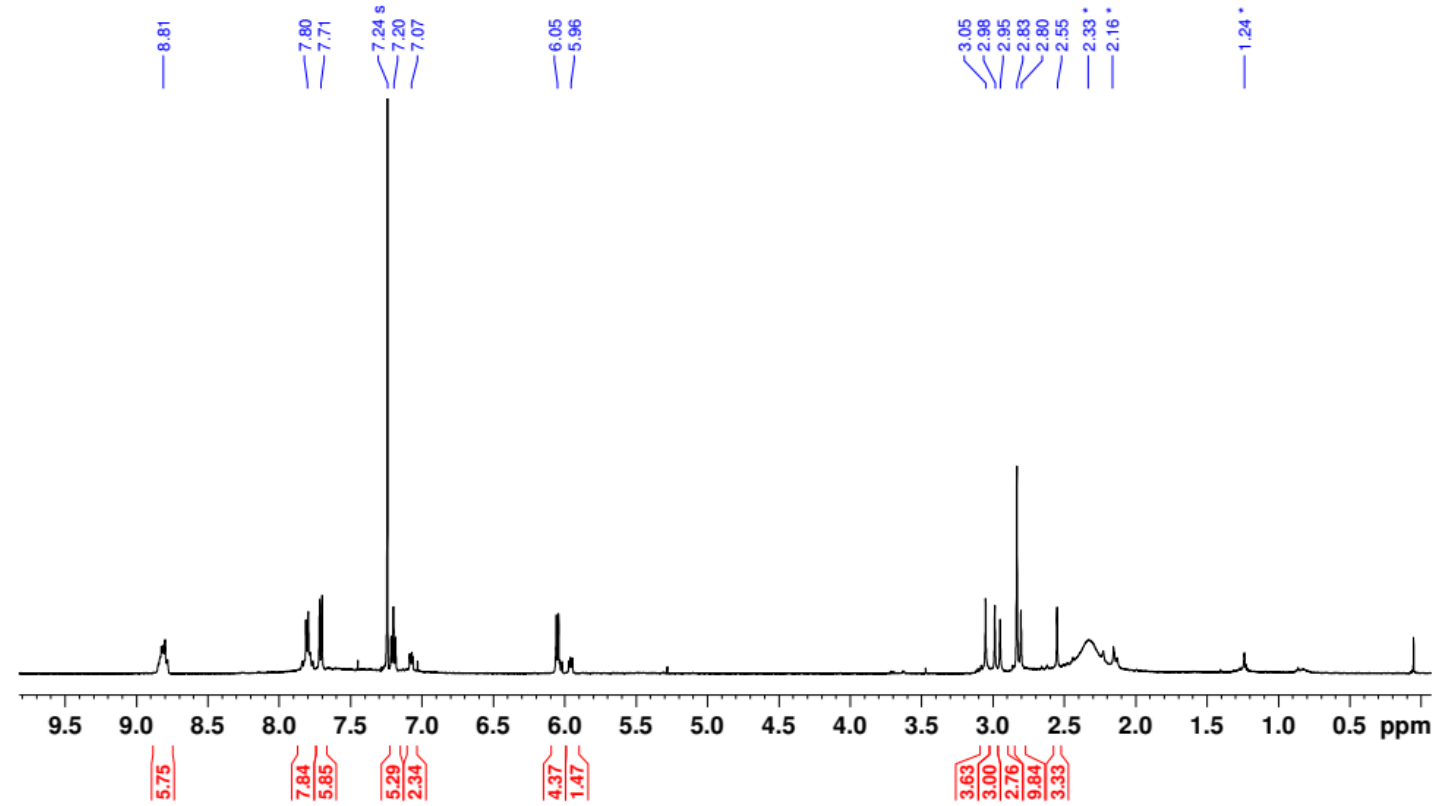

Figure S39. ^{1}H NMR spectrum of **3a**-H_2 + TFA (500 MHz, chloroform-*d* , 300 K).

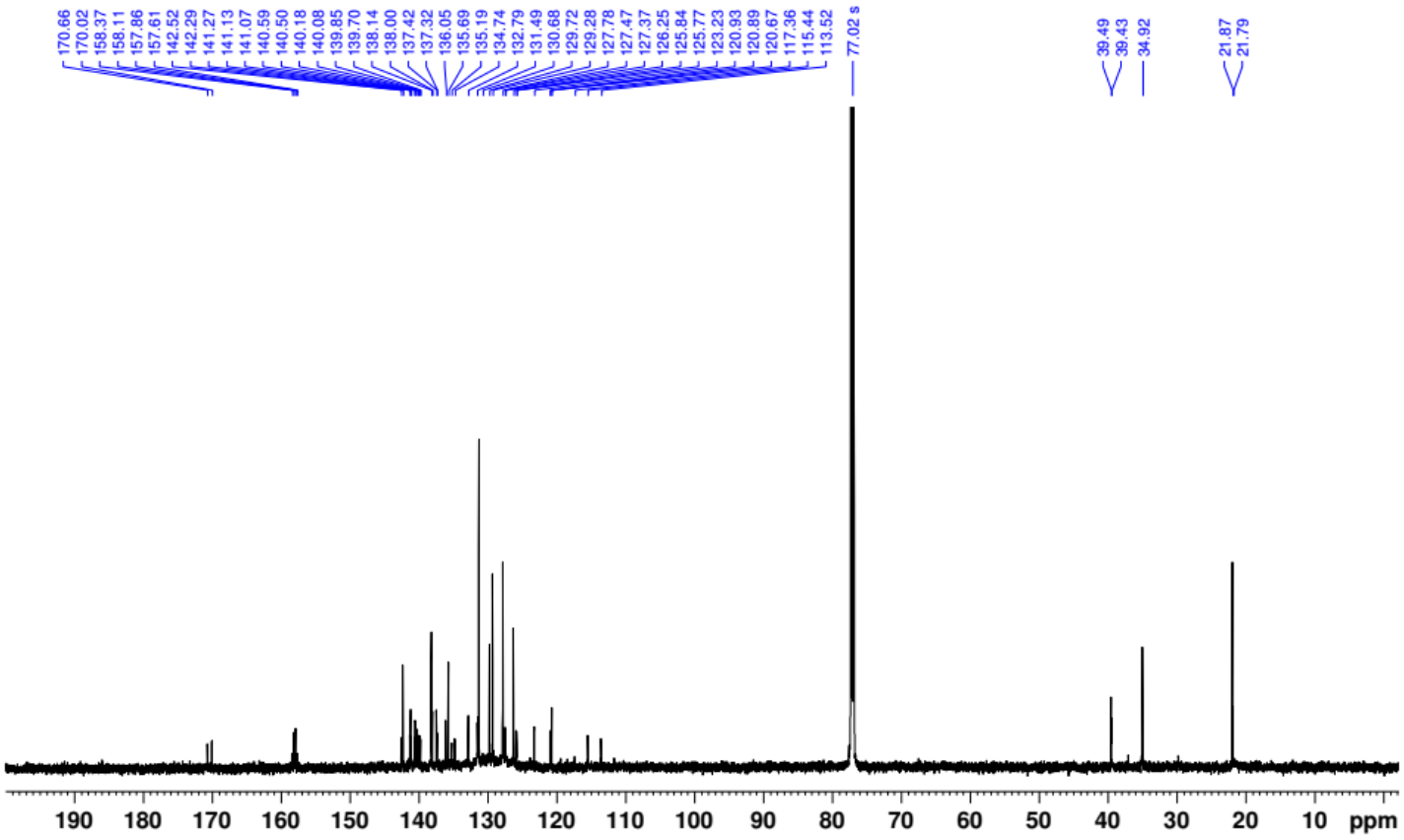

Figure S40. ^{13}C NMR spectrum of **3a**-H_2 + TFA (151 MHz, chloroform-*d* , 300 K).

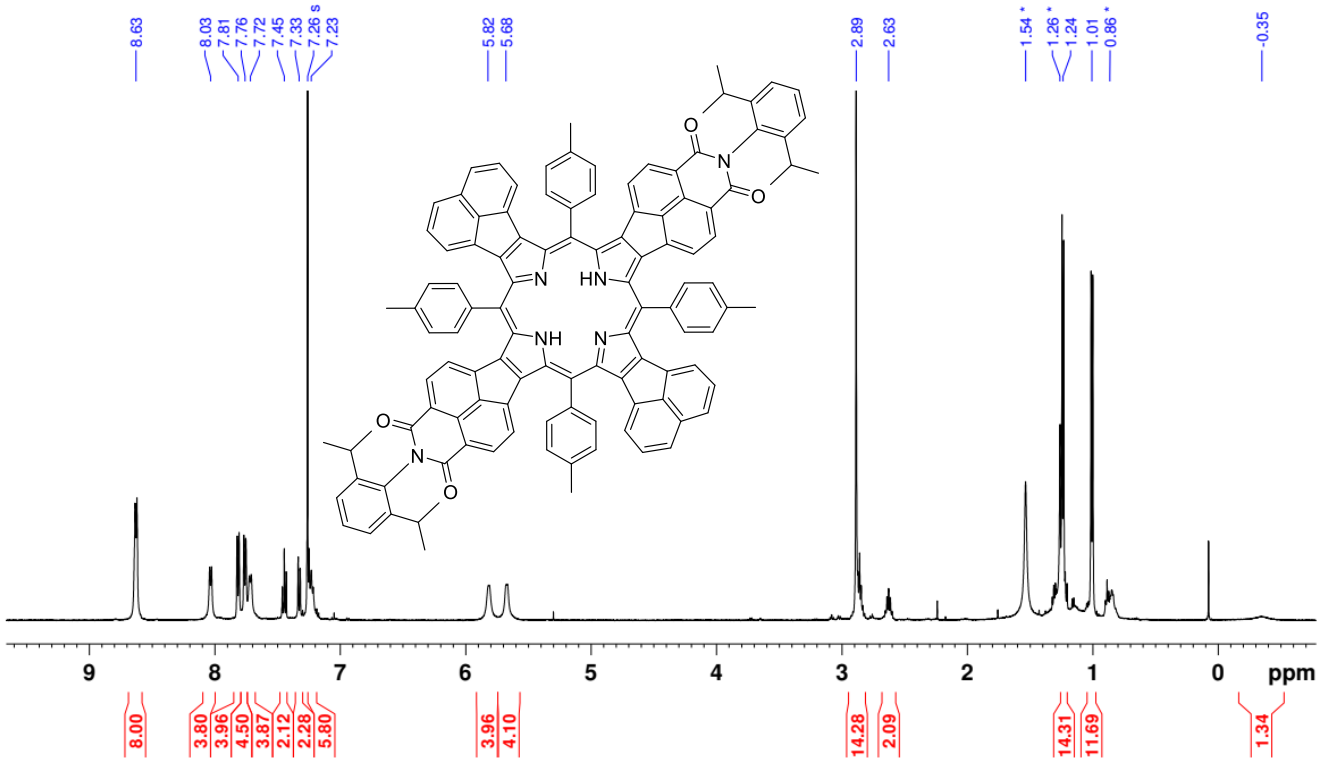

Figure S41. ^{1}H NMR spectrum of **2b**-H_2 (500 MHz, chloroform-*d* , 300 K).

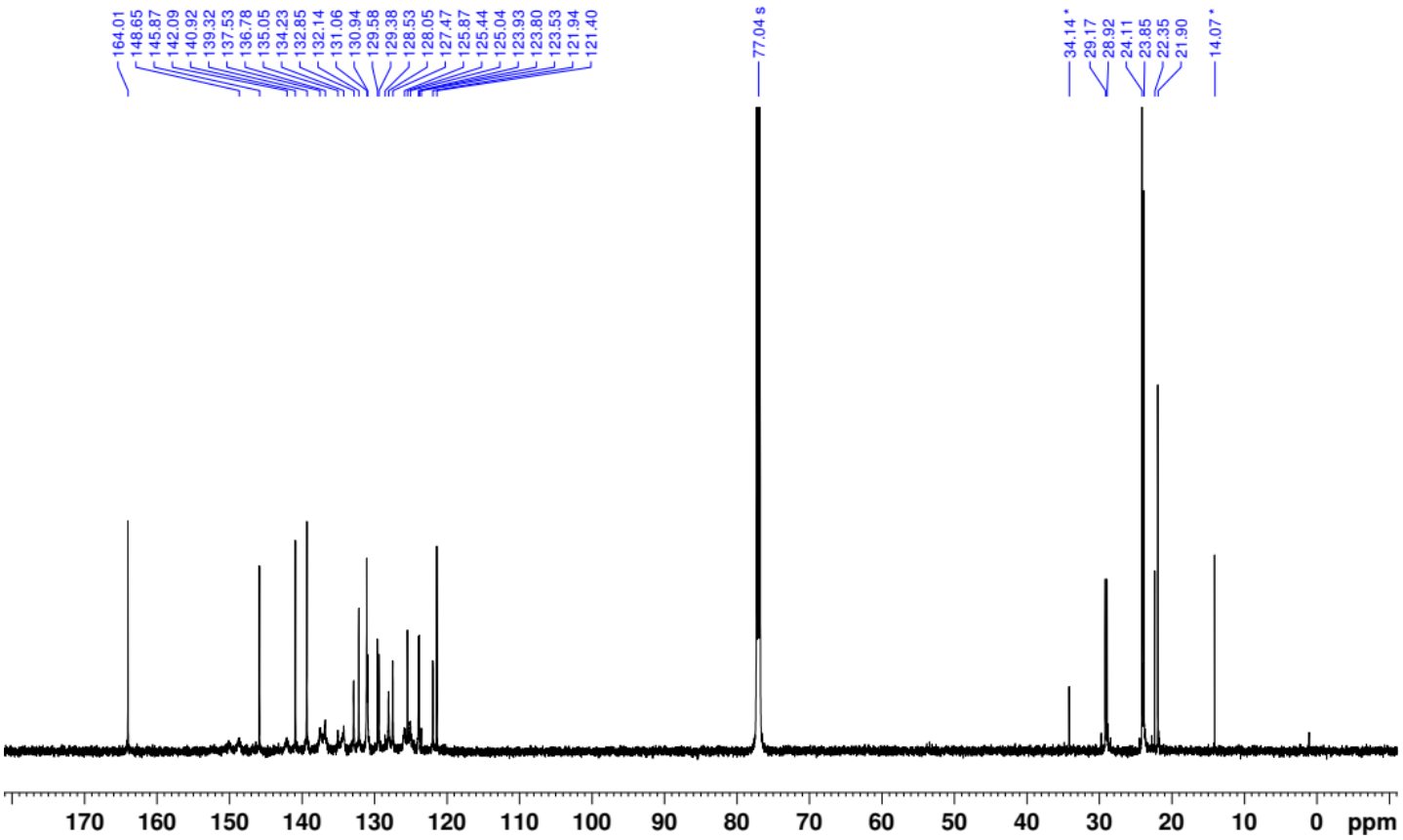

Figure S42. ^{13}C NMR spectrum of **2b**-H_2 (151 MHz, chloroform-*d* , 300 K).

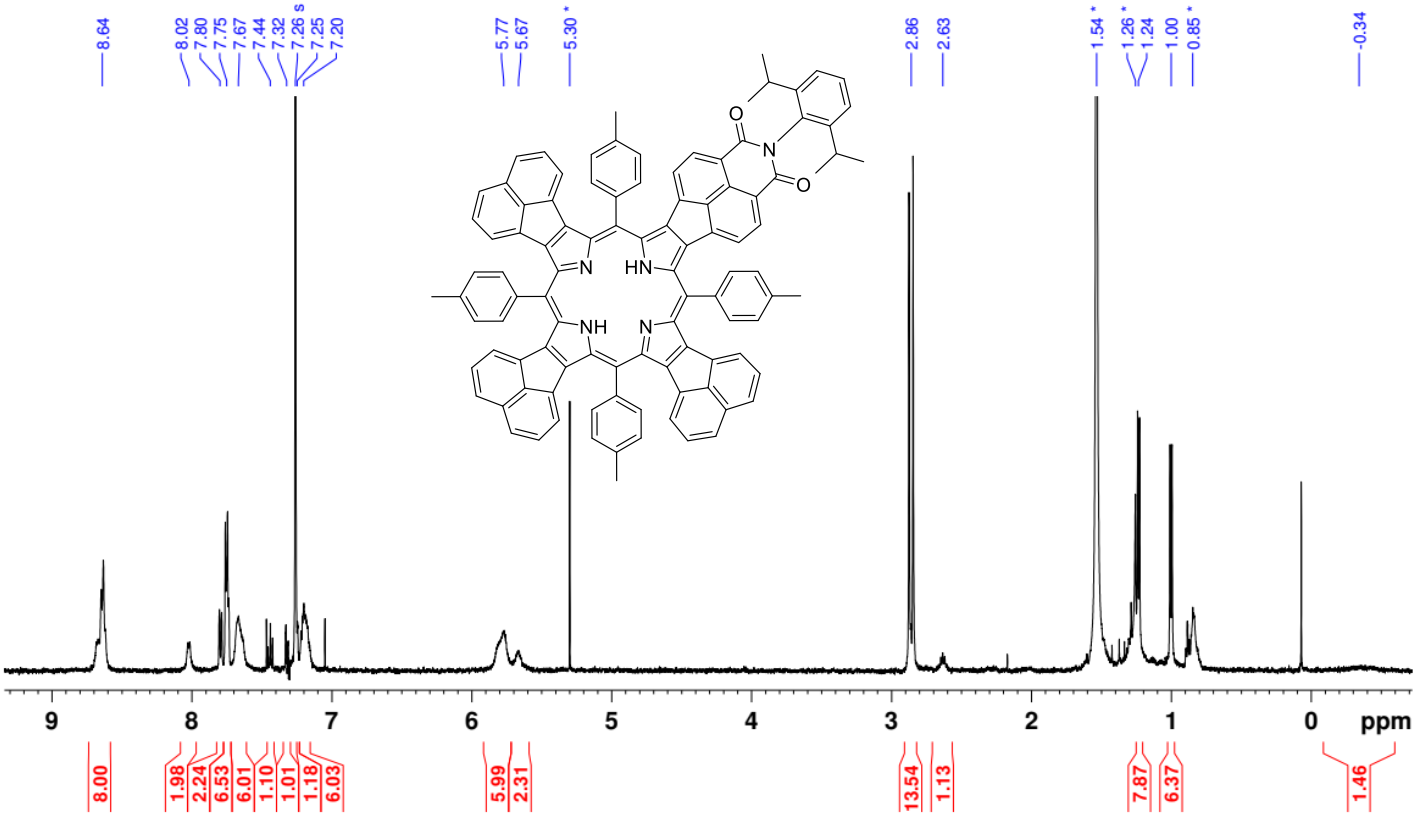

Figure S43. ^{1}H NMR spectrum of **3b**-H_2 (500 MHz, chloroform-*d* , 300 K).

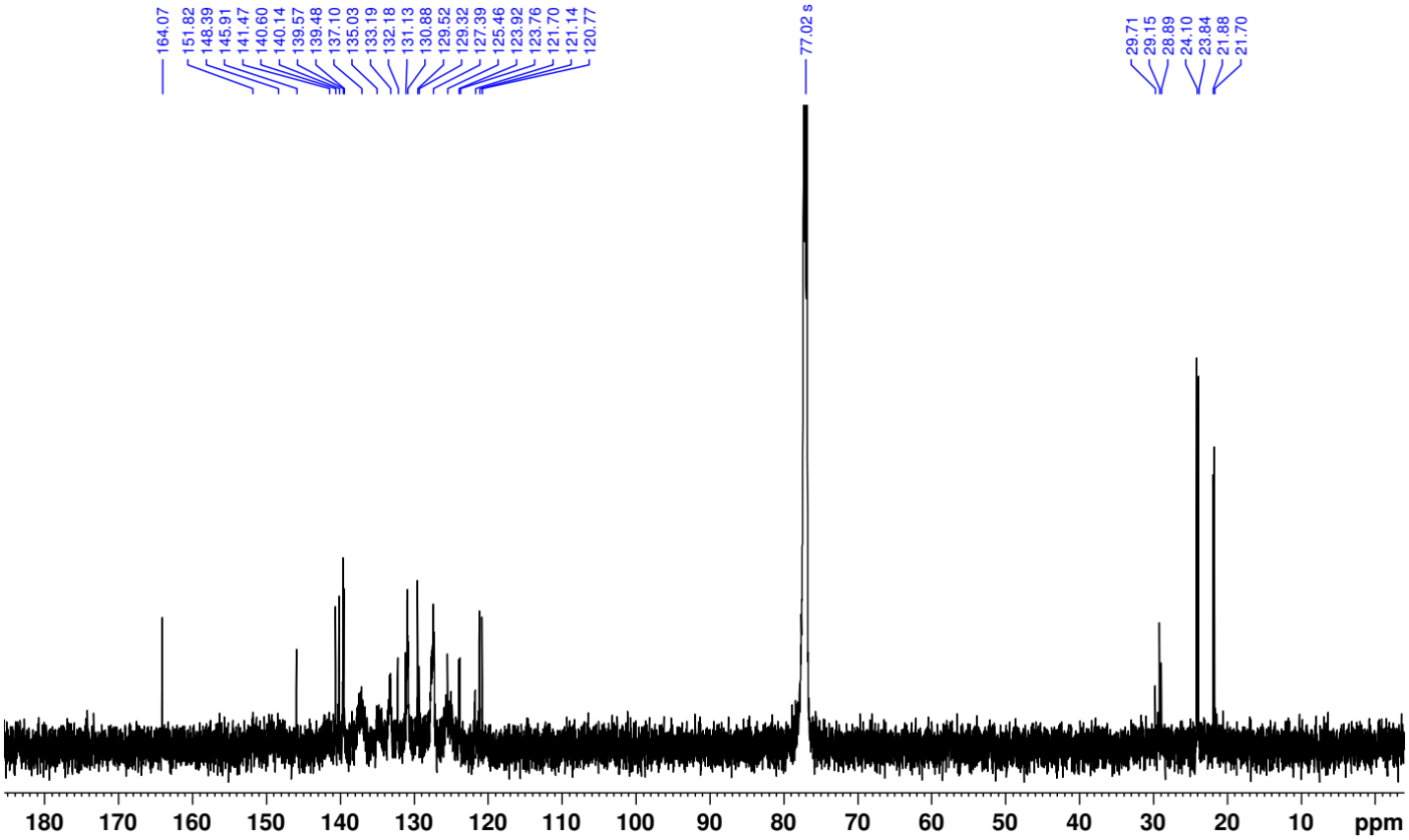

Figure S44. ^{13}C NMR spectrum of **3b**-H_2 (151 MHz, chloroform-*d* , 300 K).

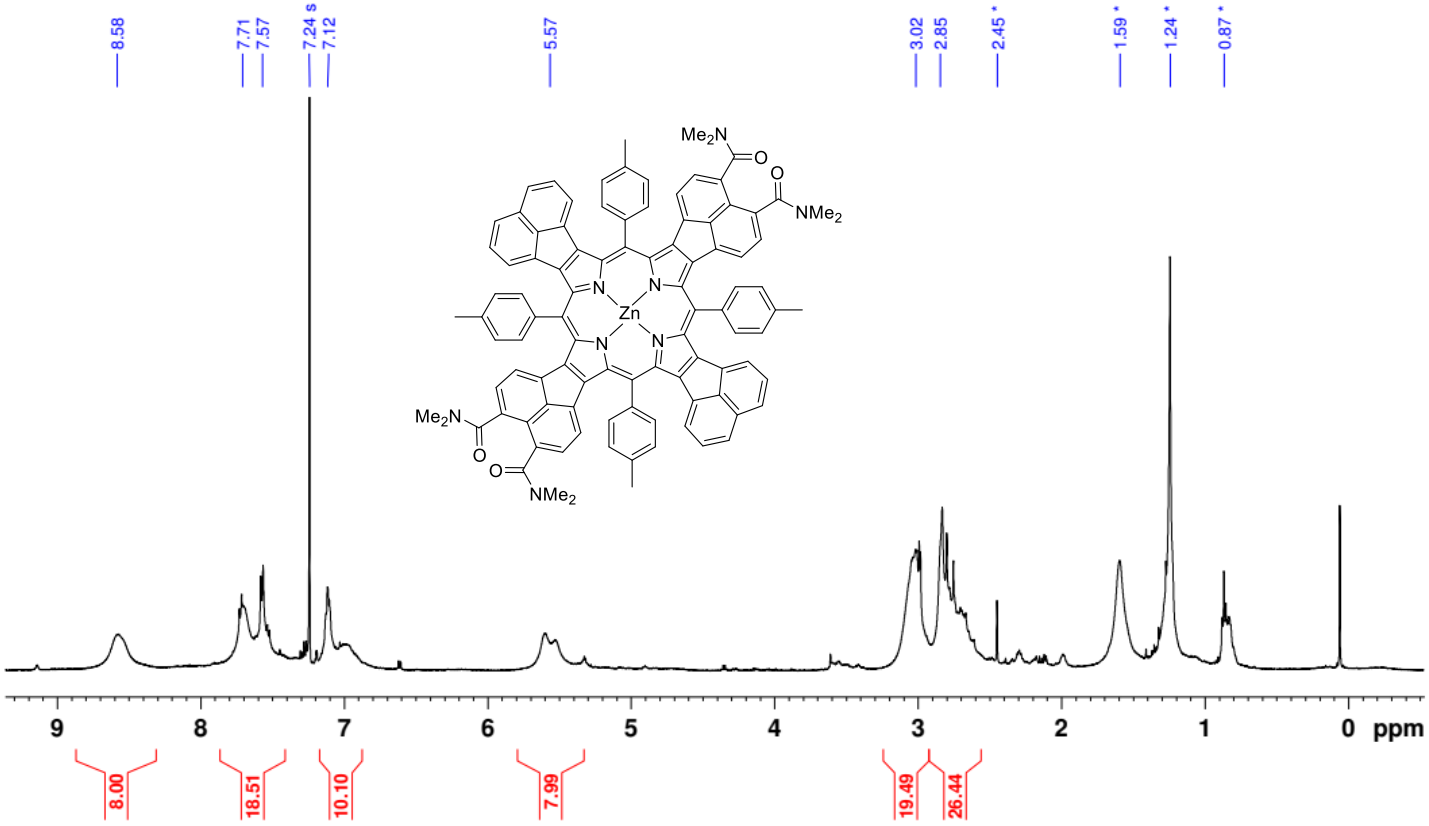

Figure S45. ^{1}H NMR spectrum of **2a**-Zn (500 MHz, chloroform-*d* , 300 K).

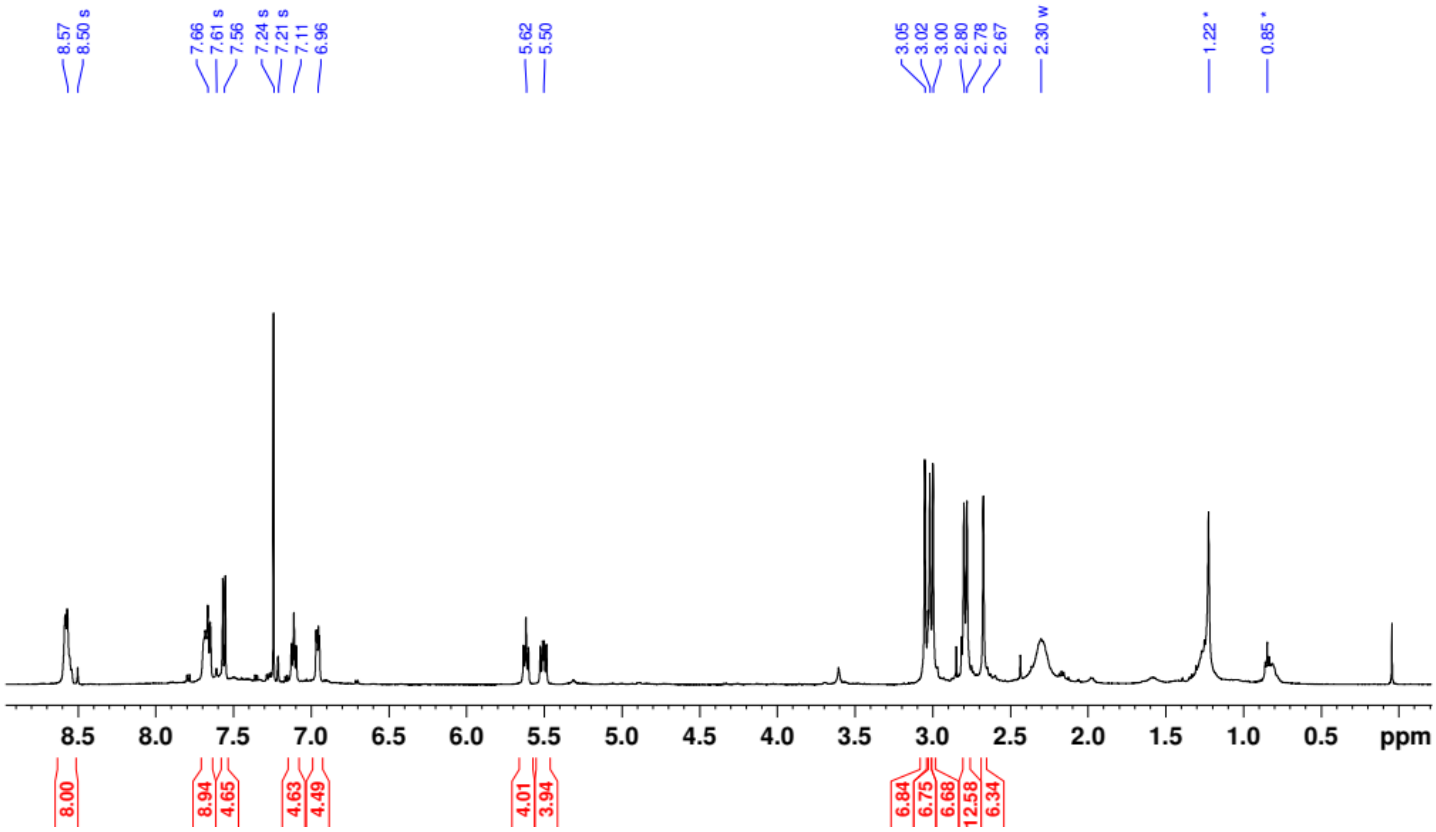

Figure S46. ^{1}H NMR spectrum of **2a**-Zn + Pyridine d_5 (500 MHz, chloroform-*d* , 300 K).

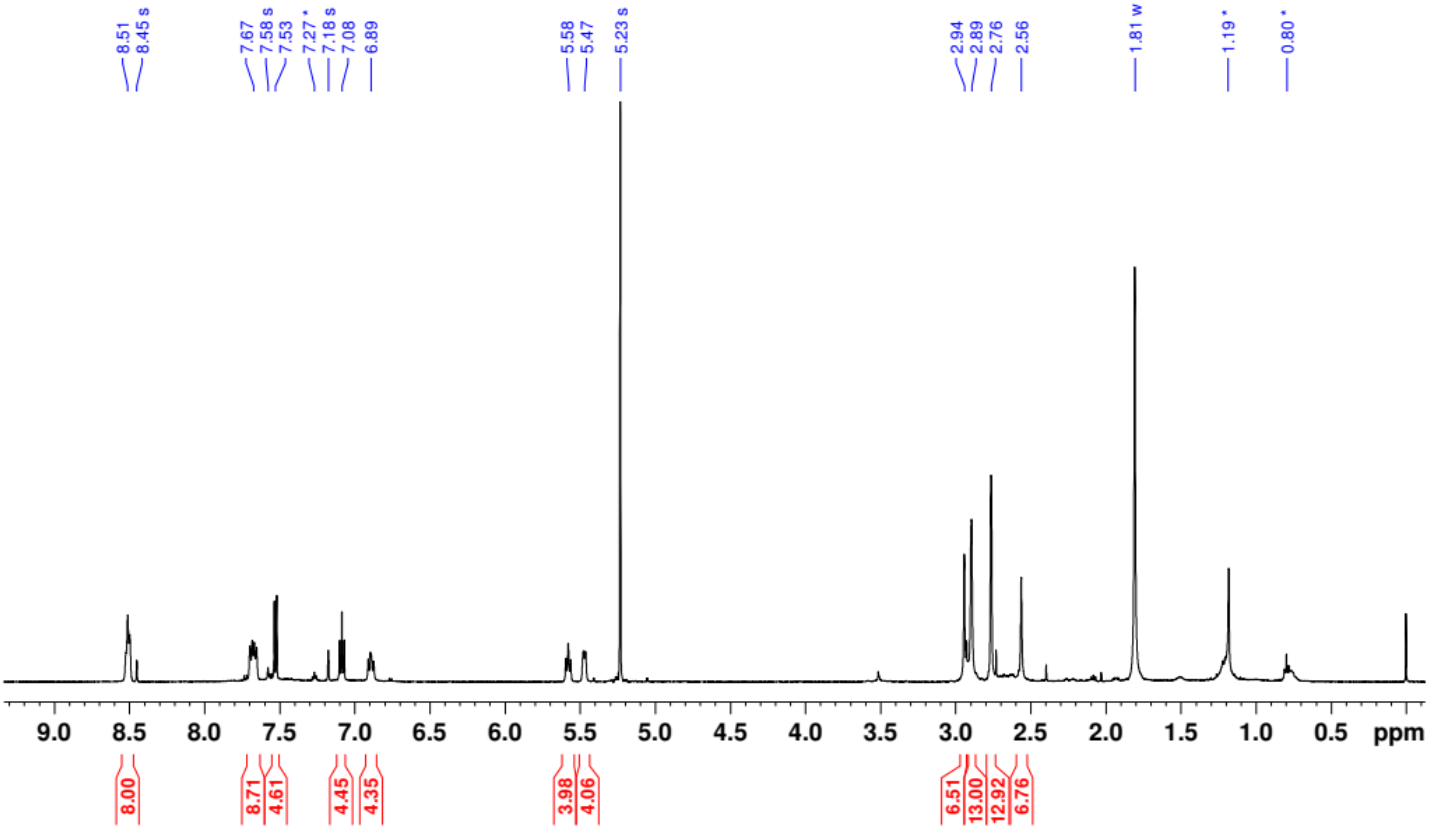

Figure S47. ^{1}H NMR spectrum of **2a**-Zn + Pyridine d_5 (500 MHz, dichloromethane-*d* , 300 K).

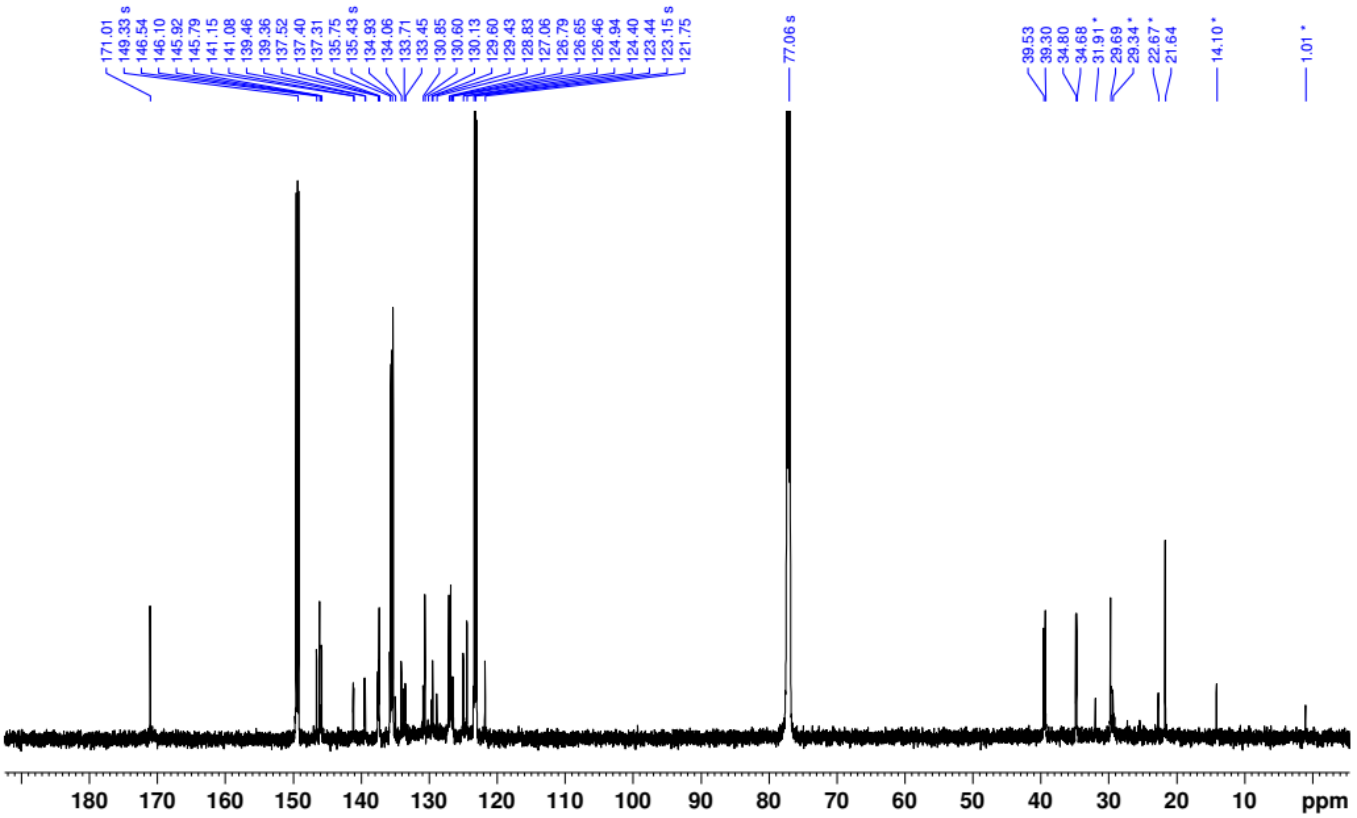

Figure S48. ^{13}C NMR spectrum of **2a**-Zn + Pyridine d_5 (151 MHz, chloroform-*d* , 300 K).

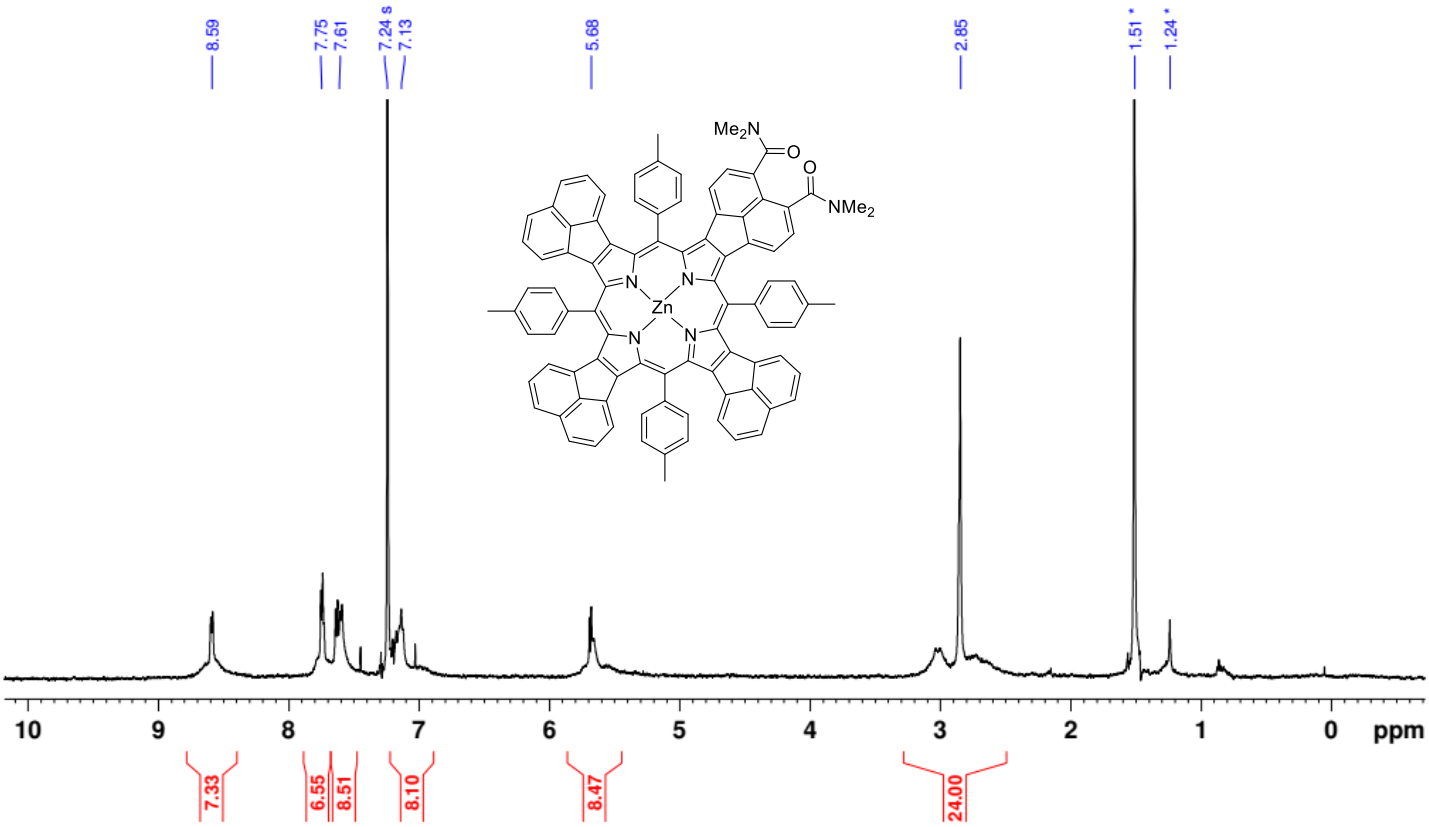

Figure S49. ^{1}H NMR spectrum of **3a**-Zn (500 MHz, chloroform-*d* , 300 K).

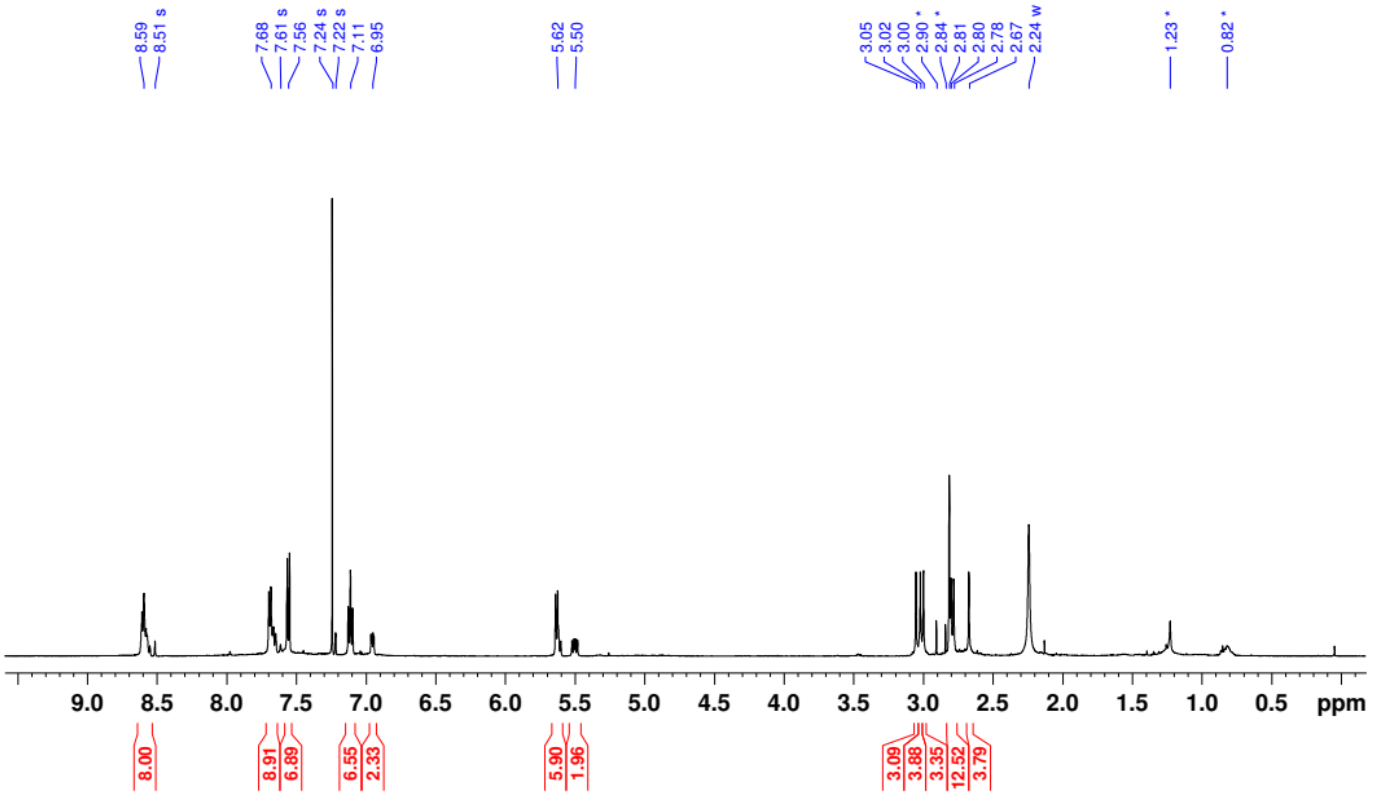

Figure S50. ^{1}H NMR spectrum of **3a**-Zn + pyridine d_5 (500 MHz, chloroform-*d* , 300 K).

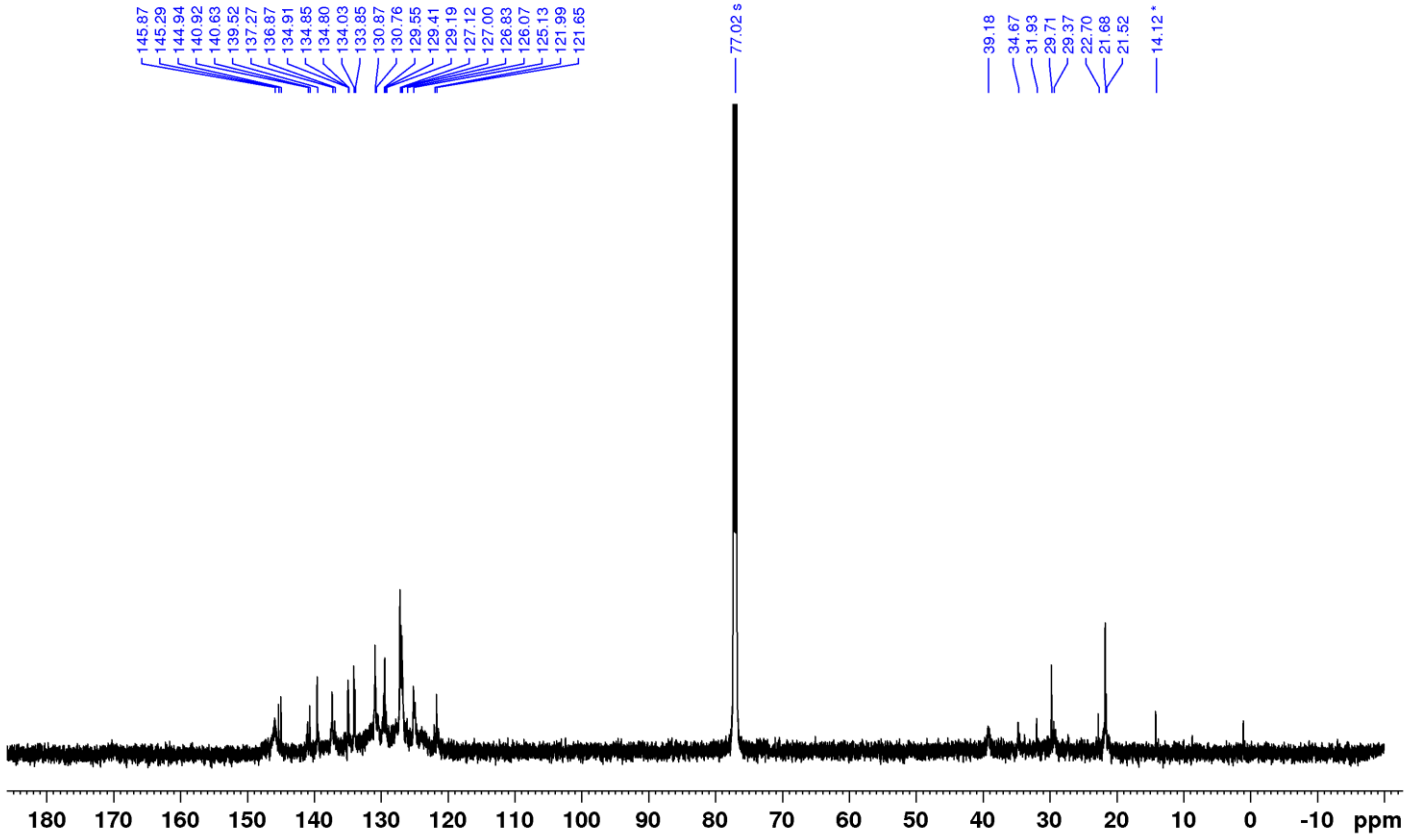

Figure S51. ^{13}C NMR spectrum of **3a**-Zn (151 MHz, chloroform-*d* , 300 K).

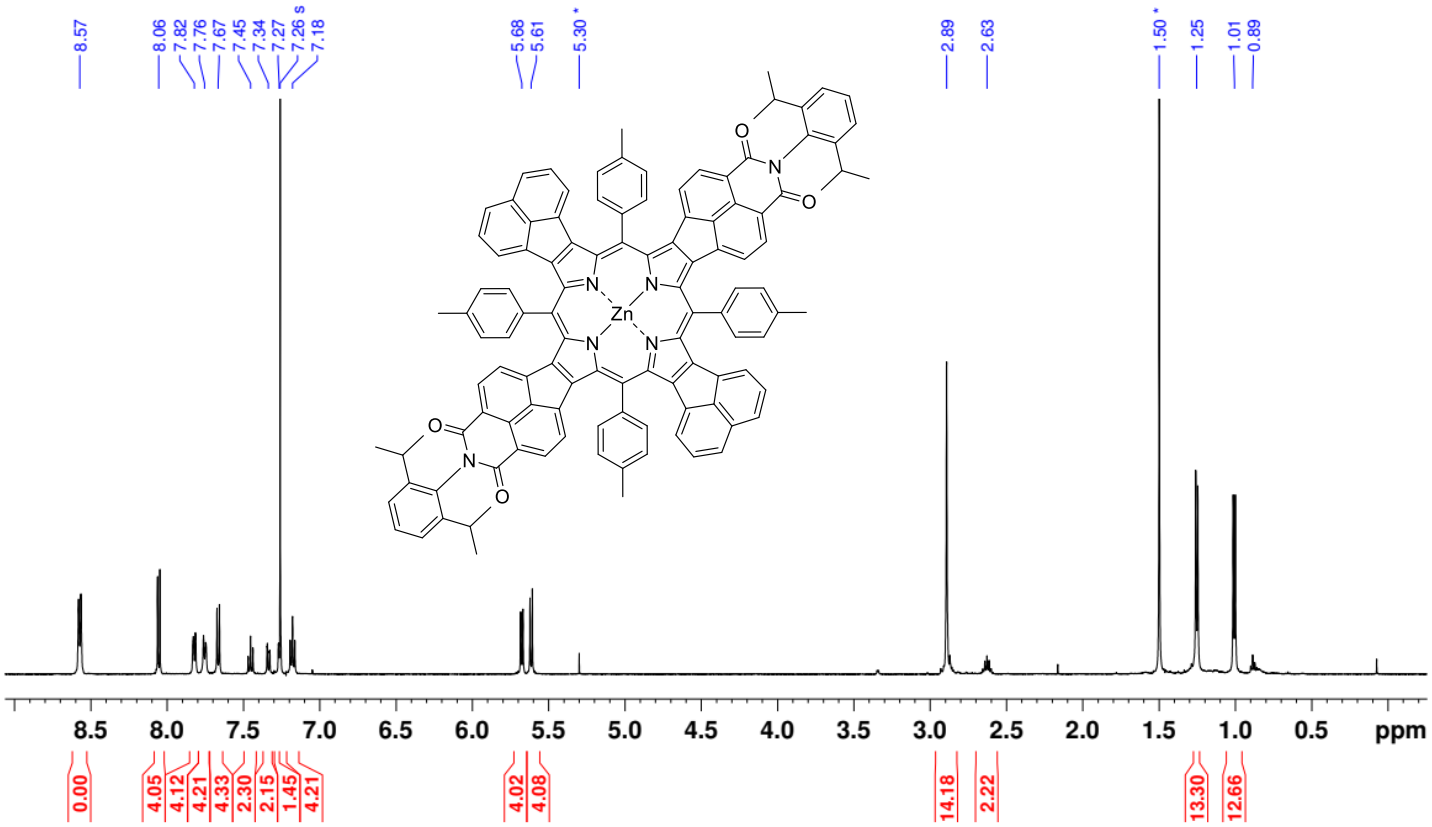

Figure S52. ^{1}H NMR spectrum of **2b**-Zn (500 MHz, chloroform-*d* , 300 K).

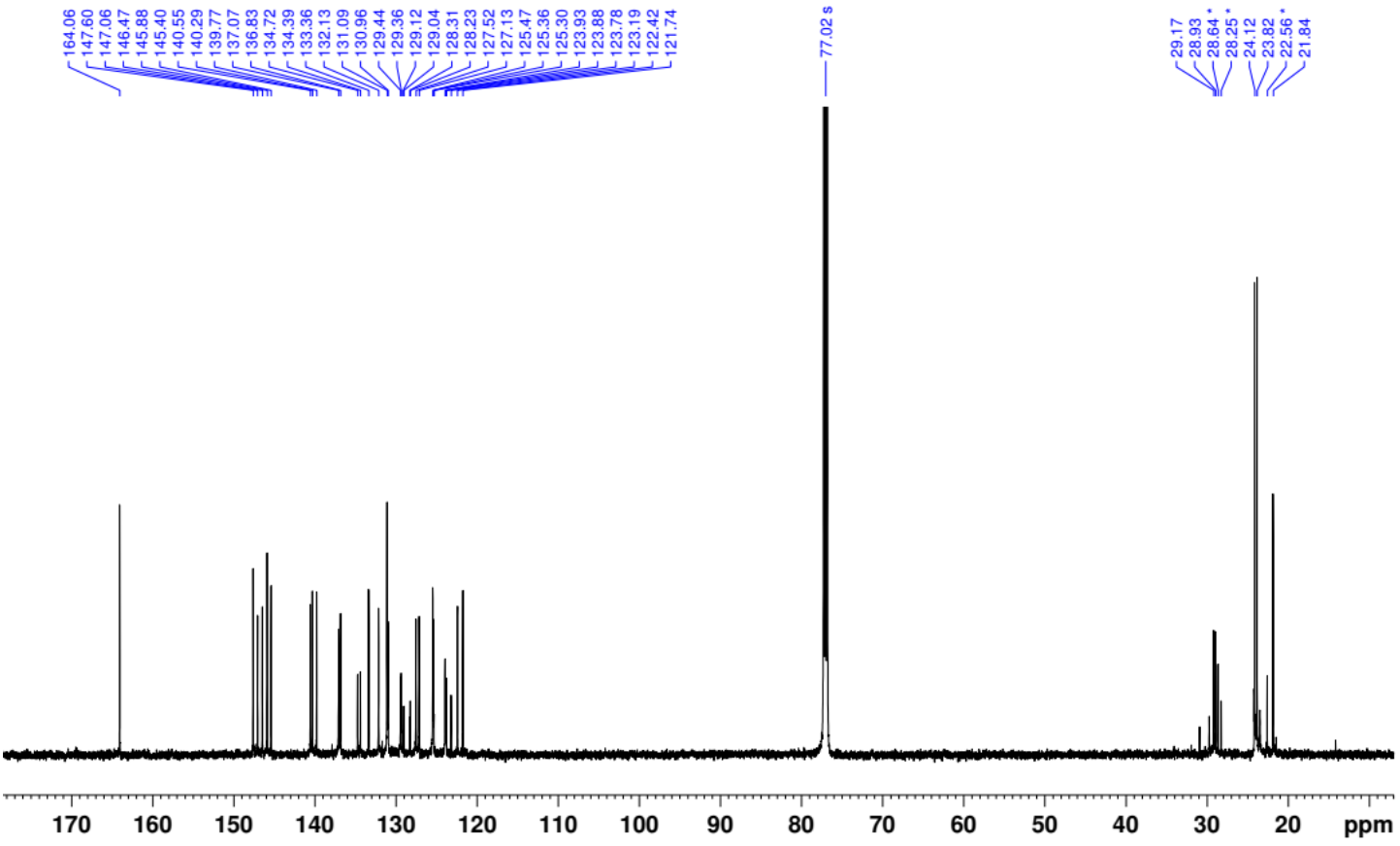

Figure S53. ^{13}C NMR spectrum of **2b**-Zn (151 MHz, chloroform-*d* , 300 K).

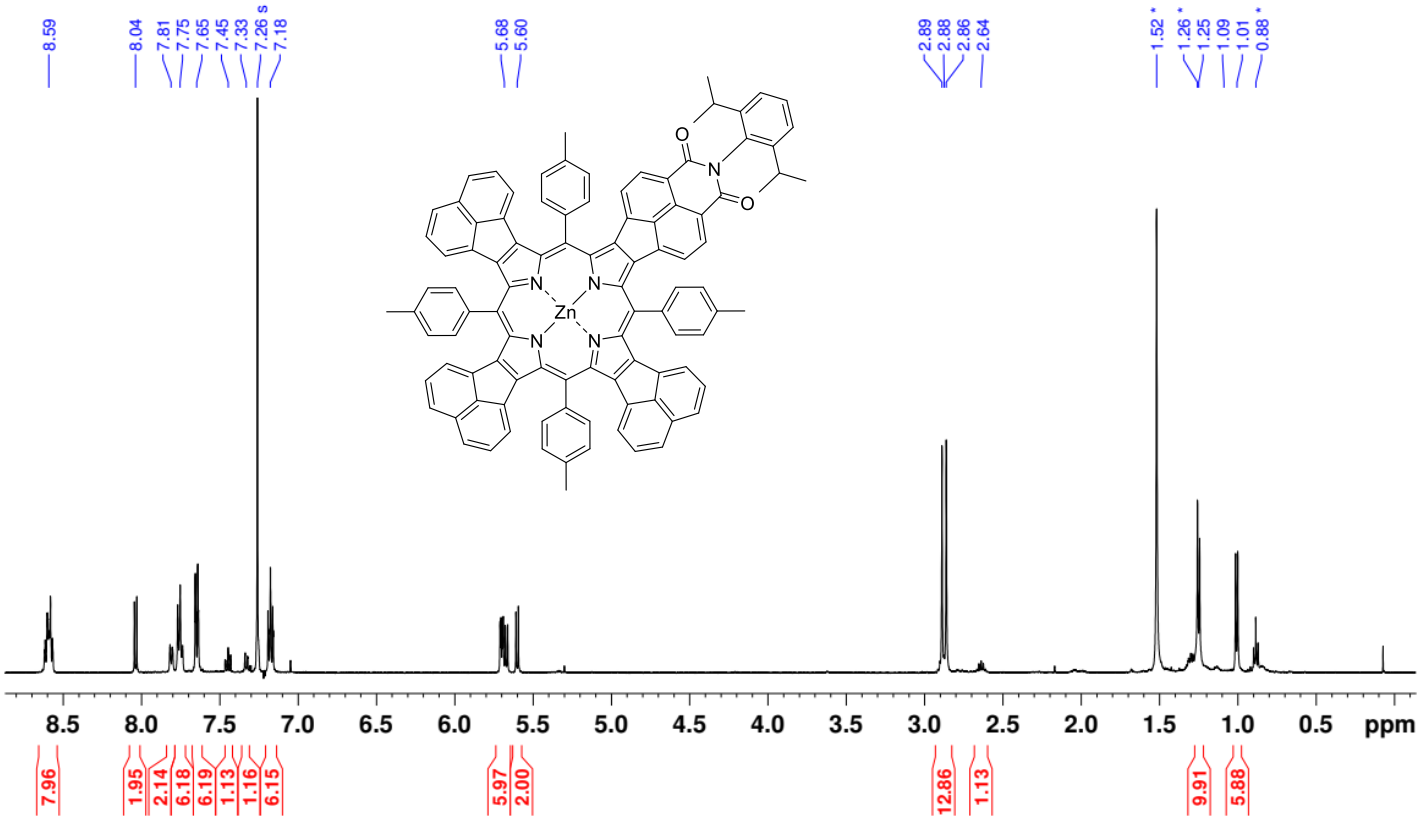

Figure S54. ^{1}H NMR spectrum of **3b**-Zn (500 MHz, chloroform-*d* , 300 K).

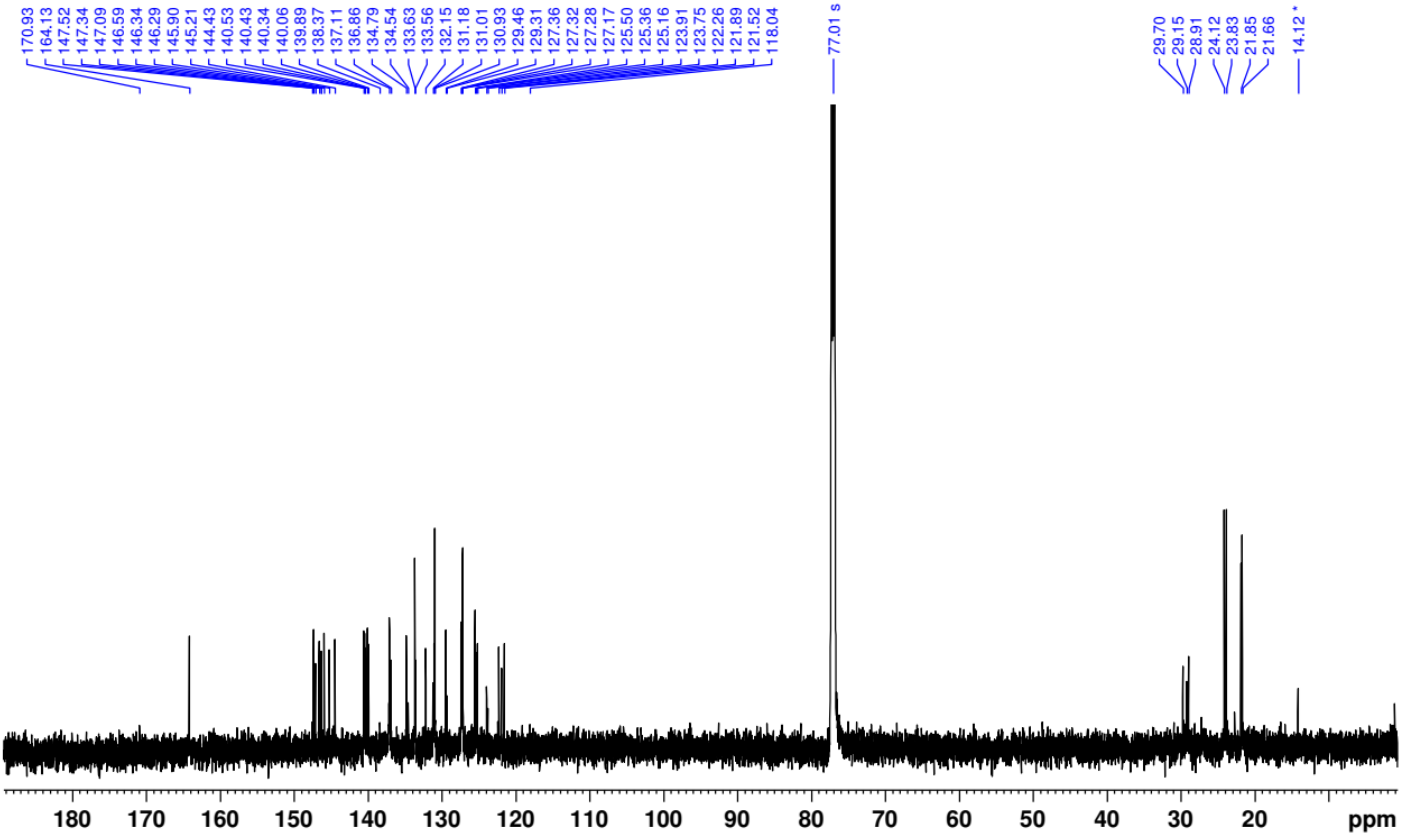

Figure S55. ^{13}C NMR spectrum of **3b**-Zn (151 MHz, chloroform-*d* , 300 K).

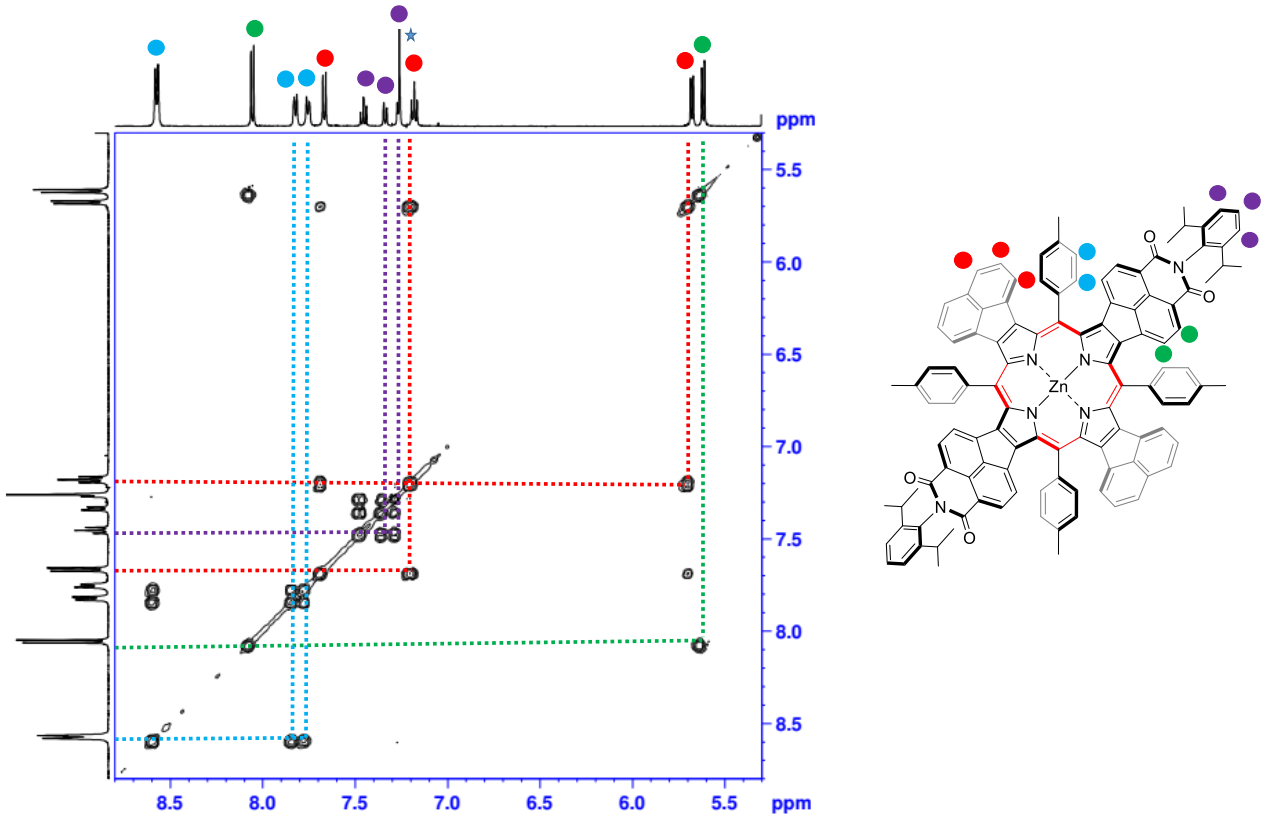

Figure S56. ^{1}H-^{1}H COSY NMR spectrum of **2b**-Zn (500 MHz, chloroform-*d* , 300 K).

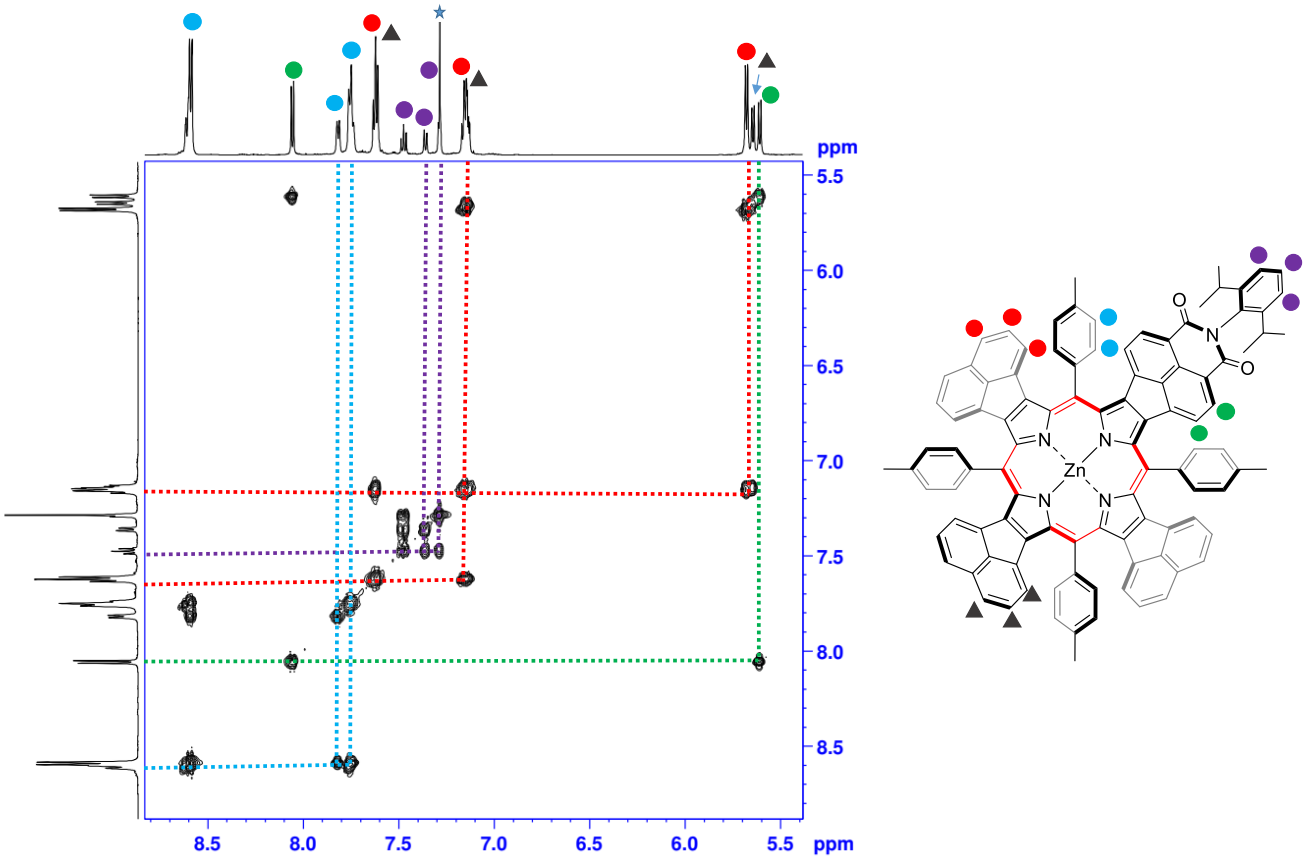

Figure S57. ^{1}H-^{1}H COSY NMR spectrum of **3b**-Zn (500 MHz, chloroform-*d* , 300 K).

Mass Spectra

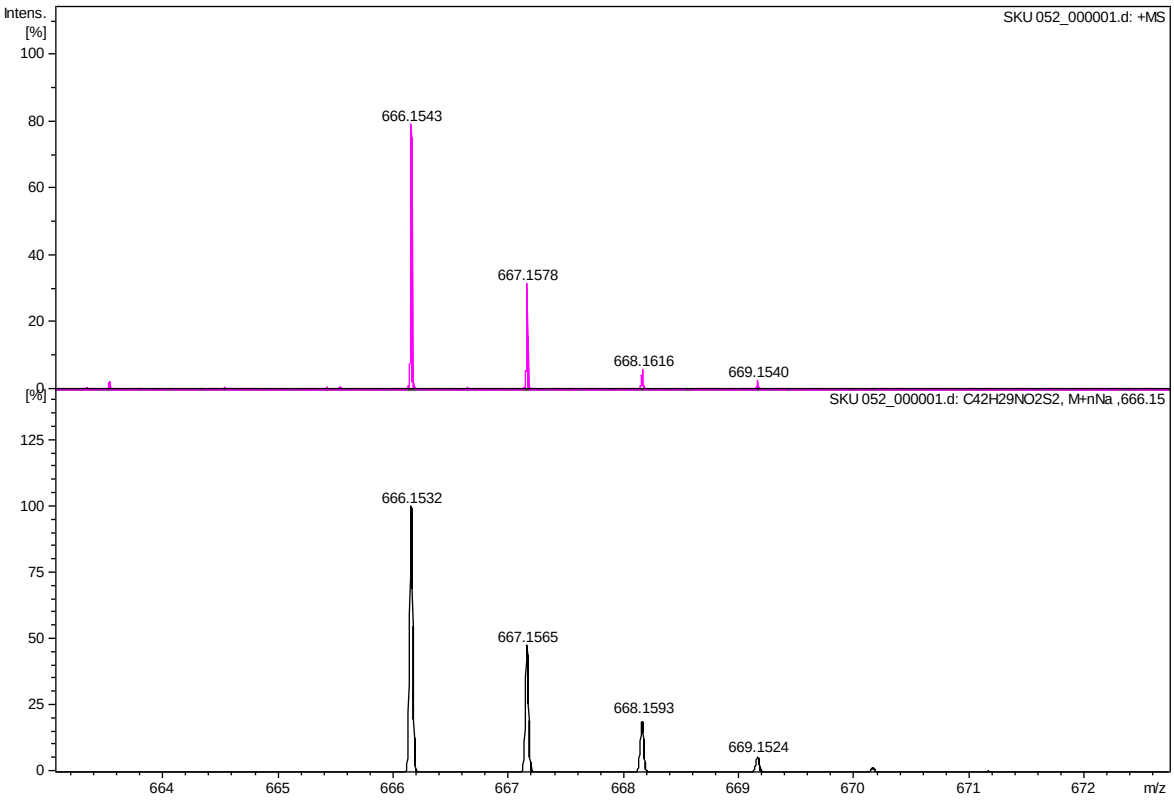

Figure S58. High resolution mass spectrum of **5** (ESI–TOF, top: experimental, bottom: simulated).

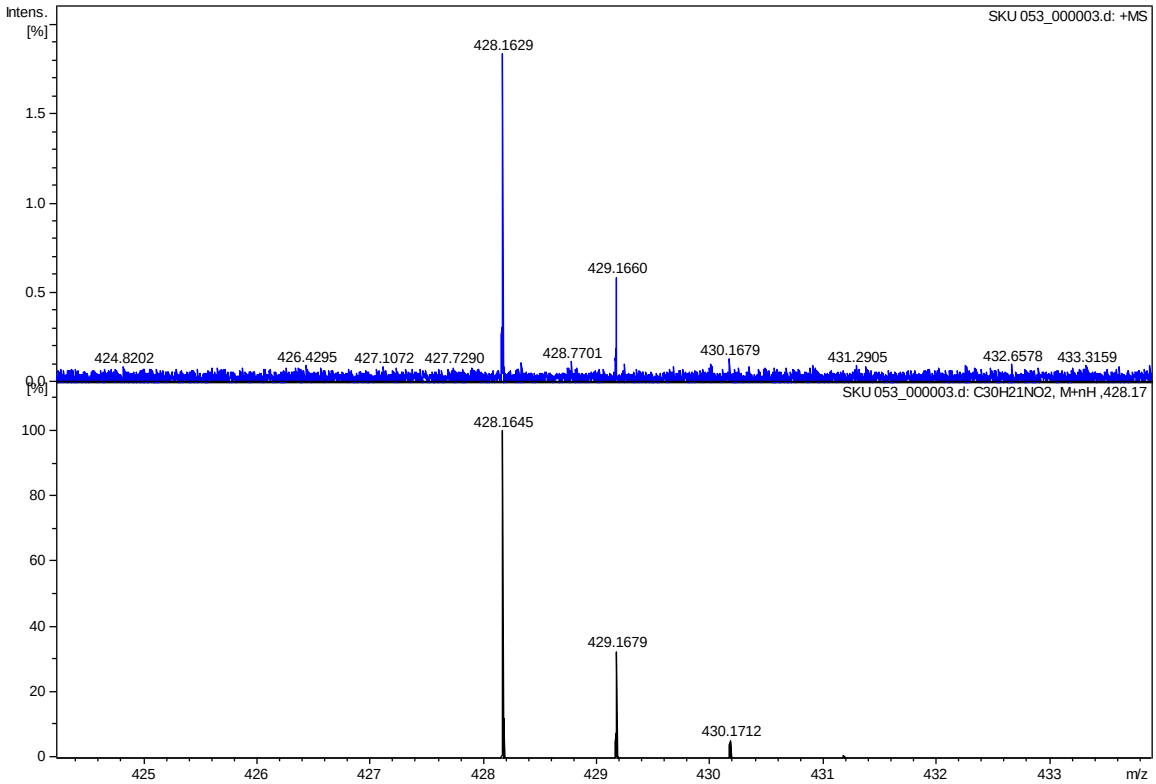

Figure S59. High resolution mass spectrum of **6** (ESI–TOF, top: experimental, bottom: simulated).

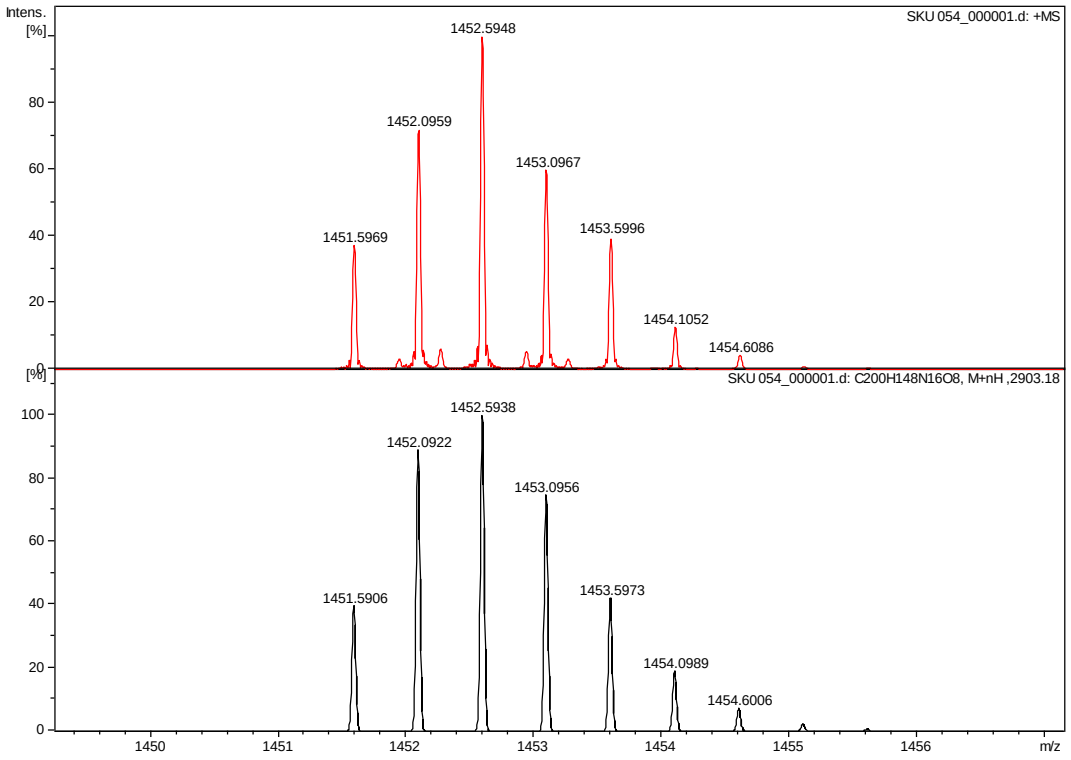

Figure S60. High resolution mass spectrum of **2a**-H_2 (ESI–TOF, top: experimental, bottom: simulated).

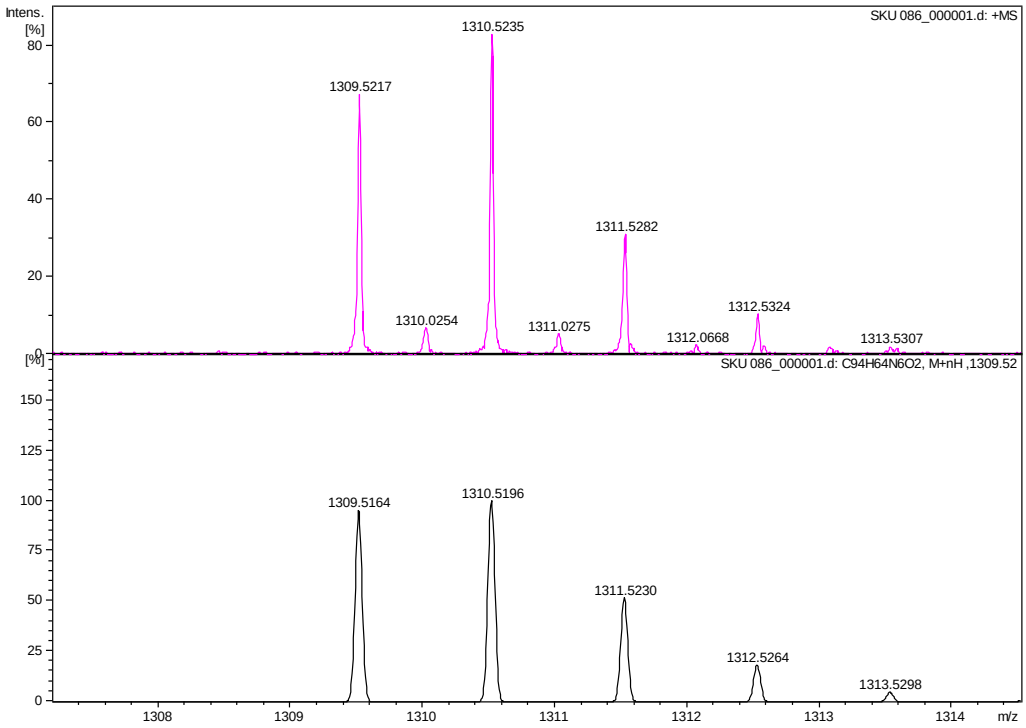

Figure S61. High resolution mass spectrum of **3a**-H_2 (ESI–TOF, top: experimental, bottom: simulated).

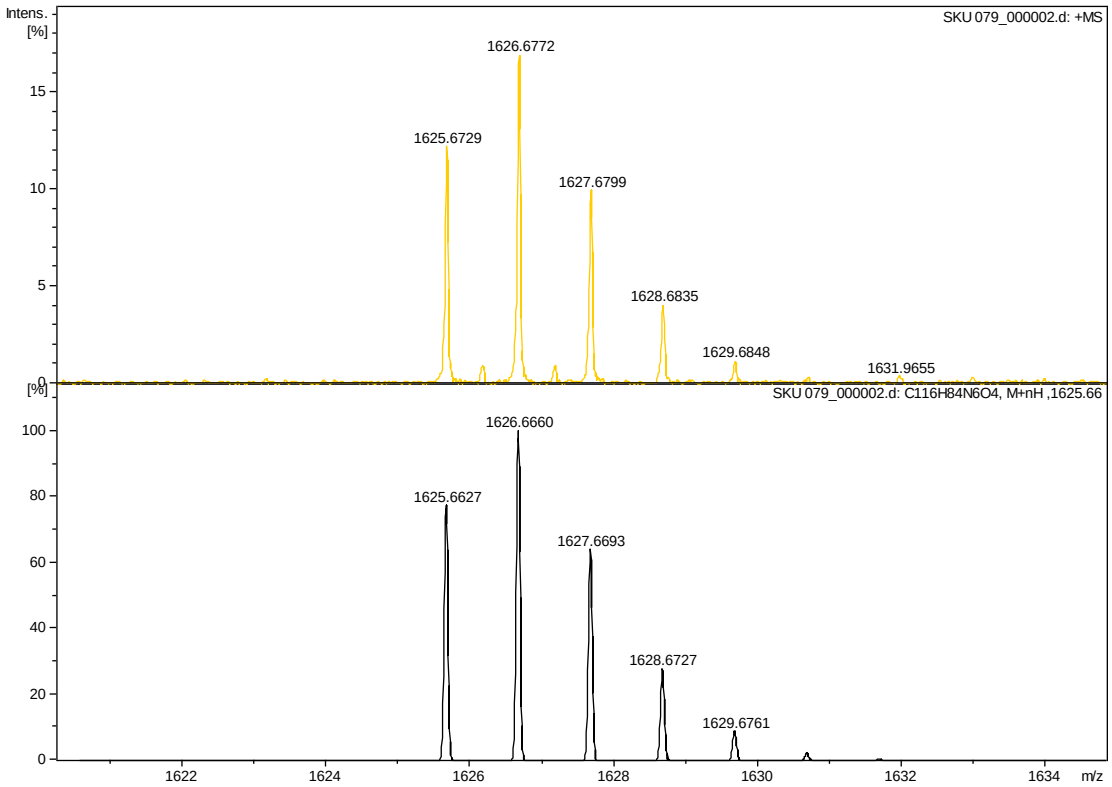

Figure S62. High resolution mass spectrum of **2b**-H_2 (ESI–TOF, top: experimental, bottom: simulated).

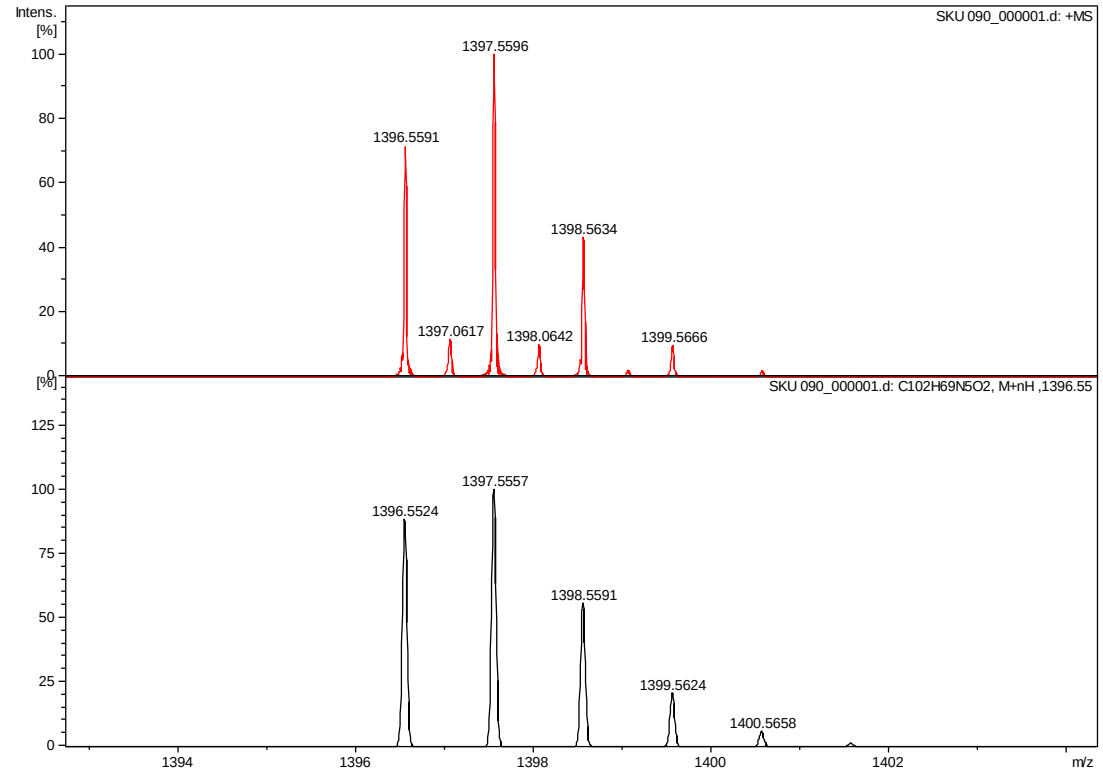

Figure S63. High resolution mass spectrum of **3b**-H_2 (ESI–TOF, top: experimental, bottom: simulated).

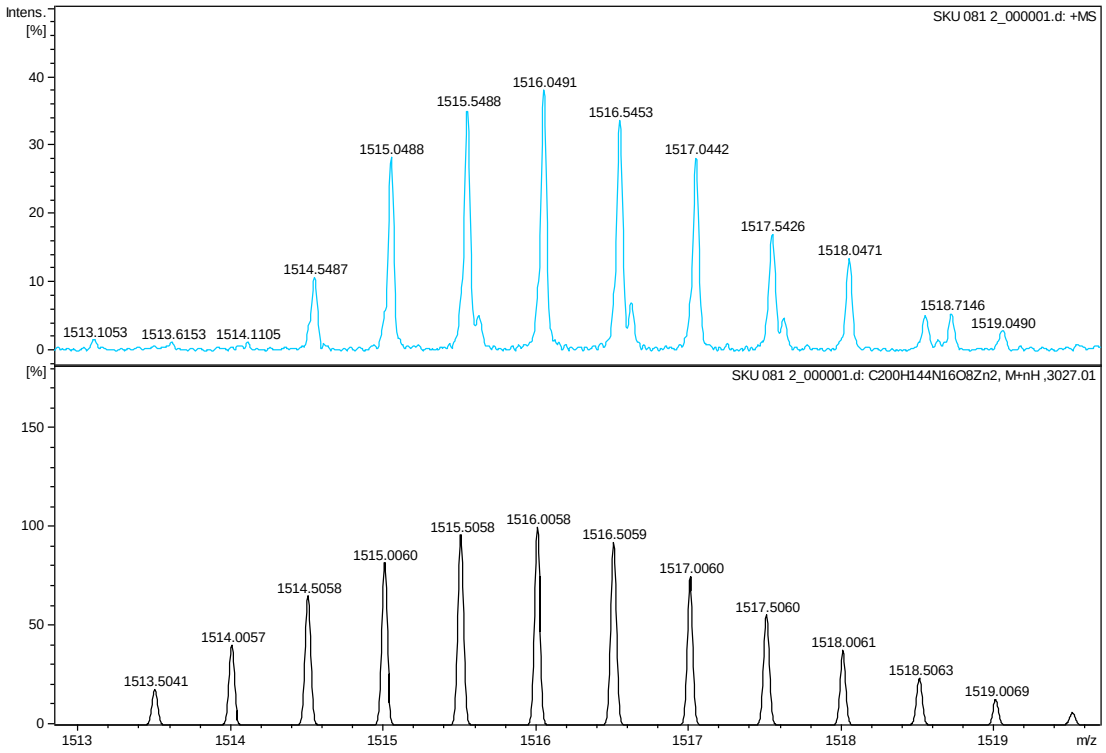

Figure S64. High resolution mass spectrum of **2a**-Zn (ESI–TOF, top: experimental, bottom: simulated).

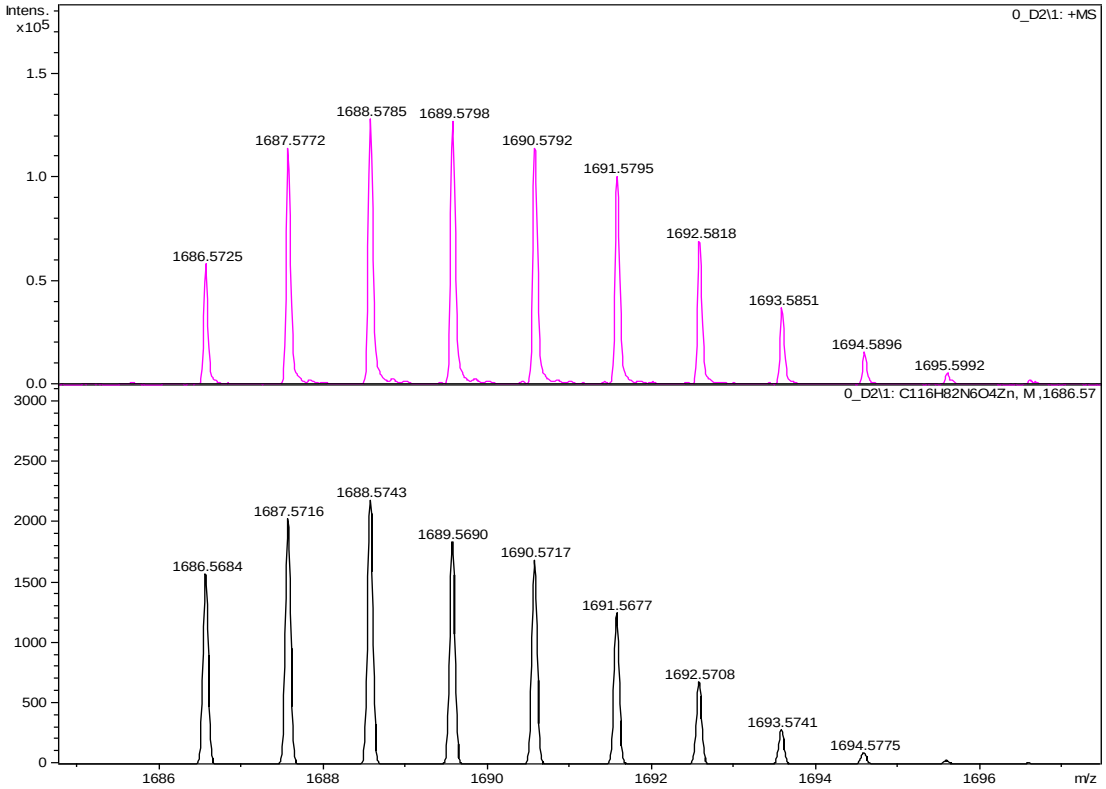

Figure S65. High resolution mass spectrum of **2b**-Zn (MALDI–TOF, top: experimental, bottom: simulated).

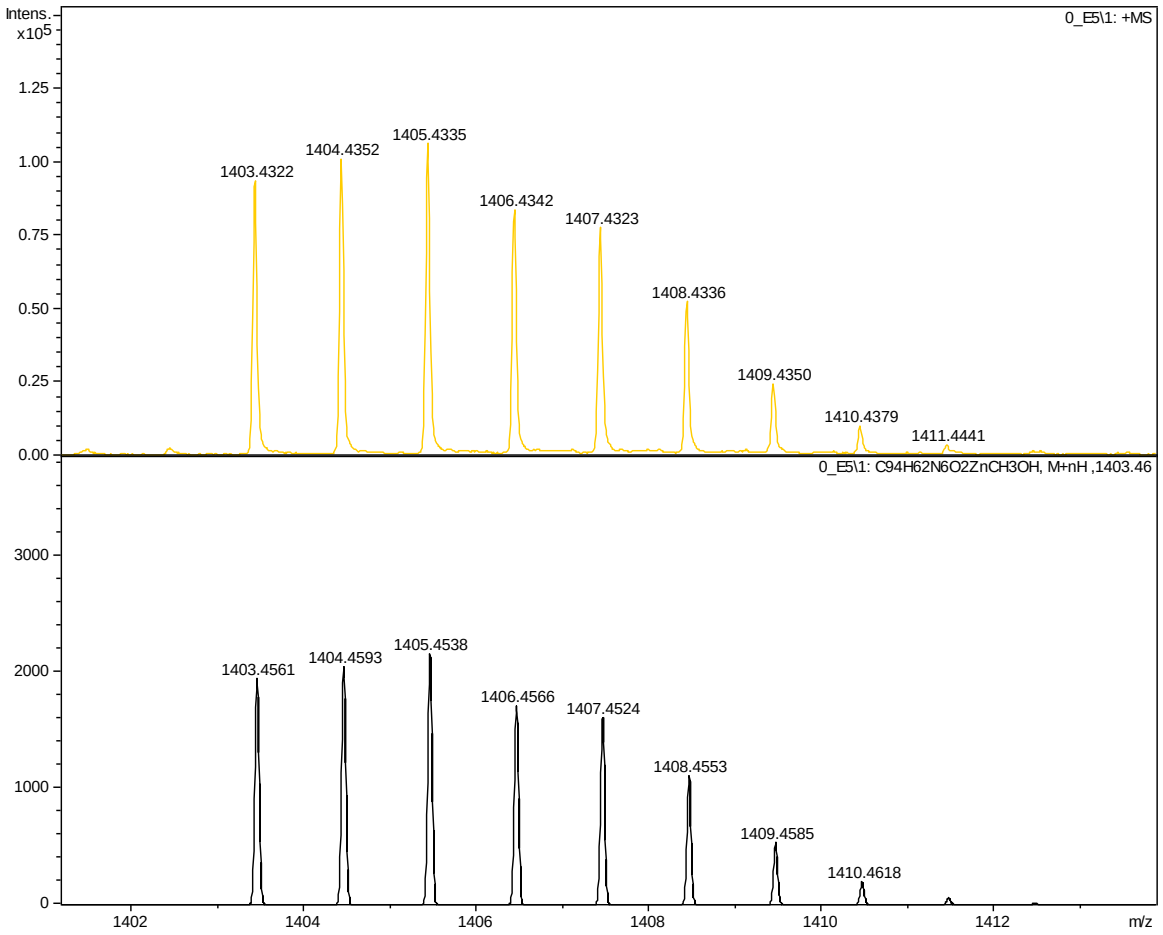

Figure S66. High resolution mass spectrum of **3a**-Zn (MALDI–TOF, top: experimental, bottom: simulated).

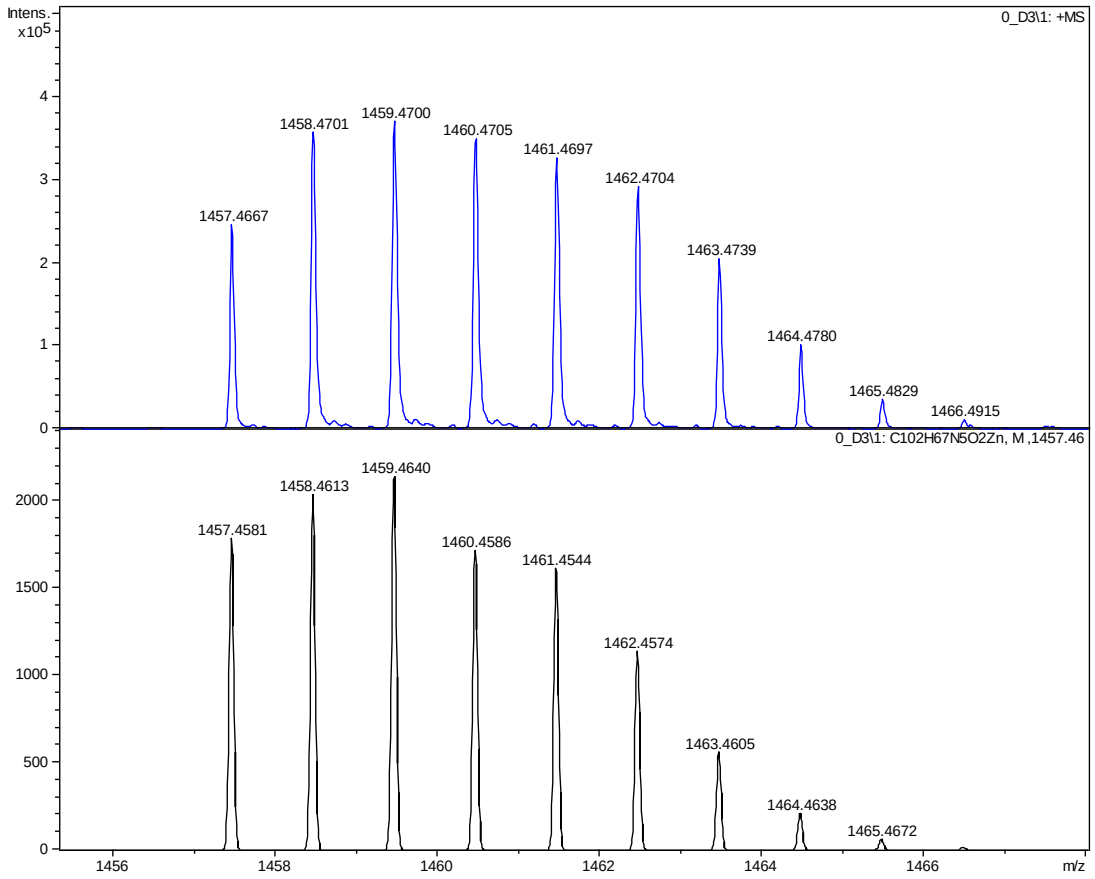

Figure S67. High resolution mass spectrum of **3b**-Zn (MALDI–TOF, top: experimental, bottom: simulated).

References

(1) Sheldrick, G. M. A Short History of SHELX. *Acta Crystallographica Section A Foundations of Crystallography* **2008**, *64* (1), 112–122.
(2) Spackman, M. A.; Jayatilaka, D. Hirshfeld Surface Analysis. *CrystEngComm* **2009**, *11* (1), 19–32.
(3) Turner, M. J.; McKinnon, J. J.; Jayatilaka, D.; Spackman, M. A. Visualisation and Characterisation of Voids in Crystalline Materials. *CrystEngComm* **2011**, *13* (6), 1804–1813.
(4) Frisch, M. J.; Trucks, G. W.; Schlegel, H. B.; Scuseria, G. E.; Robb, M. A.; Cheeseman, J. R.; Scalmani, G.; Barone, V.; Petersson, G. A.; Nakatsuji, H.; Li, X.; Caricato, M.; Izmaylov, A. F.; Zheng, G.; Sonnenberg, J. L.; Hada, M.; Ehara, M.; Toyota, K.; Fukuda, R.; Hasegawa, J.; Ishida, M.; Nakajima, T.; Honda, Y.; Kitao, O.; Nakai, H.; Vreven, T.; Montgomery, Jr., J. A.; Peralta, J. E.; Ogliaro, F.; Bearpark, M.; Heyd, J. J.; Brothers, E.; Kudin, K. N.; Staroverov, V. N.; Kobayashi, R.; Normand, J.; Raghavachari, K.; Rendell, A.; Burant, J. C.; Iyengar, S. S.; Tomasi, J.; Cossi, M.; Millam, J. M.; Klene, M.; Adamo, C.; Gomperts, R.; Stratmann, R. E.; Yazyev, O.; Austin, A. J.; Cammi, R.; Pomelli, C.; Ochterski, J. W.; Martin, R. L.; Morokuma, K.; Zakrzewski, V. G.; Voth, G. A.; Salvador, P.; Dannenberg, J. J.; Dapprich, S.; Daniels, A. D.; Farkas, O.; Foresman, J. B.; Fox, D. J. *Gaussian 16, Revision B.01*; Wallingford CT, 2016.
(5) Grimme, S.; Bannwarth, C.; Shushkov, P. A Robust and Accurate Tight-Binding Quantum Chemical Method for Structures, Vibrational Frequencies, and Noncovalent Interactions of Large Molecular Systems Parametrized for All Spd-Block Elements (Z = 1–86). *J. Chem. Theory Comput.* **2017**, *13* (5), 1989–2009.
(6) Bannwarth, C.; Ehlert, S.; Grimme, S. GFN2-XTB—An Accurate and Broadly Parametrized Self-Consistent Tight-Binding Quantum Chemical Method with Multipole Electrostatics and Density-Dependent Dispersion Contributions. *Journal of Chemical Theory and Computation* **2019**, *15* (3), 1652–1671.
(7) Becke, A. D. Density-Functional Exchange-Energy Approximation with Correct Asymptotic Behavior. *Phys. Rev., A* **1988**, *38* (6), 3098–3100.
(8) Becke, A. D. Density-functional Thermochemistry. III. The Role of Exact Exchange. *J. Chem. Phys.* **1993**, *98* (7), 5648–5652.
(9) Lee, C.; Yang, W.; Parr, R. G. Development of the Colle-Salvetti Correlation-Energy Formula into a Functional of the Electron Density. *Phys. Rev. B* **1988**, *37* (2), 785–789.
(10) Tomasi, J.; Mennucci, B.; Cammi, R. Quantum Mechanical Continuum Solvation Models. *Chem. Rev.* **2005**, *105* (8), 2999–3094.
(11) Spence, J. D.; Lash, T. D. Porphyrins with Exocyclic Rings. 14. Synthesis of Tetraacenaphthoporphyrins, a New Family of Highly Conjugated Porphyrins with Record-Breaking Long-Wavelength Electronic Absorptions. *The Journal of Organic Chemistry* **2000**, *65* (5), 1530–1539.
(12) McNeece, A. J.; Chang, M.-C.; Filatov, A. S.; Anderson, J. S. Redox Activity, Ligand Protonation, and Variable Coordination Modes of Diimino-Pyrrole Complexes of Palladium. *Inorg. Chem.* **2018**, *57* (12), 7044–7050.
(13) Zhylitskaya, H.; Cybińska, J.; Chmielewski, P.; Lis, T.; Stępień, M. Bandgap Engineering in π-Extended Pyrroles. a Modular Approach to Electron-Deficient Chromophores with Multi-Redox Activity. *J. Am. Chem. Soc.* **2016**, *138* (35), 11390–11398.